# Processing and Interpretation of Vibroseismic Data from Ekstroem Ice Shelf, Antarctica 2011

MASTER THESIS

eingereicht am Fachbereich Geowissenschaften,
Universität Bremen,
Oktober 2013
von

Jens Rose

durchgeführt am
Alfred-Wegener-Institut, Helmholtz-Zentrum für Polar- und Meeresforschung (AWI)

Prof. Dr. Angelika Humbert
Prof. Dr. Wilfried Jokat


# I. Erklärung

Erklärung gem. § 22 Abs. 9 Allg. Teil d. Master-PO

Ich versichere hiermit, dass ich meine Masterarbeit selbständig verfasst und keine anderen als die angegebenen Quellen und Hilfsmittel benutzt habe. Wörtliche oder dem Sinn nach aus anderen Werken entnommene Stellen sind unter Angabe der Quellen kenntlich gemacht.

Weiterhin erkläre ich, dass die Masterarbeit in unveränderter Fassung der Öffentlichkeit **zur Verfügung / nicht zur Verfügung*** gestellt werden kann.

*Zutreffendes bitte markieren

Ort/Datum: _____

Unterschrift: _____

# II. Zusammenfassung

Reflektionsseismologische Untersuchungen ermöglichen eine Abbildung der geologischen Strukturen des Untergrundes in einer Tiefe von mehreren Kilometern aber auch im nahen Oberflächenbereich. Durch eine Quelle wie einen Vibrator werden an der Oberfläche Raumwellen erzeugt, die sich innerhalb des Erdkörpers fortbewegen. Durch einen Wechsel der geologischen Schichten, ändert sich das Material und damit verändert sich die akustische Impedanz. Raumwellen werden hier reflektiert, refraktiert und gebeugt. Dies wird an der Erdoberfläche durch Geophone registriert. Nach einer umfangreichen Bearbeitung, dem Prozessieren, der seismischen Daten ergibt sich im Idealfall ein seismisches Querprofil des Untergrundes, das die Lage von Schichten und Störungen gut erkennen lässt und in dem Störsignale wie Mehrfachreflektionen eliminiert oder wenigstens gedämpft sind. In glazial geprägten Gebieten wie einem Eisschild wird üblicherweise Sprengstoff als Quelle für seismische Erkundungen verwendet. Das hat Nachteile in Hinsicht auf die Sicherheit und auf die Produktivität, da für jede Registrierung ein Loch gebohrt werden muss, in dem die Sprengladung platziert wird. Ferner wird unter Verwendung von Sprengstoff eine spezielle Mehrfachreflektion generiert. Mehrfachreflektionen stören bei der Auswertung der Daten. Ein neuer Ansatz, ist einen Vibrator zu benutzen, so können mehr Untersuchungen an einem Tag durchgeführt werden, bei gleichzeitigen Wegfall eines Sicherheitsrisikos. Außerdem sind die Aufnahmen von fast gleich hoher Qualität bei einer größeren Penetrationstiefe.

Diese Arbeit befasst sich mit der Auswertung und Interpretation zweier reflektionsseismischer Datensätze, die 2011 im Königin-Maud-Land, Antarktis, entlang zweier Profile erhoben wurden. Das Untersuchungsgebiet ist der Ekströmen Eisschelf und der angrenzende Halvarryggen, ein Eisdom mit 900 m Mächtigkeit. Das erste Profil reicht vom Fuß des Halvarryggen über die grounding line weit in den Ekströmen Eisschelf hinein. Das zweite Profil erstreckt sich längsseits, über einen Teil des Schelfs bis zur Deutschen Antarktisstation Neumayer III. Damit reicht es bis zum Kontinentalhang der Antarktis, der von einem Keil aus erstarrten Vulkangesteinsschichten bedeckt ist, abgesehen von einer Sedimentschicht, die ihrerseits auf dem Keil liegt.

Der glaziologischen und geologischen Interpretation geht das Prozessieren der seismischen Daten voraus. Die im Feld aufgezeichneten Daten müssen einer umfangreichen Abfolge der Datenverarbeitung unterzogen werden. Ein wesentlicher Aspekt dabei ist die

Verbesserung des Signal-Rausch-Verhältnisses und in dem Zusammenhang die Unterdrückung von Mehrfachreflektionen bzw. Echos eines einzigen Reflektionspunktes im Untergrund. Letzteres ist ein bedeutendes Problem in der Seismologie. Im Rahmen dieser Arbeit wurden aus den Rohdaten zwei seismische Querprofile erstellt. Verschiedene Ansätze zur Eliminierung der Mehrfachreflektionen werden vorgestellt und getestet. Es wird gezeigt, dass die Mehrfachreflektionen nur bedingt gedämpft werden konnten. Das hängt vor allem mit der Aufnahmegeometrie zusammen, aber auch die geringe Überdeckung eines jeden Reflektionspunktes wirkt sich negativ auf die Ergebnisse der Mehrfachreflektionsfilterung aus. Trotzdem konnten die Resultate für eine geologische Interpretation genutzt werden. Die Querprofile veranschaulichen die oben erwähnten geologischen Charakteristika deutlich und ermöglichen eine Interpretation des Untergrundes.

# III. Abstract

This thesis deals with processing and interpretation of data from a seismological survey, on Ekstroem Ice Shelf Dronning Maud Land, Antarctica. This data was obtained with a new approach: using a vibrator to generate spatial waves on ice, Vibroseismics. One advantage is that more energy is transmitted into the subsurface with a deeper penetration than the typically used explosives in firn/ice covered areas. Seismic surveys are indispensable for investigations with sub-ice glaciological and geological objectives. Two profiles were shot, one is passing a shear zone of two different ice flows and the grounding line, where ice shields slide into water and contribute to the sea level. The second profile shows the buildup of the continental basement and shelf sediments. An outstanding problem during processing of this data was removal of multiple reflections. Attenuation of multiples was reached and seismic cross sections about two profiles which outline glaciological and geological important features are presented and interpreted.

# IV. Acknowledgements

Many thanks to my adviser Coen Hofstede, he taught me in glaciological and geophysical subjects and helped me with the processing stuff; Angelika Humbert for sharing her profound knowledge about ice streams and ice flows; Wilfried Jokat and Olaf Eisen for giving hints for writing and multiple removal. I also want to thank a special person in my life, Antje Marschalk for supporting me.

# Table of Contents

# List of Figures

# 1 Introduction

Glaciers and polar ice shields are playing a decisive role for the climate of the Earth. Due to their attribute to reflect the solar radiation (albedo) they prevent that Earth absorbs solar heat. The result is a cooling effect for climate. They are also an important reservoir for fresh water and they influence the global and regional sea level by their mass balances. The mass balances include how much ice on the land (glaciers, ice sheets) and floating in the water (sea ice, icebergs, and ice shelves) is available. They enable conclusions about the rate at which ice forms on the land and how much ice flows with which speed into water. The transition zone from ice sheet to ice shelf, called the "grounding line", plays a crucial role. The change of environment results in changes of the stress regime in the ice, as the basal shear force which greatly slows the flow movement of the ice is removed. This in turn has an influence on the speed with which the ice flows into the sea. Ice core drilling in ice enable paleoclimatic climate reconstructions. Air bubbles in the ice allow statements about the composition of the atmosphere at the time of inclusion. Concentrations of certain isotopes in the ice core allow conclusions on temperature, rainfall distribution and wind direction. These parameters could be reconstructed for the last 890,000 years, showing that ice is an important research object.

Seismic investigations can obtain geological and glaciological objectives for the shallow subsurface and its basement. After processing of seismic data from a survey it is possible to produce a structural map of the subsurface down to tens of kilometers of depth, depending on device delivery. To examine large areas, e.g. in the Antarctic, most of geophysical investigations are carried out usually from aircraft. That has logistic advantages such as no need for heavy vehicles and a high amount of measurements per day. But seismic investigations cannot be carried out by an airplane. Radar is used instead, it is appropriate for ice but for geology objectives it has problems with the conductivity. A better result will be achieved from land-based methods. Normally, on ice sheets (ice grounded on land) or on the connected ice shelves (floating ice) or on glaciers explosives will be used to produce seismic waves (explosive seismics). Unfortunately a hole has to be drilled in which to place the explosives for every shot. This practice is more dangerous, costly and time consuming. From a geophysical point of view, a lot of the explosive energy gets lost due to scattering caused by the firn – snow that survived one seasonal melting (ablation) period. So most of the seismic waves triggered by explosives in firn will be redirected to the surface and only a small portion

travels directly down to the underground. Furthermore a strong, special kind of multiple reflections will be caused by a source placed underneath the surface, the ghost. Ghosts are reflected by the surface-to-air boundary and travel downwards. Multiples can overlap with primary seismic signals and change their waveforms, or they appear as single event. However, the geological interpretation will be interfered.

A new approach on ice is the use of a vibrator (Vibroseismics) to record seismic shots. Hofstede et al. (2013) and Eisen et al. (2010) proved recently that it works on firn and ice covered areas. It enables records with alike richness in detail like explosive seismics but with a higher production rate and safety and the vertical motion prevents the ghost. The aim was to record seismic reflections for a seismic survey for glaciological and geological objectives.

This project was accomplished by LIMPICS ("Linking micro-physical properties to macro features in ice sheets with geophysical techniques"), a junior research group of the Emmy Noether Programme from 2008 till 2013. This programme was founded by the Deutsche Forschungsgesellschaft (DFG). LIMPICS is located at the Alfred Wegener Institute, Helmholtz Centre for Polar and Marine Research, Bremerhaven (AWI) and the Institute of Environmental Physics, University of Heidelberg, both in Germany.

In August 2010, LIMPICS carried out a geophysical campaign on the alpine glacier “Colle Gnifetti” in its accumulation zone. The aim was to test new geophysical measurement techniques (e.g. Vibroseismics) and to provide new physical properties close to an already existing borehole. The previously collected borehole radar data enables an estimation of the amount of ice between underneath the borehole and the bedrock. This is important because older ice has a higher density and thus a higher seismic velocity for seismic waves. From the drill core a density profile was produced that enables a calculation of seismic velocity (Kohnen, 1972). So the quality of the results of Vibroseismics was evaluated.

First time Vibroseismics measurements on an ice shelf were carried out in the 2009/10 field season on Ekstroem Ice Shelf Dronning Maud Land (DML), Antarctica (Kristoffersen, et al., 2010). In 2011 a Vibroseismics survey was carried out acquiring two profiles. The first profile reaches from Halvarryggen, a local ice dome with a thickness of 900 m, to Ekstroem Ice Shelf (around 30 km) with traverse of the grounding line (Fig. 24).

The grounding line is the transition zone from an ice sheet to its swimming portion, an ice shelf. The second profile is perpendicular to profile 1 and reaches from the turning point of profile 1, northward along the Ekstroem Ice Shelf, ending at the German Antarctic station Neumayer III (around 41 km). The north section of this profile includes a sub-ice outcrop belonging to an unconformity overlying the continental slope, the Explora volcanic wedge. This outcrop is marked by seaward dipping reflectors.

The aim of this thesis is to process the seismic data of the Vibroseismic surveys, with special interest in removing or attenuating multiple reflections. Two seismic profile sections should be created, which allow a geological and glaciological interpretation of the subsurface in respect to the grounding line (profile 1), the Explora Wedge (profile 2) and other features.

# 2 Field of activity: Ekstroem Ice Shelf, Antarctica

This chapter gives an outline about the origin of Antarctica (Fig. 1); it provides geographical information and the geological formation of the survey area.


*Fig. 1; Antarctica with the main geographic components. The red filled area in the north is the Ekstroem Ice Shelf. Adapted from the British Antarctic Survey.*

## 2.1 Geological origin of Antarctica

Antarctica at present day is the result of a very long and complex process of plate tectonics. It was a central component of the amalgamation of the supercontinent Gondwana its breakup. Alfred Wegener's book "The origin of continents and oceans", 1915, and his works and lectures, which introduced the movement of continents, was the first important step to reconstruct the paleogeography of continents and oceans. Decades of scientific investigation were necessary to understand this process. With the disclosure of the paleogeographical reconstruction of Antarctica it was possible to make conclusions and assumptions about the development of the supercontinents Rodinia, Pangaea, Gondwana and Laurasia. Geological structures like rift systems which can overlap whole continents were also hard to explain or even unknown. Pangaea was a supercontinent which contained all landmasses. Sea floor spreading about the Atlantic magmatic province between Africa and America 190-180 Ma ago led to split up Pangaea into two parts (Fig. 2) (Veevers, 2012).

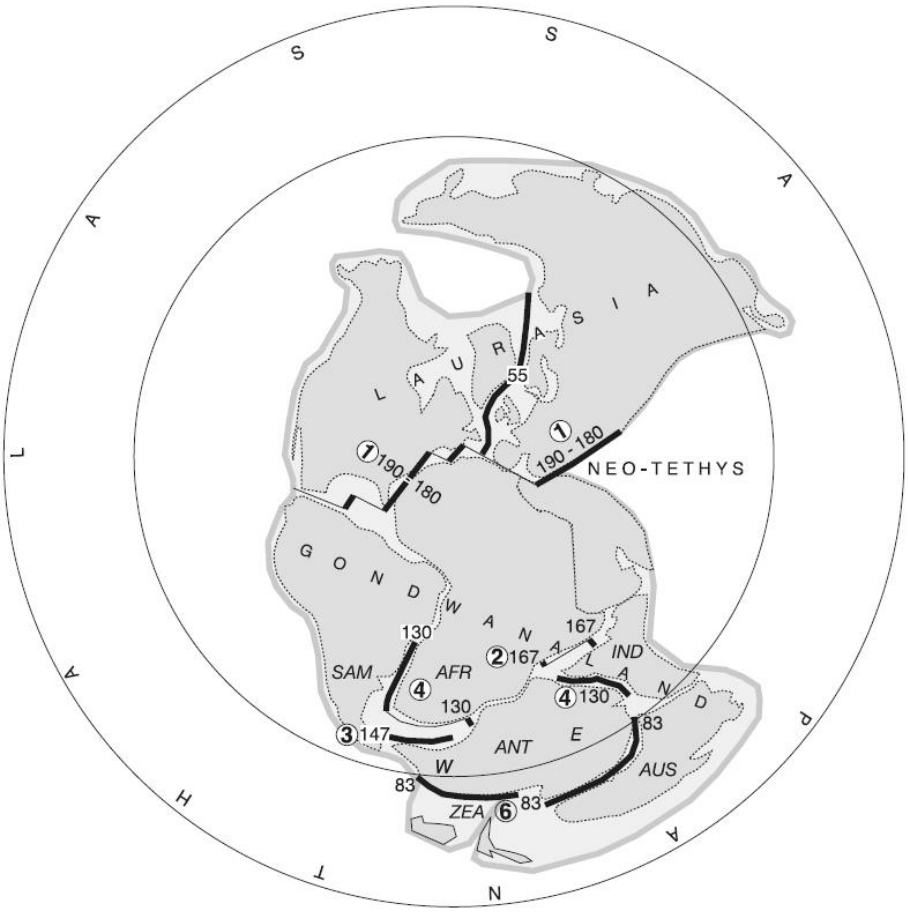


*Fig. 2; Pangaea and Panthalassa, during the middle to late Triassic with ages (Ma) of breakup. Heavy lines mark onsets of sea floor spreading. The numbers in circles mark subsequent stages in which Gondwana splits up. Abbreviations in text below. From Veevers (2012).*

The northern part was Laurasia, or more uncommon Laurentia, containing the recent continents North America, Europe and Asia. The southern part was Gondwanaland or Gondwana, or very uncommon Gondwania, and contained South America (SAM), Africa (AFR), Arabian Peninsula, India (IND), Australia (AUS), Zelandia (ZEA) and Antarctica (ANT). Panthalassa was the all-embracing Ocean, including the re-entrant Neo-Tethys. 13 till 23 Ma later the breakup of Gondwana begun, stage 2 (Fig. 2). Several parts of Gondwana broke away from Antarctica due to sea floor spreading. Although the splitting of Gondwana began in the Middle Jurassic, Antarctica was only isolated at the early Oligocene, about 29 to 33 Ma. The result was circumpolar deep water flows, which led to a general cooling of the oceans and started the glaciation of Antarctica (Lawver & Gahagan, 2003). Due to the fact that 98 % of Antarctica is covered with ice with an average thickness of two kilometers and the severe climatic conditions – mean annual temperature -55° C – the geology is only roughly mapped and discovered (Fig. 3). Antarctica is divided by the Transantarctic Mountains which is the fifth largest mountain range of the world, into West- and East Antarctica. Those mountains are in places completely covered by ice and snow. East Antarctica is a Precambrian block which is composed predominantly of granitoid and metamorphic rocks. West Antarctica consists of several terranes which have been added to the East coast during the Ross-orogenesis and the Cenozoic (Boger, 2011; Veevers, 2012, Fig. 4).

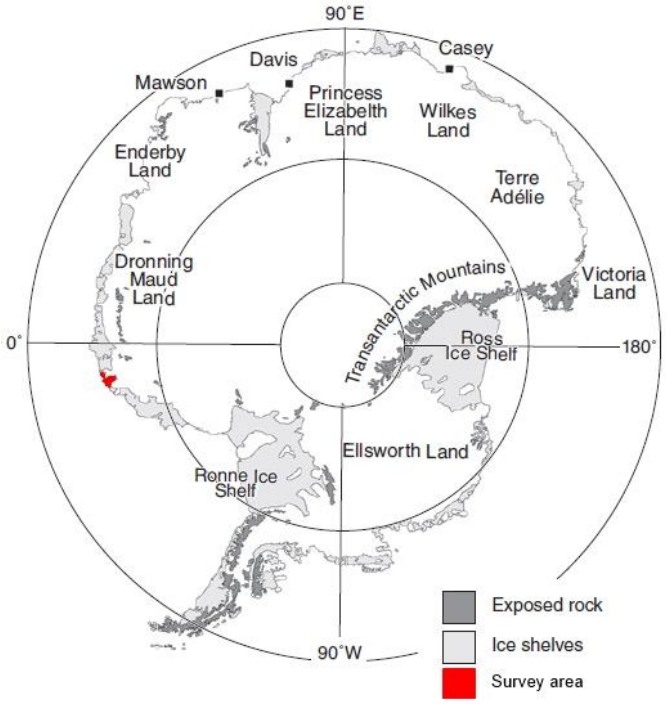


*Fig. 3; presentday Antarctica with distribution of rock exposures and major geographic place names. Mawson, Davis and Casey are the three Australian research stations. Modified after Boger (2011).*

### 2.1.1 **Geology of the survey area**

Boger (2011) presents in Fig. 4 the relationship between tectonic domains in Antarctica and their correlatives within Gondwana. Besides it is shown that the Ekstroem Ice Shelf belongs to the Archaean Grunehogna Craton which is a fragment of the Kalahari Craton, the Precambrian shield of Southern Africa (Jacobs, et al., 2008). The Grunehogna Province was divided by the breakup of Gondwana, it consists of a granitic basement with an age between 2960 Ma and 2820 Ma (Barton, et al., 1987; Halpern, 1970). Riedel et al. (2012) suggest a total crustal thickness from 24 km (northward from Neumayer III) up to 38 km (southern Halfvar Ridge), estimated from gravity inversion. Above the basement there is a flat layer of Mesoproterozoic sediments, the Ritscherflya Supergroup. It contains both, sub-aqueous and sub-aerial sediments intercalated with basaltic to andesitic lavas and lesser volcaniclastic sediment (Boger, 2011).

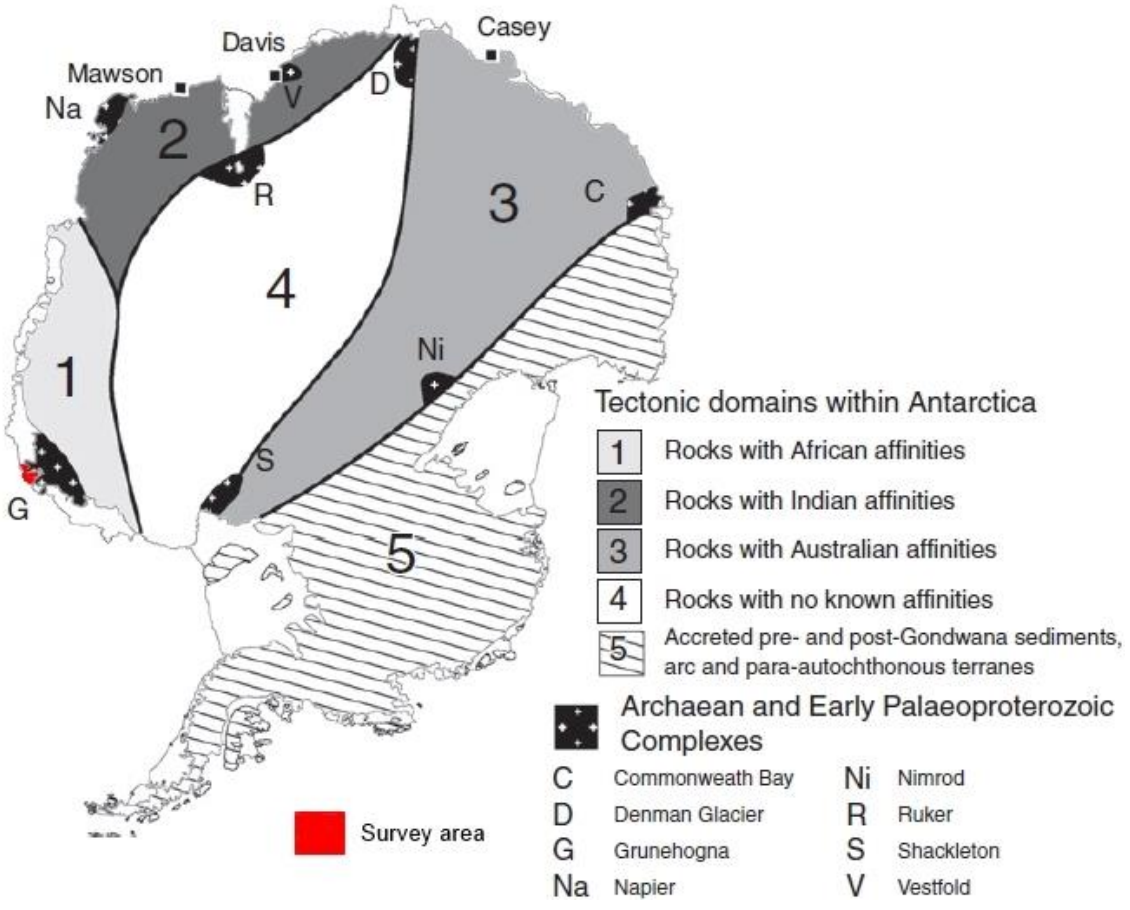


*Fig. 4; tectonic domains of Antarctica differentiated on the basis of their affinities with Antarctica's correlatives within Gondwana. Modified after Boger (2011).*

### 2.1.2 Explora Volcanic Wedge

A 1700 km part of a volcanic unconformity over the continental slope of Dronning Maud Land was mapped by a multichannel marine seismic survey in 1978 (Hinz & Krause, 1982). The unconformity is an Explora Wedge with seaward dipping volcanic units, and uncertain base is (Fig. 5). A strong, positive magnetic anomaly (Riedel, et al., 2013) 14 km southward of Neumayer III, at the margin of the landward extent of the wedge, indicates that the extent of the wedge is along the greater Dronning Maud Land continental slope (Kristoffersen, et al., submitted). The landward extent is uncertain due to the severe conditions like floating ice sheets/shelves with several hundred meters in thickness. The wedge was build up shortly before Gondwana broke up (Jokat, 2003).

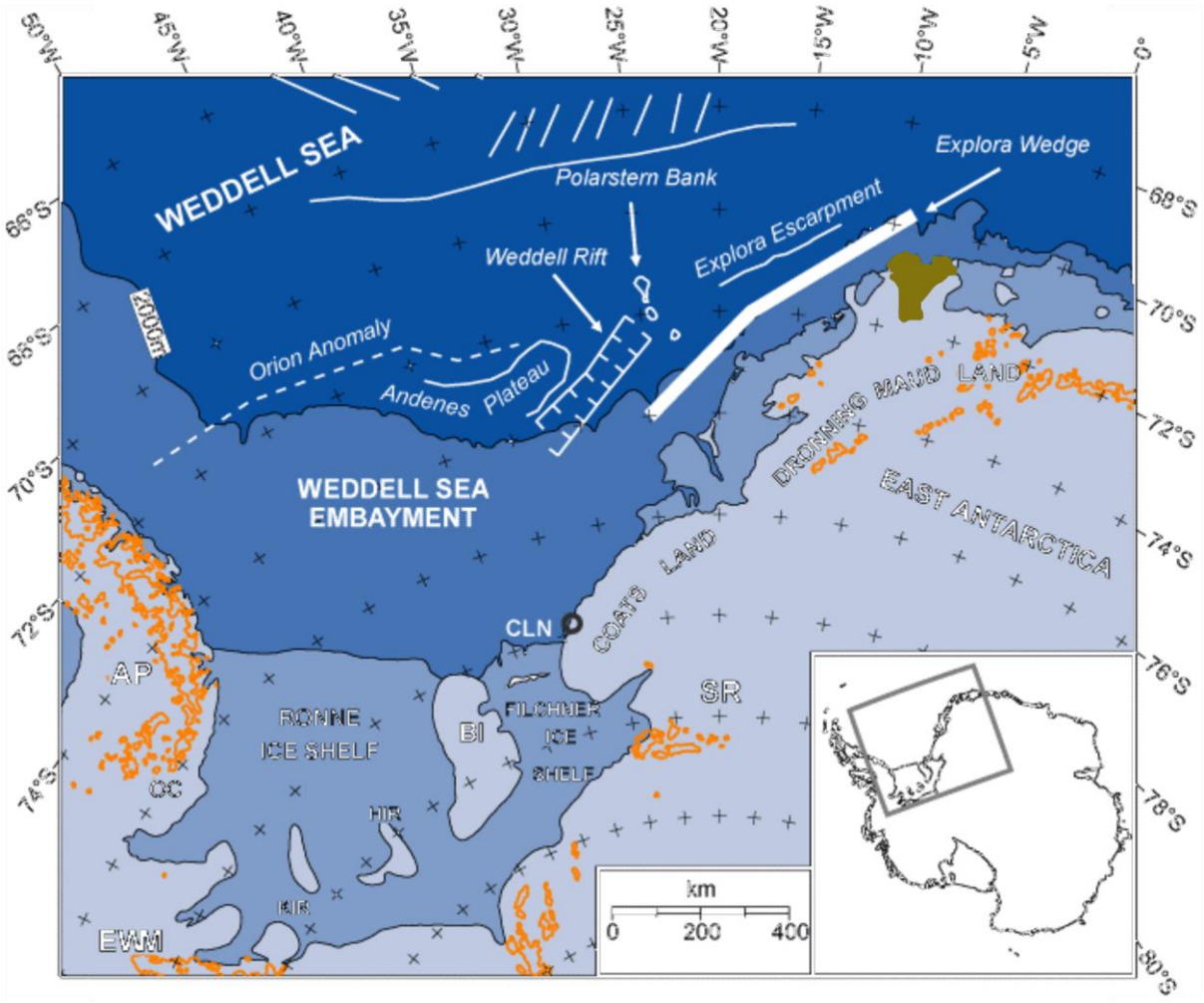


*Fig. 5; tectonic features of the Weddell Sea. Abbreviations are: AP, Antarctic Peninsula; BI, Berkner Island; CLN, Coats Land Nunataks; EWM, Ellsworth Whitmore Mountains. (Studinger & Miller, 1999). The olive filed area is the Ekstroem Ice Shelf.*

## 2.2 Overview of the survey area, the Ekstroem Ice Shelf

The Ekstroem Ice Shelf is part of the polar ice shelves (section 2.3.1) of Antarctica. It is located in Dronning Maud Land (DML), the Atlantic coastal zone of East Antarctica (Fig. 6). The shelf reaches into the eastern Weddell Sea which is part of the southern Atlantic Ocean and into the Atka Bay. It ranges about 140 km from 10,00°W to 6,25°W and about 170 km from 70,25°S to 71,75°S (WGS84). The area is about 8,700 km² in size and thus one of the smaller ice shelves of Antarctica (Müller, et al., 2000). The floating ice shelves in the coastal zone of DML are more or less flat, with an average height of 40 m above sea level (Riedel, et al., 2012). To the east Ekstroem Ice Shelf is bounded by the Halfvar Ridge, a local ice dome. The southern boundary is Ritscherflya, a marginal region of the East Antarctic Ice Sheet. In the West there are Auståsen and Soräsen, two other ice domes. Ekstroem Ice Shelf is subdivided by the Atka Bay and the northwestern part of Halfvar Ridge into a small eastern part (~2000 km²) and a major western part (~6700 km²). There is a passage between Halfvar Ridge and Atka Bay that connects the two parts. This area was first mapped by the Norwegian–British–Swedish Antarctic Expedition (NBSAE) from 1949 till 1952 (Robin, 1958) and was named after Bertil Ekström, a Swedish mechanical engineer who died on 24. Feb. 1951 because he fell from the edge of the Quar Ice Shelf, which is located in western direction. The German Antarctic Station Neumayer III, which is open for the whole year, is settled on the western part of the ice shelf, close to the Atka Bay (Fig. 6).

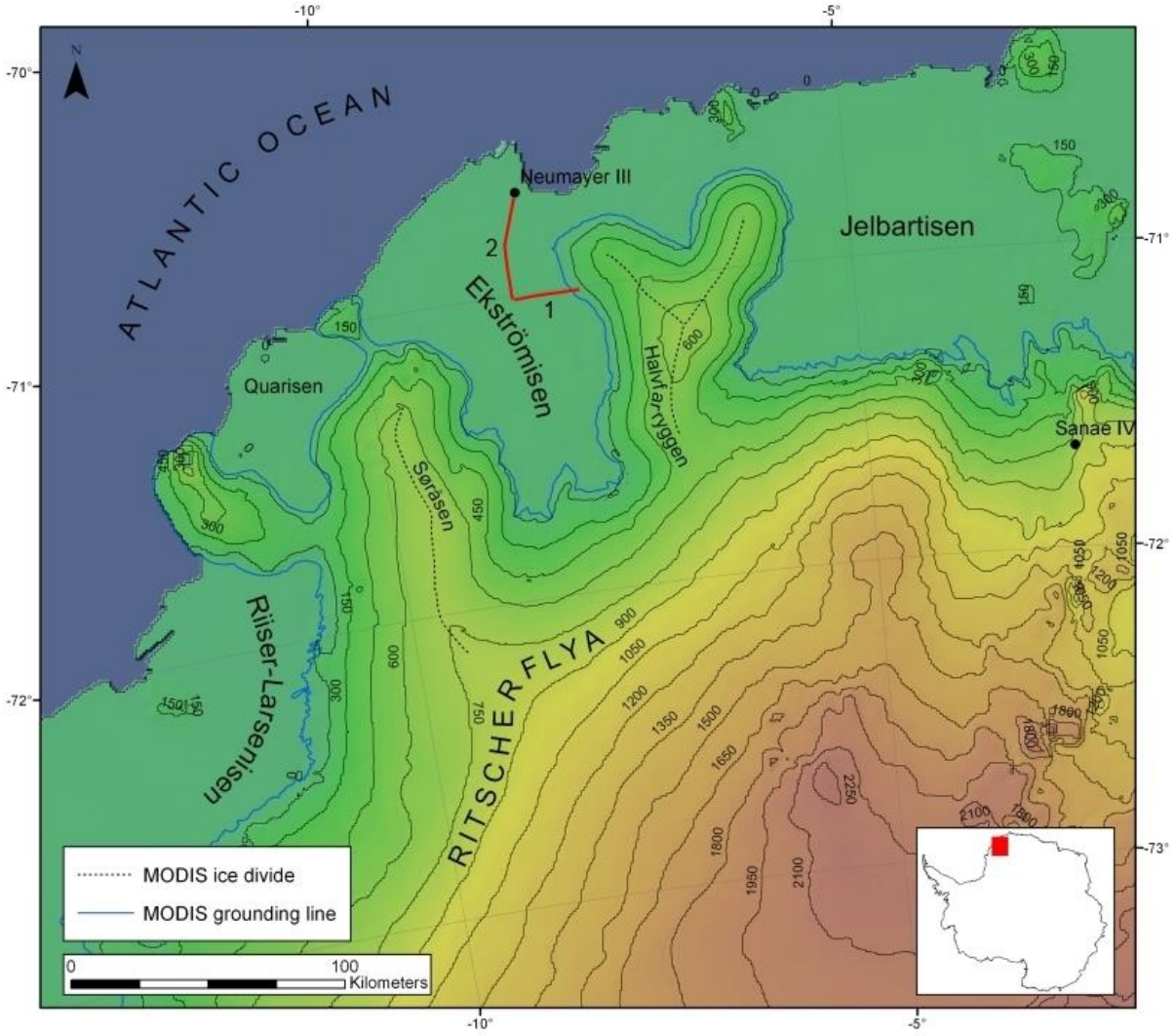


*Fig. 6; overview of the survey area with profile lines (red), elevation lines and grounding line (6), adapted from Niklas Neckel (2010)*

## 2.3 Glaciology

### 2.3.1 Ice sheet/shelf and grounding line

"An ice sheet is a continent-sized mass of ice and snow thick enough to flow under its own weight" (Hughes, 1977). It may have also floating portions called ice shelves (Fig. 7). Ice sheets and ice shelves are active, dynamic components of the climate system of the Earth (Greve & Blatter, 2009), since they have a cooling effect on the climate. The grounding line (Fig. 7 and Fig. 6) marks the zone where the ice slides into the sea. So the grounding line is by definition the transition from continental ice sheet to marine ice shelf (Thomas, 1979). The term "line" is unfortunate, since the grounding of the ice is more a zone with up to several kilometers in width. In the following it is named grounding zone. It is a very important subject in polar research. Basal shear forces prevent ice from sliding fast. In the grounding zone a basal shear force does not exist. So the ice movement is accelerating and the ice slides into water and contributes to sea level from that point. The ice flux in this zone gives information about the rate with which the Antarctic Ice Sheet loses mass due to changes in accumulation and ablation (Rignot, et al., 2011). "For numerical models of ice sheet dynamics, ice sheet mass budgets, ice-ocean interactions, oceanic tides and subglacial environments use the grounding zone for boundary condition" (Rignot, et al., 2011). Its position can vary due to changes in sea level and ice thickness (Hughes, 1977, Thomas, 1979).

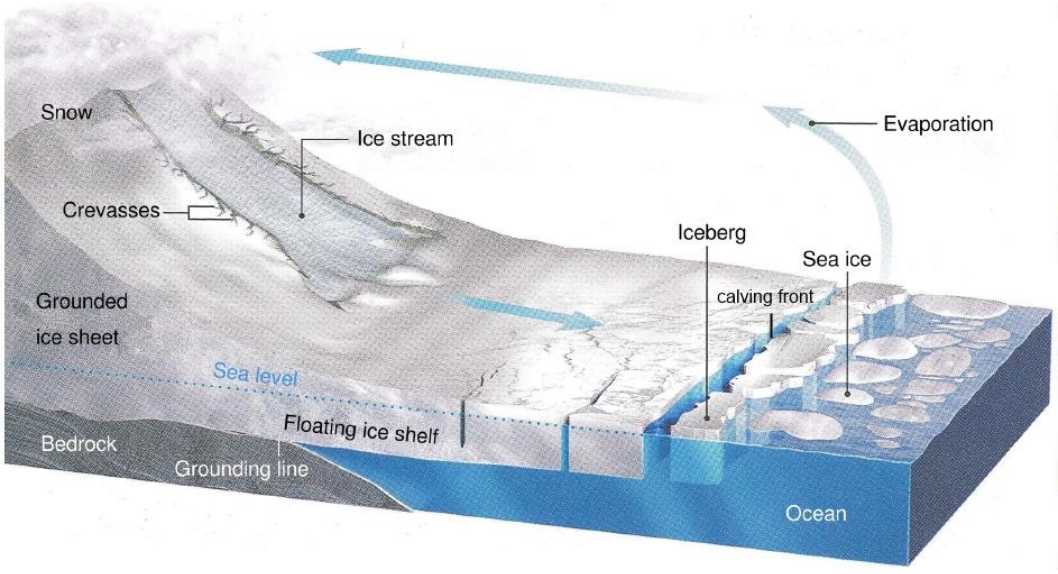


*Fig. 7; an outline of the Antarctic ice system which marks the grounding line, modified after (Bell, 2008). Ice streams are parts of an ice sheet, where ice moves significantly faster than the surrounding ice. Their shear forces create crevasses. 90 % of the Antarctic ice discharge is drained through ice streams (Bamber, 2000), although they account for only 10 % of the volume of an ice sheet.*

### 2.3.2 **Firn**

The top layer of most ice sheets and glaciers in their accumulation area is firn. That is snow which has not molten in the ablation period (Greve & Blatter, 2009). Firn consists of a mixture of air and ice crystallites. Unlike ice, it has a bigger porosity and is therefor compressible. Thus, ice has a greater density. This is an important factor for the propagation of seismic waves. At some depth, the firn is transformed into ice, due to its densification (Fig. 8). Firn has a porosity of 60 to 70 %, which means that 60 to 70 % of the volume is air, so the density is around 350 $kg/m^3$ at the first layering. This high porosity is the reason why firn acts as an energy trap, much of explosion energy crackles here, firn acts as a waveguide (Albert, 1998). Much of seismic energy is generally lost in the first few meters of the firn due to inelastic deformation around the shot location (Diez, et al., 2013). In ongoing time through further snow accumulation the density of firn rises up to 830 $kg/m^3$ and most of the air will be pressed out. The continuous densification with depth causes a diving wave (Hofstede, et al., 2013). At a density of about 820 $kg/m^3$ (Stauffer, et al., 1985) ice with isolated air bubbles exists. Ice can get a density over 900 $kg/m^3$. The firn-ice-transformation is very complex and depends on inter alia of the presence of melt water, the amount of accumulation, temperature and other factors.

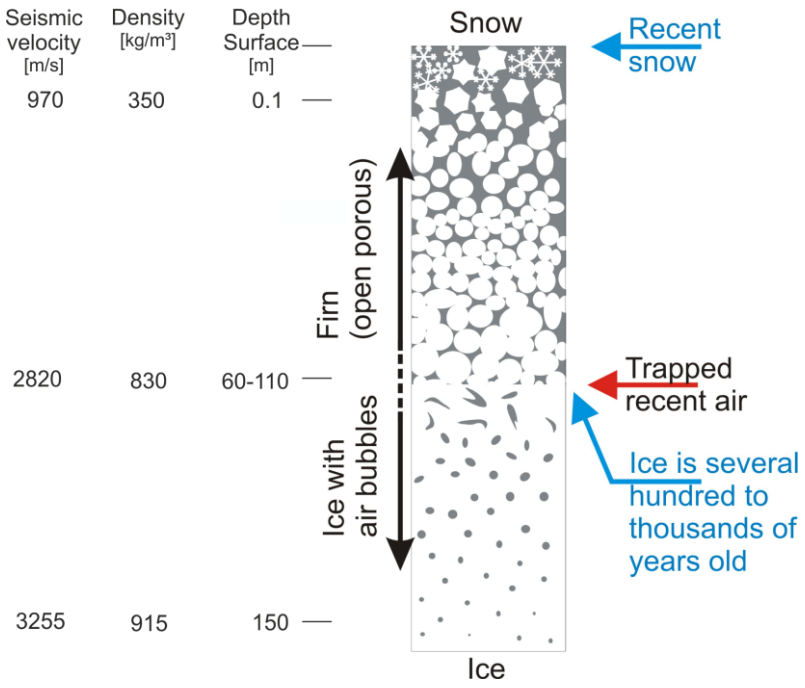


*Fig. 8; a schematic outline how snow becomes ice added with root mean square (rms) seismic velocity from Halvfar Ridge ice core DML-94 (Fernandoy, et al., 2010). Courtesy of Centre for Ice and Climate, University of Copenhagen, modified.*

# 3 Principles of seismic data processing

## 3.1 Fundamentals of reflection seismics

The basic idea behind seismic surveys is that at the surface or in boreholes an impulse will be produced. As a result the subsurface gives a response and this response will be recorded. After processing the recorded data, an image in form of a structural map of the subsurface is generated. There are several techniques which can act as a source of such an impulse like Vibroseismics (section 3.2) or explosives. Geophones ("*something like a microphone*" (Claerbout, 1985)) serve as receivers, they record the seismic movement. The impulse generation of energy at the surface (called shot) triggers space waves which travel through ice and soil like a ray. These waves have a continuous amplitude loss due to geometric spreading and attenuation. Each time a seismic ray passes a boundary layer, the wave passes through an impedance contrast interface (Fig. 10). Impedance is the product of velocity ($v$) and density ($\rho$).

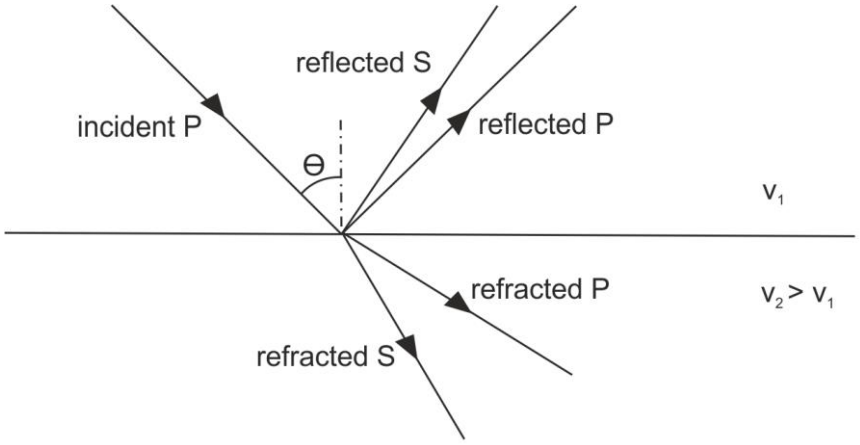


*Fig. 9; a compression-wave (P-wave) gets reflected at a boundary layer, generating reflected and transmitted P- and S-waves (shear waves). Courtesy of the Department of Earth Sciences, University College London.*

The amplitude here is scaled by a transmission coefficient, which is different for upward and downward propagating waves. The factor of this coefficient depends on the kind of material of the layer, in particular of its density and its transmission velocity. The passage through various layers results in a cumulative transmission loss and to reflection, diffraction and also to refraction. There are several kinds of seismic waves, for reflection seismics compression waves (P-waves) and shear waves are important. P-waves are more typically used because they penetrate better and travel through fluids.

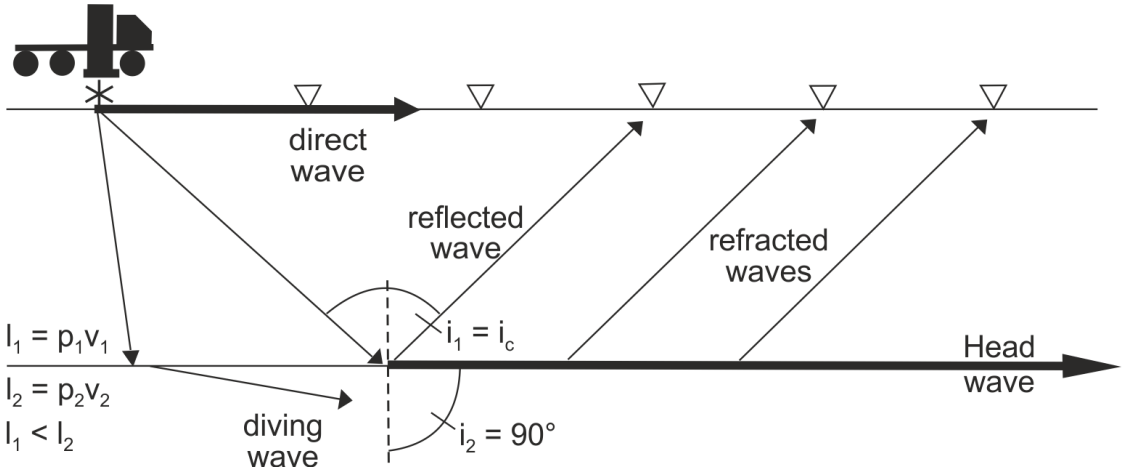


*Fig. 10; simple model of the propagation of P-waves. A direct wave propagates along the air-surface interface. A reflected wave has an exit angle that equals the incidence angle, is this angle 90° in lower medium it is called the critical angle and a critical refracted head wave runs along the boundary between layer 1 and layer 2. The head wave creates refracted waves. A diving wave is a continuously refracted wave that travels back to surface with a diffracted ray path. The star symbol denotes the source, triangles mark receivers, arrows are wave ray paths, l = layer, p = density, v = velocity, $i_c$ = angle of incoming ray path.*

The amplitude of a reflected wave is scaled by an angular reflection coefficient, which depends on the medium of the layers. Propagating to the receiver, seismics waves lose further energy by geometric spreading, absorption and attenuation. A seismogram is the record of all geophones, also called shot gather (Fig. 11). The geophones are often combined to channels and record one trace. For the surveys in this thesis, eight geophones are combined to one channel, due to advantages in recording. So the shot gather in Fig. 11 is a multichannel system and every channel is represented in this shot gather by a wiggle line. The distance from the source to the first channel, called first-geophone-offset, is 62.5 m (Trace 1), the channel spacing is 25 m and the total offset is about 1500 m. The geophones are arranged on only one side of the source.

The shot gather in Fig. 11 has not undergone any processing, except a correction for spherical divergence (section 4.2.4). At 0.25 s (trace 1) inserts a reflection event down to 0.5 s (trace 60), that is the ice-bed boundary. The impedance contrast interface between the ice and Mesoproterozoic sediments is strong. That causes multiple reflections of this boundary. Some traces (channels) were removed because they were distorted. Surface waves are direct waves which travel along the surface (Fig. 10). Due to a rising temporal difference at recording at each geophone, they occur continuously descending in a shot gather. A diving wave is a refracted wave with a diffracted ray path, see also Fig. 10.

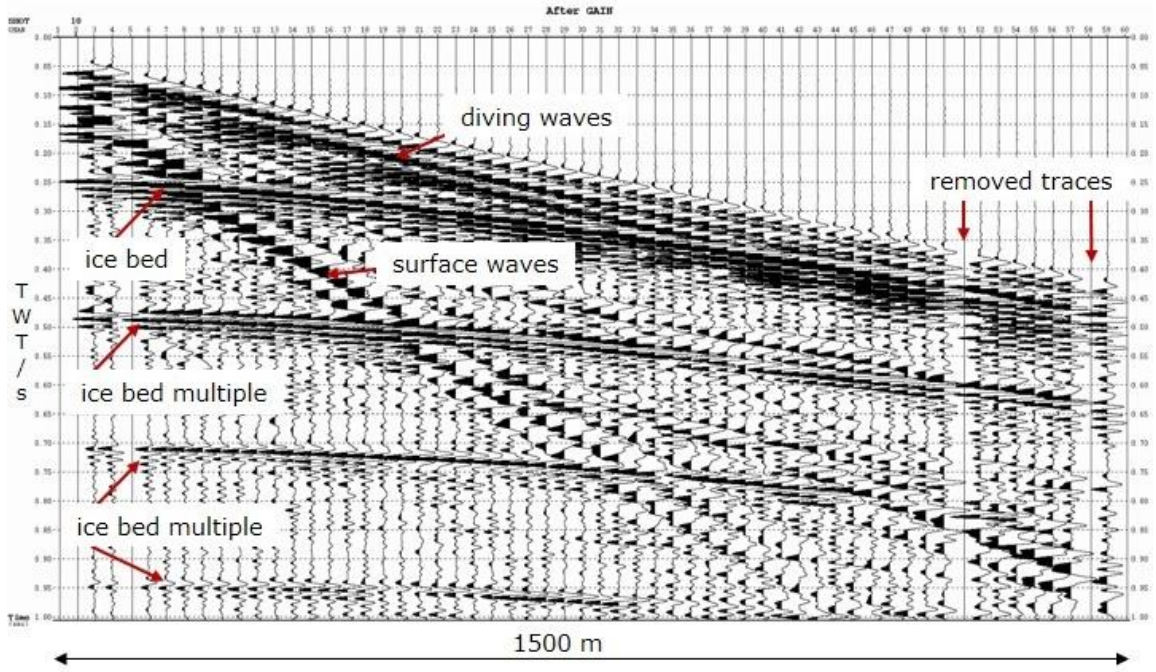


*Fig. 11; a shot gather from the beginning of profile 1 (section. 4.1, Fig. 24) up to 1 s two-way travel time (TWT). The recorded channels displayed as wiggle lines against TWT of the seismic waves. Every time a receiver registers an impulse the wiggle line draws an amplitude. In this picture the negative amplitudes are filled out with black. Solid black lines denote a reflection or refraction.*

After the processing, the seismic data has undergone an improvement of the signal-to-noise ratio and three main steps in processing. With Deconvolution, every trace will be examined for a reflection event. Stacking compresses the data volume along the offset, the traces of a common reflection point will be resorted and stacked together. Thirdly, Migration insures that reflection events will appear at their true subsurface positions. The reward is a seismic profile, an image of regional and local structures of the geology of the subsurface. So the processing has an important role and is different for every case study. There is a wide field of possible applications for reflection seismics. The exploration industry uses reflection seismics for hydrocarbon surveys and development within a depth of up to 10 km and geophysicists use it for investigation of the Earth's crustal structure within a depth of up to 100 km (Yilmaz, 2001) or for shallow surface investigations with a penetration depth of several meters for e.g. archaeological surveys. It is also possible to estimate elastic parameters like the Poisson's ratio for geotechnical tasks, but for this purpose it is necessary to work with shear waves in addition to the compression waves, which are normally used for reflection seismics.

## 3.2 Introduction to Vibroseismics

Vibroseismics mean that the source of energy which produces seismic waves will be created by a vibrator. This vibrator is attached for instance to a vehicle (Fig. 12). The plate underneath the load floor is lowered to the ground. It creates a vibration with a duration of several seconds, called a sweep. Vibroseismics are very common as reflection survey method for the hydrocarbon exploration with a range from several hundreds of meters up to tens of kilometers of depth.

*Fig. 12; a truck-mounted vibrator, the black rectangle marks the plate, which will be lowered down. Photo from Lambrecht et al. (2010).*

The major difference compared to explosives or weight-drop is the duration of the impulse transmission. Explosives or weight-drop have a short impulse transmission, while Vibroseismic sweeps have durations of several seconds. The motion of the vibrator is vertical, so the impulse goes straight down in opposite to explosives. Explosives in seismic surveys detonate in boreholes. The force is transmitted in all directions and a high amount of the energy crackles in the firn layer. But the shot gathers have a higher resolution than Vibroseismic shot gathers, because explosives clearly reach into higher frequencies, up to 600 Hz and the energy of Vibroseismics are limited to the sweep frequency, the common sweep frequency is 100 Hz. The disadvantages of explosives are strong surface waves respectively strong ground rolls and the creation of a ghost, a multiple reflection created at the surface-to-air boundary. Seismic waves triggered underneath the surface are reflected downwards at this boundary. Vibroseismics have a higher reproducibility and production rate, because there is no borehole needed for explosives and it is repeatable opposed to the use of explosive sources – every explosion has another character. In our survey Vibroseismic sweeps

are in the range of 10 to 100 Hz. LIMPICS has proved that Vibroseismics penetrate well through firn, while explosives are still necessary for a higher resolution (Eisen, et al., 2010). Furthermore it is also non-destructive and has advantages in logistics, costs and safety. The disadvantages are that vibrators can not be used in jungle or marshy areas and very hard surfaces tend to distort vibrator signals (Gadallah & Fisher, 2009).

### 3.2.1 **Sweep**

The input sweep of a vibroseis source has a sinusoidal character (Fig. 13a). The input sweep frequency ramp can be exactly controlled and thereby the tapering at the end of the signal ("windowed") to reduce truncation effects as Gibbs phenomena (Fig. 13b).

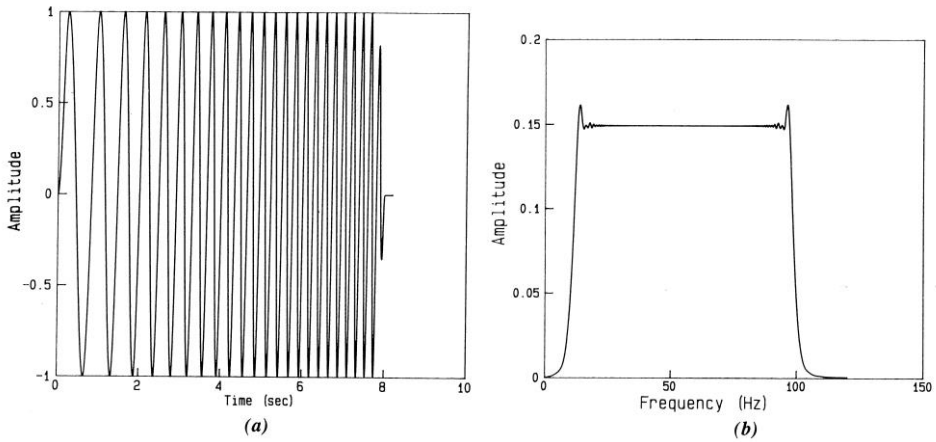


*Fig. 13; an 8 s, 10-100 Hz sweep with a taper length of 250 ms. a) the sweep in time domain but the frequency range is 1-5 Hz for display purposes. b) the amplitude spectrum of the sweep. From Baeten & Ziolkowski (1990).*

The instantaneous frequency of a linear sweep as a time function $q(t)$ is given by Baeten & Ziolkowski (1990)

$$q(t) = a(t)\sin\left[2\pi(f_0 + \frac{1}{2}\frac{f_1 - f_0}{T}t)t\right] \qquad (1)$$

with $a(t)$ for tapering, $f_0$ = first sweep frequency, $f_1$ = last sweep frequency, T = sweep duration and t = time. If $f_0 < f_1$ the sweep is called an upsweep and vice versa a downsweep.

Due to the fact that Vibroseismics do not work with a short impulse as source, an additional processing step for the recorded seismic data is necessary, the crosscorrelation (section 3.2.6). The recorded data yields several information, the sweep signal and reflection signals from all reflection points. With crosscorrelation the long sweep signal (Fig. 13a) will be contracted to a short impulse signal (Fig. 14). That enables a distinction between the input sweep and the reflectivity events. After that process, a reflection event appears as pulsed coherent input (peak amplitude). Autocorrelation (section 3.2.6) is a special case of crosscorrelation and is useful for detecting repeating periods within signals in the presence of noise. The sweep is band limited, so the autocorrelation function is not a perfect impulse. Resulting correlation noise arises, which can be reduced with tapering. A more detailed discussion on Vibroseismic correlation is presented in section 4.2.2.2.

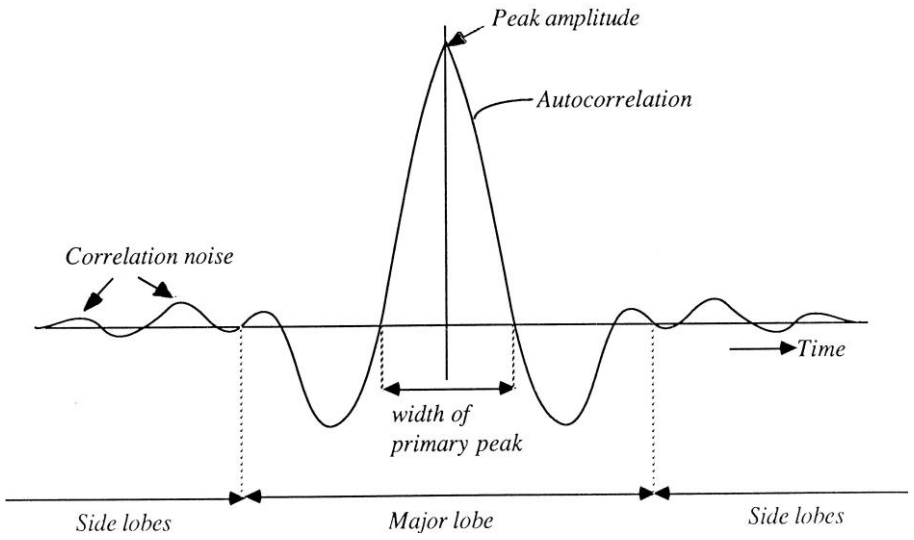


*Fig. 14; the contracted sweep after correlation, (Baeten & Ziolkowski, 1990).*

### 3.2.2 **Listening time**

An important point is the record length of the geophones and the duration of the sweep. The recording length has to be the same length as sweep duration plus the "listening time". The listening time is the final record length. For this surveys a final record length of 3 s was desired, the sweep length was 10 s, so the total raw recording time had to be 13 s.

### 3.2.3 **Fourier Transform**

A record of a trace $x(t)$ where $(t)$ is time, is in digital form nothing more than a time series, that is a discrete time function, for a specific time a specific value of amplitude is stored. With forward Fourier Transform the time-domain signal can be analyzed into its sinusoidal components in the frequency $(f)$ domamin (Yilmaz, 2001), each with a unique peak amplitude, peak frequency and phase-lag (Fig. 15). After Yilmaz (1987) the forward Fourier transform is defined by

$$X(\omega) = \int_{-\infty}^{\infty} x(t) e^{-i\omega t}\, dt \qquad (2)$$

with: $\omega = 2\pi f$. Now we are able to create filters to remove undesired frequencies. With the Inverse Fourier Transform the corresponding time function is given by Yilmaz (1987)

$$x(t) = \int_{-\infty}^{\infty} X(\omega) e^{i\omega t} d\omega \qquad (3)$$

$X(\omega)$ is a complex function, it is expressed as two other functions of frequency, (Yilmaz, 1987)

$$X(\omega) = A(\omega) e^{i\phi(\omega)} \qquad (4)$$

where $A(\omega)$ and $\phi(\omega)$ are the amplitude and phase spectra. These are computed by the following equations, (Yilmaz, 1987)

$$A(\omega) = [X_r^2(\omega) + X_i^2(\omega)]^{1/2} \qquad (5)$$

$$\phi(\omega) = \arctan[X_i(\omega)/X_r(\omega)] \qquad (6)$$

where $X_r(\omega)$ and $X_i(\omega)$ are the real and imaginary parts of the Fourier Transform, further details in Yilmaz, (1987, Appendix A). The basic theorems that are useful in various applications of the Fourier Transformation in reference to two functions $x(t)$ and $y(t)$ are given in table 2.

*Table 1 Fourier Transform theorems, (Yilmaz, 1987)*

| Operation | Time Domain | Frequency Domain |
|---|---|---|
| Addition | $x(t) + y(t)$ | $X(\omega) + Y(\omega)$ |
| Multiplication | $x(t)y(t)$ | $X(\omega) * Y(\omega)$ |
| Convolution | $x(t) * y(t)$ | $X(\omega)Y(\omega)$ |
| Autocorrelation | $x(t) * x(-t)$ | $\lvert X(\omega)^2 \rvert$ |
| Derivate | $dx(t)/dt$ | $i\omega X(\omega)$ |
| Parseval's Theorem | $\int \lvert x(t) \rvert^2 dt$ | $\int \lvert X(\omega) \rvert^2 d\omega$ |

Now we are able to produce synthesized traces for further processing. The Fourier Transform applies to almost all stages of seismic data processing (Yilmaz, 1987).

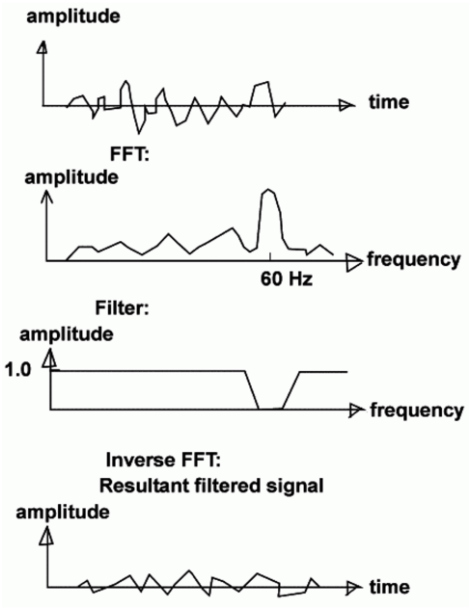


*Fig. 15; an example for a filter using Fourier Transform. The upper panel shows the signal of a trace in time domain. The second panel shows the signal after forward Fourier Transform (FFT) in frequency domain. In panel 3 a notch filter is applied, it filters out frequencies around 60 Hz. After that the signal is transformed back in time domain (the lowermost panel).Courtesy of School of Geology & Geophysics, University of Oklahoma.*

### 3.2.4 **Radon Transform**

The Radon Transform (RT) is established 1917 by Johann Radon. RT has become very popular in tomography, image processing and even in seismic data processing. RT is an integral transform, the integral of a function will be determined over all straight lines in a x, t plane (Fig. 16). Here the straight lines are defined as ray parameter $p$, see section 3.3.7 for a more detailed discussion. The Radon Transform is the base of three important multiple attenuation techniques, slant stack (linear RT), parabolic RT and hyperbolic RT (Gu & Sacchi, 2009). The forward RT is given by Yilmaz (2001)

$$u(\mathrm{v},\tau) = \int_{-\infty}^{\infty} d[h, t = \tau + \phi\,(\mathrm{v},\mathrm{h})]\, dh \qquad (7)$$

$d(h,t)$ represents the CMP gather ($h$ = *half-offset*, $t$ = *two-way traveltime*), and $u(v,\tau)$ its Radon transform ($v$ = *stacking velocity*, $\tau$ *is the intercept time*). $t - \phi\,(\mathrm{v},\mathrm{h})$ defines the traveltime curve in a CMP gather, assuming a horizontally layerd earth model with $\phi$ as slope.

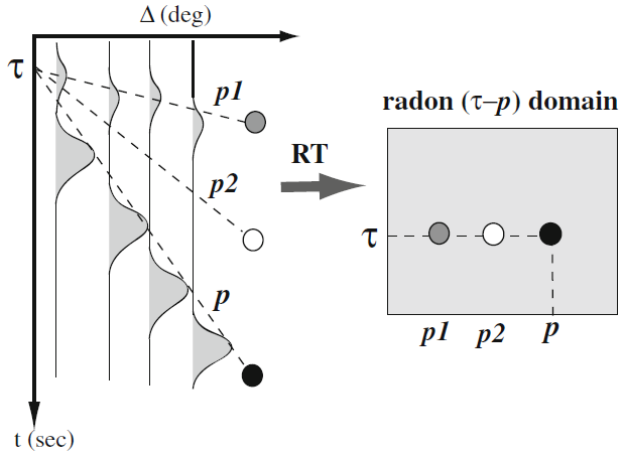


*Fig. 16; schematic diagram of a forward Radon Transform (linear RT). Stacking along the ray parameter p maps the time domain peaks into a strong energy focus in the Radon domain (dark solid circle). Conversely, stacking along p2 results in negligible Radon energy due to major mismatches with the traveltime slope of the major arrivals. From Gu & Sacchi, 2009.*

The inverse RT is given by their integral expression, Yilmaz (2001)

$$\mathrm{d}(\mathrm{h},\mathrm{t}) = \int_{-\infty}^{\infty} \rho(\tau) * u[v, \tau = t - \phi\,(\mathrm{v},\mathrm{h})]\, dv \qquad (8)$$

$\rho(\tau) = FT\ of\ \sqrt{\omega^{\frac{\pi}{4}}}$, with $\omega$ = temporal frequency, $*$ denotes convolution.

### 3.2.5 **Correlation**

Correlation quantifies, how much two or more traces are associated. The output is the correlation coefficient $(r)$ (for a 2D plot), if $r$ is zero, the traces are totally independent; if $r$ is one the traces are identical and if it is minus one they are identical except the phase is shifted by 180°. The correlation of $r(t)$ by $s(t)$ is written in the time domain after Mari et al. (1999)

$$\gamma(t) = r(t) * s(-t) \qquad (9)$$

### 3.2.6 **Auto- and crosscorrelation**

A crosscorrelation is the comparison of two independent traces. It compares two (adjacent) traces with each other and measures their resemblance as a function of time-lag applied to one of them (Yilmaz, 1987). The result is the time delay between two traces. The output depends on which trace is shifted and which trace is fixed. That means crosscorrelation is not commutative like convolution. It is also used to determine the time where the trace is similar to the source wavelet. That is important to push the signal-to-noise ratio and for Vibroseismic correlation. This involves crosscorrelation of a sweep signal with the recorded vibroseis trace (Yilmaz, 2001). Crosscorrelation of two complex functions $x(t)$ and $y(t)$ is expressed as Telford et al. (1990)

$$\phi_{xy}(\tau) = \sum_{k} x_k y_k + \tau \qquad (10)$$

$\tau$ is the time-lag between of $y(t)$ relative to $x(t)$. The term $\phi_{xy}(\tau)$ is rather a discrete data set than a continuous function, because $x$ and $y$ are data sets. This equation can be written as Telford et al. (1990)

$$\phi_{xy}(\tau) = \phi_{yx}(-\tau) \qquad (11)$$

Autocorrelation (also called “Klauder Wavelet”) means that a trace is cross-correlated to itself at different times. Autocorrelation is given by Telford et al. (1990)

$$\phi_{xx}(\tau) = \phi_{xx}(-\tau) \quad (12)$$

### 3.2.7 **Convolution**

Convolution is a mathematical operator which delivers for two complex functions e.g. two traces $x(t)$ and $s(t)$ a third function which is a modified version of one of the two original functions. It depicts an area overlapping between $x(t)$ and $s(t)$ as a function of comparison.

$$x(t) * s(t) = \int_{-\infty}^{\infty} s(t)x(-\tau) \quad (13)$$

Where $*$ denotes convolution and $\tau$ denotes delay or lag. The two traces $x(t)$ and $s(t)$ can be written as convolutional product $\gamma(t)$

$$\gamma(t) = x(t) * s(t) \quad (14)$$

In seismics a recorded trace is the product of a spatial wave and its interaction with the physical characteristics of the subsurface. A recorded trace x$(t)$ consists of:

- the sweep and its propagating effects in the Earth and the response of the recording system = $\omega(t)$,
- the Earth's impulse = $e(t)$
- the background noise = $n(t)$

$$x(t) = \omega(t) * e(t) + n(t) \quad (15)$$

The background noise is another factor which influences the seismogram. It can be induced by humans through traffic, heavy machinery or by natural activities like the

movement of the ocean, stress release in ice in the grounding zone or ice movement triggered by ocean tides. According to assumption no. 4 (see Deconvolution, 3.2.8) it will be neglected here. So the generated wavelet $\omega(t)$ is convolved with the reflectivity function $e(t)$. By the way the Fourier Transform of the seismogram respectively the trace will correspond to the multiplication of the Fourier Transform of the wavelet and of the reflectivity.

$$X(f) = \Omega(f)E(f) \quad (16)$$

### 3.2.8 **Deconvolution**

Deconvolution is the process of the reversal of the convolution, the deconvolution of $r(t)$ by $s(t)$ will be written as

$$\gamma(t) = r(t) * s^{-1}(t) \quad (17)$$

The aim is to extract the Earth's impulse response e$(t)$ from the recorded trace. If it is possible to compress the wavelet $\omega(t)$ into a zero-lag spike, $e(t)$ can be extracted. The recorded wavelet gets converted into a spike, hence the name spiking deconvolution. After that it will be correlated with the recorded trace. This is needed to resolve closely spaced reflections, so the temporal resolution will be improved. The way to do this is to design a filter $d(t)$ such that a convolution between the filter and the initial wavelet unmasks the Earth's response; in time domain

$$d * s = d * e * \omega = d * \omega * e = \delta * e = e \quad (18)$$

with $e * \omega = \omega * e$ and the Dirac delta function $\delta(t)$:

$$\delta(t) = d(t) * \omega(t) \quad (19)$$

The Dirac impulse $\delta(t)$ is a neutral event in convolution (Mari, et al., 1999). This works only if the wavelet is in minimum phase, so that energy is concentrated at the onset. If the wavelet is not minimum phase, spiking deconvolution can not convert it to a perfect zero-lag spike and hence the correlation with the recorded trace will not be correct. The length of initial wavelet is required; if it is unknown it can be computed with an autocorrelation of the seismogram. The filter of the spiking deconvolution, also called operator, $d(t)$ is the inverse of the amplitude spectrum. If the amplitude spectrum of the input wavelet is zero for a certain frequency, the inverse for zero is not defined and that results to artifacts produced by the deconvolution. To prevent this, a certain level of white noise is added to the input spectrum. This is called prewhitening. Deconvolution used to extract the Earth's impulse $\mathrm{e}(t)$ works only if five assumptions are true, from Yilmaz (2001).

1. The Earth is made up of horizontal layers of constant velocity
2. The source generates a compressional plane wave that impinges on layer boundaries at normal incidence. Under such circumstances, no shear waves are generated.
3. The source waveform does not change as it travels in the subsurface; i.e., it is stationary.
4. The noise component $n(t)$ is zero.
5. The source waveform is known.
6. Reflectivity is a random process. This implies that the seismogram has the characteristics of the seismic wavelet in that their autocorrelations and amplitude spectra are similar.

Deconvolution is also used as multiple removal technique. A more detailed discussion is presented in section. 3.3.4

## 3.3 Multiple attenuation

### 3.3.1 Multiple reflections

A multiple is a seismic signal that has been reflected from more than one reflector before being recorded (Fig. 17). Multiples are divided into two classes: short-path and long-path types. Short-path multiples arrive almost at same time with their primary signal at the receiver and change mainly the waveform, because they might interfere with it. Long-path multiples arrive with some time lag. They appear in a seismic section as separate events. Since they overlap with the primary reflection, and thus, masking its information, it is necessary to remove them. Multiple removal is an outstanding problem in seismic data processing and many techniques were developed in the last decades. This chapter gives an introduction to those techniques, which were tested and used in this thesis.

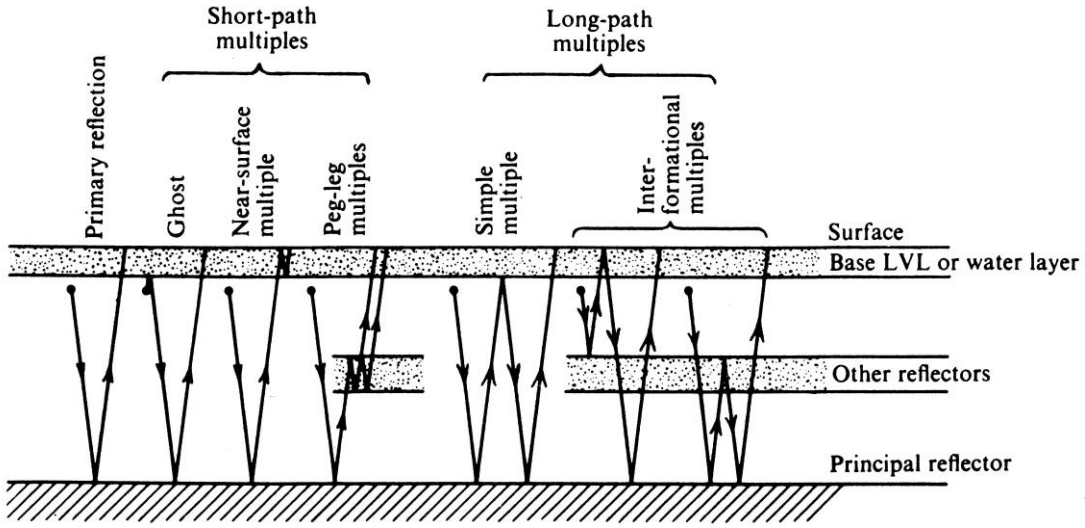


*Fig. 17; several kinds of multiples. They will be class-divided in short-path and long-path multiples. From Telford et al (1990).*

### 3.3.2 Sea floor multiple

Profile 1 and 2 on the ice shelf consist of a firn-ice column, a water column and a sea floor. In glacial overprinted shelf areas the sediments of the sea floor are compressed by the former ice load and erosional features from ice streams like lineation and furrows are visible (Stolldorf, et al., 2012). Thus, there is a strong impedance contrast interface between the sea water and the sea floor (Helm, 2003). Under this condition the water layer can trap energy for a long distance that causes multiples with strong amplitudes. They are generated at the sea bottom reflecting upwards to the sea surface (ice-sea water boundary) reflecting downwards

to the sea floor and reflecting upwards again (Fig. 18). This reflection can be repeated several times, before the signal will be recorded. Generally, this scenario belongs to the long-path multiple class, since the sea floor multiples appear as separate events in the seismogram, as in this data.

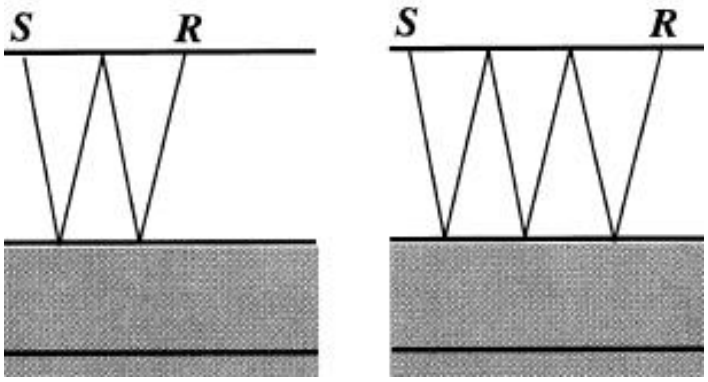


*Fig. 18; outline of a sea floor multiple reflection, of first- and second-order. S = Source, R = Receiver, from Yilmaz (2001).*

### 3.3.3 **Multiple removal strategies**

There are two approaches for removing multiples, one is to exploit their periodicity and apply a predictive deconvolution. The other approach for multiple removal is using seismic traces after normal moveout correction (NMO). The basic idea is that after applying a NMO correction, the primary reflections are flat as in Fig. 36 b, and their multiples are a hyperbola. That results in a time-moveout and it is possible to separate the multiples from the primaries. Separation will be achieved through a transform of the NMO corrected CMP gathers from the time (t) – space (x) domain into another domain like frequency (f) – wavenumber (k) (Fourier transform) or time (t) – ray parameter ($\tau$) domain (Radon transform). The flat events will be plotted into another quadrant as the multiples; a filter will be applied to omit the multiples for inverse transform. However, often the moveout differences are very small. To compensate for this disadvantage, an overcorrection can be applied either for the primary or for the multiple reflections. An overcorrection means that the velocity is set too low for a seismic event, this results in a bending downward reflector in the CMP gather and therefore in a time-moveout. Echos™ offer to apply an overcorrection function in the NMO module. After multiple removing through a chosen velocity based method, the overcorrection can be removed. In both profiles, the multiples are generated by the ice-bed boundary and by the sea floor. They are horizontal, strong in amplitude and have almost no moveout difference.

### 3.3.4 **Predictive Deconvolution**

The predictive deconvolution aims to predict the next occurrence of a multiple. Therefore, a filter operator $d(t)$ has to be designed, that identifies the predictable part, which represents the multiple of the wavelet and removes them. The filter provides an estimated value based on present values at time (t) for a future time (α). In Echos™ the modules MCDECON (Multichannel deconvolution) and DECONF (Deconvolution in Frequency domain) provide predictive deconvolution using the Wiener-Levinson-Algorithm. For both modules two important variables have to be provided. The length of the operator (n) and time lag (α). Time lag (α) is the time where the first multiple occurs and n is generously estimated, containing the source wavelet. They can be computed with autocorrelation of the seismogram. If there is at future time (α) a derivation from the estimated value, then it is a primary event, because it was not a predictable part, considering assumption no. 6, reflection events are random.

### 3.3.5 **Stacking**

The most robust and effective way to suppress multiples is stacking NMO corrected seismic gathers (Foster & Mosher, 1992). This statement is true for land-based seismic surveys, because here is the limitation of normal incidence given. After the NMO correction multiples have larger moveouts than primaries. They are undercorrected and, hence attenuated during stacking (Yilmaz, 2001). When stacking is performed on NMO corrected CMP gathers, the primaries are enhanced, because of the superposition of events at the zero offset traveltime, while the multiples are spread over a range of time to produce smaller amplitudes. The achievement depends on the moveout differences; they are smaller at near offsets and larger at far offsets. Echos™ offers several statistical based methods for stacking, each with a different weighting. On marine data, stacking results in no multiple removals.

### 3.3.6 **F – K filter**

An NMO corrected CMP gather will be transformed into F – K domain. If a velocity function between the primary and multiple velocities was chosen for NMO correction, the energy of multiple and primary events are separately displayed in two different quadrants, due to their different moveouts. One quadrant in F – K plane displays the overcorrected primaries and the other contains the undercorrected multiples. The quadrant to which the multiples are

associated will be zeroed in F – K space and the rest will be transformed back in x – t domain. That produces a multiple free, NMO corrected CMP gather (Fig. 19). In Echos™, the module ZMULT performs the F – K transformation and suppress under- or over-corrected events, depending on what the user wants to remove.

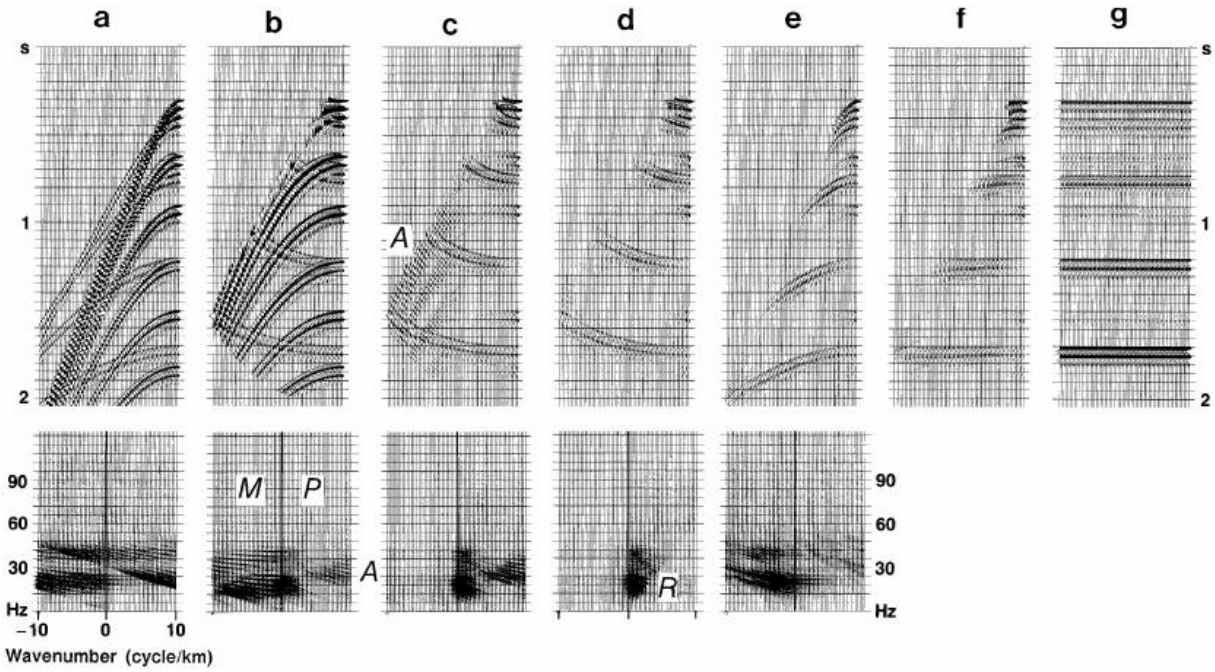


*Fig. 19; a synthetic CMP gather, from Yilmaz (2001). The bottom panels show the corresponding F – K spectra; b) after NMO correction using a velocity function between the multiple and primary trend; c) the result of zeroing the F – K quadrant associated with multiples; d) the same as c, except that in addition to zeroing the left quadrant, a portion of the right quadrant in the F – K spectra (denoted by R) also is zeroed to suppress aliased energy; e) the result of applying inverse NMO correction to a; f) the result of applying NMO correction to e, using the primary velocity function; g) stack of c, repeated to emphasize the strong events.*

At near offsets there is no significant moveout difference between primaries and multiples. Another disadvantage is that spatial aliasing occurs by Fourier Transformation, because aliased energy is wrapped around and mapped to the wrong quadrant (Yilmaz, 2001). The portion of this quadrant has to be zeroed out. Spatial aliasing effects rise through Fourier transform of seismic events with a frequency (f) higher than the Nyquist frequency($f_{max}$). $f_{max}$ is the maximum threshold frequency, which is not aliased for a given dip ($\sin\theta$), medium velocity ($f_{max}$) and CMP trace interval ($\Delta x$) (Yilmaz, 2001)

$$f_{max} = \frac{v}{4\Delta x\,(\sin\theta)} \qquad (20)$$

With $\Delta x = 25\ m$, Yilmaz (2001) provides a table about frequency thresholds for spatial aliasing for a velocity of $3000\ m/s$, for several dips and CMP trace intervals. The velocity range in this case study reaches from $1450\ m/s$ to $3000\ m/s$.

*Table 2; frequency threshold for spatial aliasing (Hz) for CMP trace interval is 25 m. Modified from Yilmaz (2001).*

| *Dip Angle (deg)* | $1450\ m/s$ | $3000\ m/s$ |
|---|---|---|
| 10° | 83.5 | 173 |
| 20° | 42.4 | 88 |
| 30° | 29 | 60 |
| 40° | 22.6 | 47 |

In our data the input sweep has a frequency of 100 Hz and there are layers with low seismic medium velocities with gentle dips. That can cause spatial aliasing.

### 3.3.7 Linear Radon Transform (Slant-Stack) or $\tau - p$ Transform

For filtering purposes in frequency-wavenumber space (F – K filter), the wavefield is decomposed with 2-D Fourier Transformation into its plane-wave components. Similar to this process, there are other transformation methods that decompose a wavefield into its plane-wave components. The $\tau - p$ Transform produces a slant stack by transforming data in time-offset domain via Radon Transform in $\tau - p$ domain ($\tau$ = intercept time, $p$ = slowness). Slant-stacking involves that a linear moveout will be applied to the wavefield via coordinate transformation (Fig. 16). Therefore, this decomposing process is also called linear Radon Transform. The amplitudes will be summed over the offset axis. Furthermore the offset axis will be replaced with the ray parameter $p$ axis. $p$ is the inverse of the horizontal phase velocity and is defined by Yilmaz (2001)

$$p = \sin\theta / v \qquad (21)$$

with $\sin\theta$ = incidence angle and $v$ = seismic velocity. A linear moveout correction will be applied to the data in $x - t$ domain via coordinate transformation (Yilmaz, 2001)

$$\tau = t - px \qquad (22)$$

$t$ = two-way traveltime, $x$ = offset and $\tau$ is the intercept time at $p = 0$. Finally the summing of the amplitudes along a linear path in time-offset domain is given through Yilmaz (2001)

$$S(p,\tau) = \sum_{x} P\,(x, \tau + px) \qquad (23)$$

$S(p,\tau)$ represents a plane wave. $P(\tau + px)$ is the input data. $p = 0$ equates to a plane wave that travels vertically (Fig. 20). Fig. 20 shows also that hyperbolas and linear events in offset – time domain map as an ellipse respectively as a point in intercept – slowness domain.

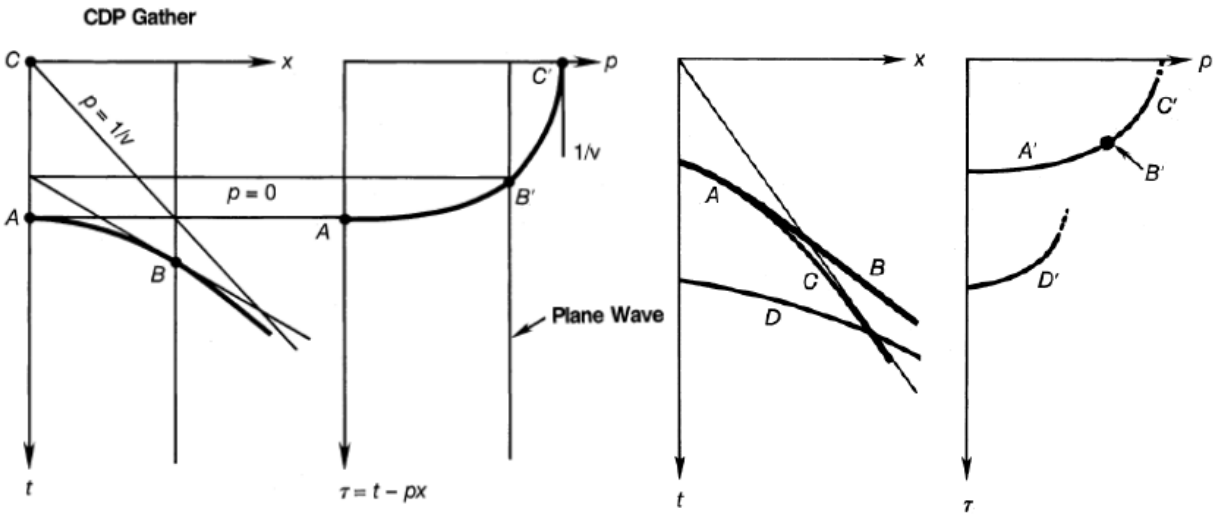


*Fig. 20; outline of a linear Radon Transform (Slant Stack). p is the ray parameter, capital letters are seismic events in offset – time (x,t) domain and mapped onto A', B', C', D' in $\tau - p$ domain. Amplitudes are summed along a slant, linear path. A hyperbola in a CDP gather maps onto an ellipse in the $\tau - p$ domain and a linear event as a point. (Yilmaz, 2001).*

Multiple attenuation with Slant Stack Transform is based on the prediction of multiples. Attenuation of multiples is achieved with predictive deconvolution in $\tau - p$ domain. The application of predictive deconvolution is valid strictly for vertical incidence and the zero-offset case; multiples are not periodic at nonzero-offsets (Yilmaz, 2001). Taner

(1980) recognizes that the arrivals of a primary and its multiples on a radial direction, the dashed line in Fig. 21, has equal time separations. A predictive deconvolution needs an operator length n and a prediction lag α , both variables are determined from the autocorrelation of the slant gather, after Yilmaz (2001)

$$\alpha(p) = \alpha(0)\sqrt{1 - p^2 v_\omega^2} \qquad (24)$$

with prediction lag $\alpha(0)$ at $p = 0$ and $v_\omega$ is the veloctiy of the primary reflection.

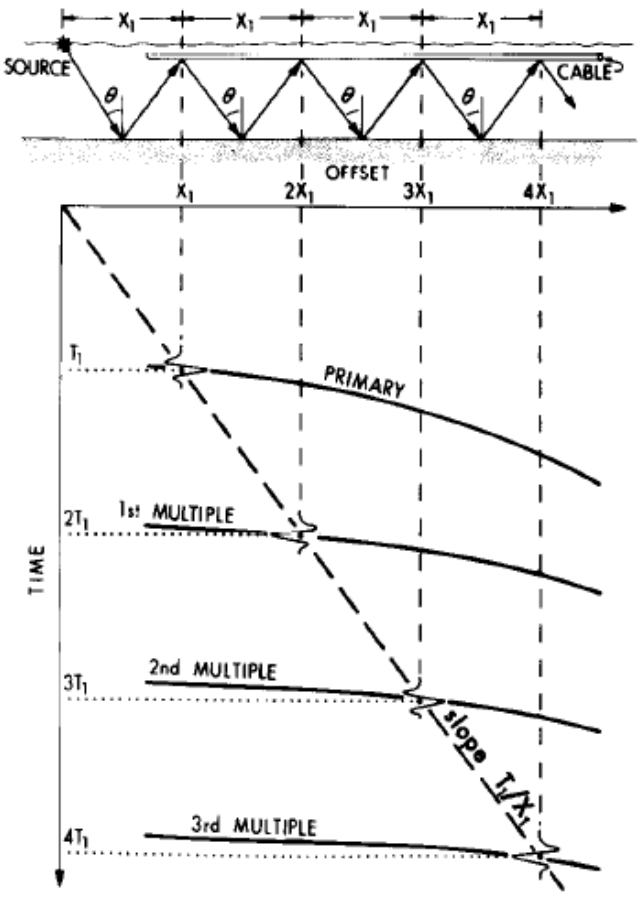


*Fig. 21; Offset-Time relationship of a portion of the wave front for horizontal sea-floor, from Taner (1980).*

### 3.3.8 **Hyperbolic Radon Transform (Velocity Stack)**

The velocity stack transform is similar to the slant stack transform, discussed in the previous section. A Radon Transform (RT) will be applied to input data in time – offset domain with a hyperbolic moveout correction and amplitudes will be summed up along offset-axis. As a result of this mapping, the offset-axis is replaced with the velocity axis (Yilmaz, 2001). The input data $(h, t)$ with $h$ = half-offset, $t$ = two-way traveltime will be transformed via Radon Transform with following transformation coordinates: $(v, \tau)$ where $v$ = stacking velocity and $\tau$ equals two-way zero-offset time. The relationship is given by Yilmaz (2001)

$$t^2 = \tau^2 + \frac{4h^2}{v^2} \qquad (25)$$

Mapping and summing over offset is achieved by Yilmaz (2001)

$$u(v, \tau) = \sum_h d(h, t = \sqrt{\tau^2 + 4h^2/v^2}) \qquad (26)$$

where $d(h, t)$ represents the CMP gather and $u(v, \tau)$ represents the velocity stack gather. An inverse transformation is possible through applying an inverse hyperbola moveout correction and summing over velocity given by Yilmaz (2001)

$$d'(h, t) = \sum_v u(v, \tau = \sqrt{t^2 + 4h^2/v^2}) \qquad (27)$$

Hyperbolas in time-offset domain will be mapped as points in the velocity stack gather and not as ellipse as in a slant stack gather. Now primary and multiple events can be distinguished by their different velocities (Fig. 22).

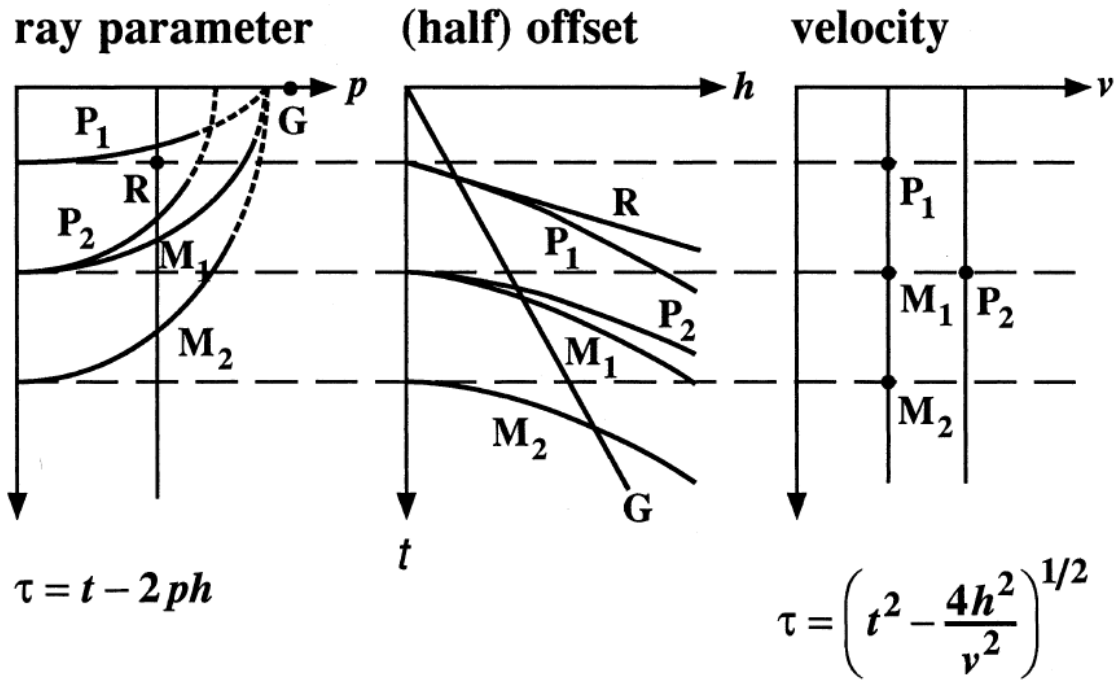


*Fig. 22; left) Slant stack and velocity stack (right), mapping of a CMP gather (center). P = primary and M = multiple reflections. G equals linear noise, R is a refracted arrival and t = two-way traveltime. From (Yilmaz, 2001).*

Fig. 22 shows an ideal case that does not hold in reality. A conventional CMP gather of constant velocity stacked traces emphasizes the energy of events that follow hyperbolic traveltime trajectories in the CMP gather (Yilmaz, 2001). A hyperbola of a reflection is imaged incomplete after transformation in the velocity stack, due to discrete sensing along offset-axis and because of the finite streamer length. These and the density of hyperbolic summation paths at near offsets cause smearing of the stacked amplitudes along the velocity axis. That reduces the velocity resolution of two seismic events with little moveout difference. To prevent amplitude smearing a time stretching function can be used. In other words the coordinates in time direction will be stretched by setting $t' = t^2$ and $\tau' = \tau^2$. As result hyperbolic events become more parabolic events in the velocity stack with the distinction that the moveout of parabolic events are time-independent (Yilmaz, 2001). Another solution is a hyperbolic NMO correction before summation, called Parabolic Radon Transform.

### 3.3.9 **Parabolic Radon Transform**

After NMO correction using a hyperbola moveout correction, events with a moveout (multiples) become parabola shaped. The correction is given by Yilmaz (2001)

$$t_n = \sqrt{t^2 - 4h^2/v_n^2} \qquad (28)$$

where $t_n$ is the time after NMO correction, $v_n$ is the hyperbolic moveout correction velocity function. Originally hyperbolic events are now approximately parabolic, (Yilmaz, 2001)

$$t_n = \tau + qh^2 \qquad (29)$$

with $\tau$ = two-way zero-offset time, $q$ defines the curvature of the parabola, $h$ equals half-offset. Transformation is given by Yilmaz (2001)

$$u(q,\tau) = \sum_h d(h, t_n = \tau + qh^2) \qquad (30)$$

$u(q,\tau)$ is the resulting velocity gather, $d(h,t_n)$ represents the input CMP gather after hyperbolic moveout correction. The inverse transformation is given by Yilmaz (2001)

$$d'^{(h,t_n)} = \sum_q u(q, \tau = t_n - qh^2) \qquad (31)$$

The summation runs along parabolas, their shapes depending on the velocity. So it is possible to limit the used parabolas for transformation of a certain velocity interval. Before inverse transformation, the primaries and an arbitrary area around them will be filtered out by defining the range of their curvature. Only the multiples will be transformed back in offset – time plane, and will be subtracted from the original seismic gather (Echos™ Manual).

### 3.3.10 **Karhunen-Loeve Transform**

The concept of the K – L transform is that the offset-time data (gather) are decomposed in components, the eigenimages. The first eigenimage contains the highest degree of correlation with seismic events. The following ones have decreasingly correlated events. The K – L transform is reached by forming a covariance matrix from the dot products of all the pairs of traces in the gather. Then it computes "eigenvalues" and "eigenvectors" for this matrix (Echos™ Manual), which are the components of eigenimages. Flat events as primaries or multiples have the highest correlation from trace to trace in the gathers, hence these events will map into the first eigenimage (Yilmaz, 2001). If a NMO correction applies to the multiples, they will be flat and primaries are overcorrected, if the moveout difference is not too small. KLTRANS – which compute K – L transform in Echos – offers to filter out the flat events. After removal of the NMO correction a seismic gather only with primaries is produced. It is also possible to go the other way around, which is to filter out events with moveout, if a NMO correction was applied to the primaries. The difference of the normal moveouts for primary and multiple events are critical. If the velocity curves are very close to each other, as at near offsets, primary energy may also be filtered out as multiple energy.

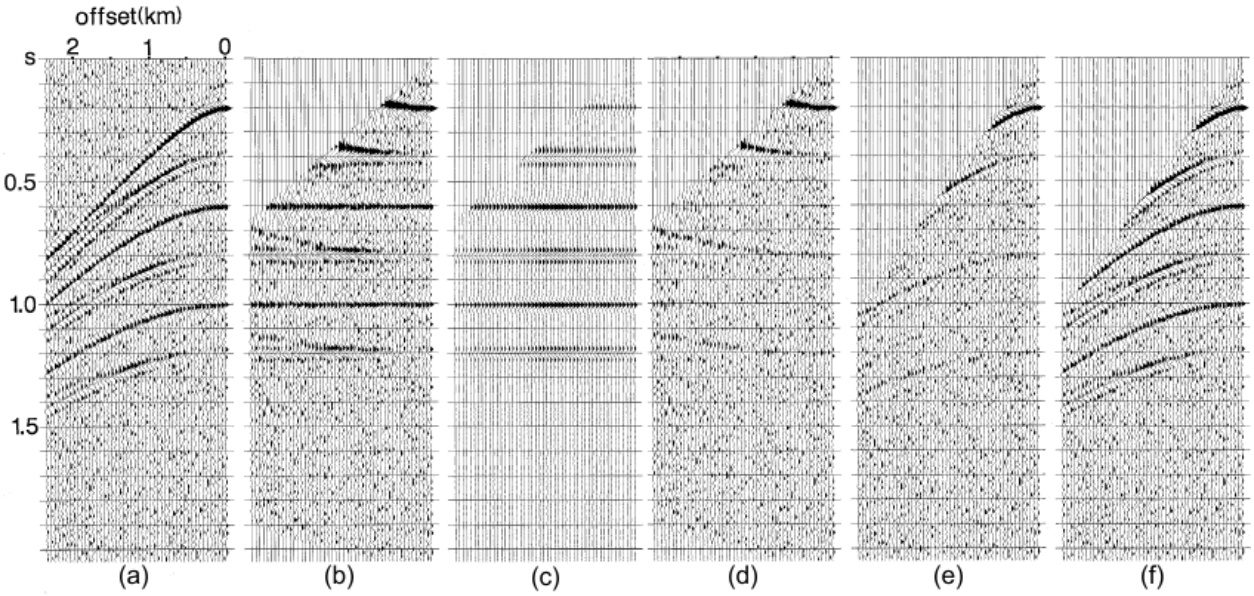


*Fig. 23; a) CMP gather with a primary at 0.2 s zero-offset time and its multiples, and three additional primaries at 0.4 s, 0.8 s and 1.2 s zero-offset times. The gather also contains band-limited noise; b) the same gather after NMO correction for the multiples (3000 m/s) and muting; c) the eigenimage associated with the first eigenvalue derived from (b), this eigenimage contains the primary at 0.2 s zero-offset time and its multiples; d) the difference gather derived from subtracting the first eigenimage gather (c) from the NMO corrected gather (b); e) same gather as in (d) after inverse NMO correction; f) original modeled gather as in (a) with the stretch mute as in (b). The gathers (f) and (e) are before and after multiple attenuation using the K – L Transformation. From Yilmaz (2001).*

# 4 Applied seismic data processing

## 4.1 Vibroseismic data acquisition

Two Vibroseismic surveys were carried out in 2011 (Fig. 24). Profile 1 reaches from Halvfar Ridge to the Ekstroem Ice Shelf. Profile 2 is continued from the turning point of profile 1 and goes northward to Neumayer III Station. Although, profile 2 is not a straight line, it was treated as such.

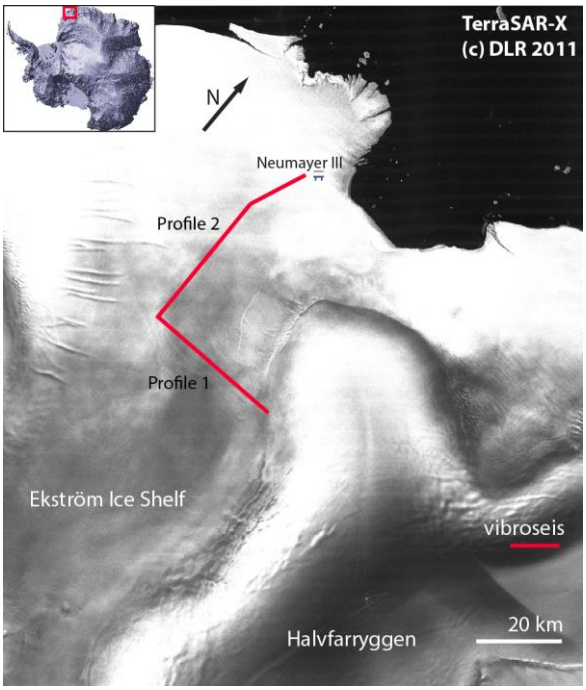


*Fig. 24; the setting of Vibroseismic surveys. Profile 1 strike in E-W and Profile 2 in S-N direction. A TerraSAR-X image, provided by Hofstede et al. (2013), modified.*

The data were taken by a vibroseis source mounted to a truck on skis that was pulled by a PistenBully (Fig. 25). The vibrator was a Failing Y-1100 with a weight of 16 tons and 12 tons peak actuator force (Eisen, et al., 2010). The size of the base plate area was 2.5 $m^2$ with a reaction mass of 1769 kg and a stroke of 10 cm (Hofstede, et al., 2013) .


*Fig. 25; the PistenBully pulled the vibroseis source, which was mounted on skis, after that the snowstreamer. From Kristoffersen et al. (submitted).*

A snowstreamer in a straight line was pulled behind the vibrator truck. The snowstreamer had a length of 1500 m with 60 channels and a channel spacing of 25 m (Fig. 26); (Hofstede, et al., 2013). Eight single gimballed geophones were dedicated to one channel.

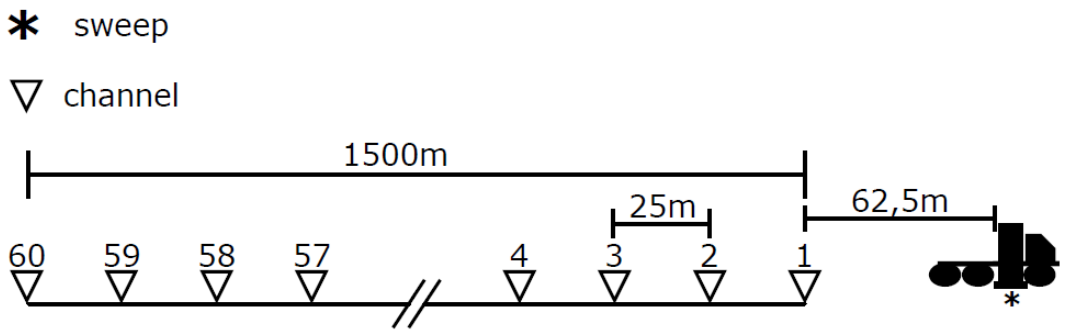


*Fig. 26; setup of the Vibroseismics Survey 2011. The streamer has a length of 1500 m and the channel spacing of 25 m.*

***Table 3; Key facts of the Vibroseismics Survey 2011.***

| *Vibroseismic Survey 2011* | *Profile 1*<br>*Grounding Line*<br>*Halvfar Ridge to Ekstroem Ice Shelf* | *Profile 2*<br>*Explora Wedge*<br>*Southward to Neumayer III* |
|---|---|---|
| *Start point [WGS84]* | S 71.03328°<br>W 7.64872° | S 71.02148°<br>W 8.48255° |
| *End point [WGS84]* | S 71.02148°<br>W 8.48255° | S 70.53442°<br>W 8.18176° |
| *Total length [km]* | 30 | 41 |
| *Source* | sweep, 10 s,<br>10-100 Hz | sweep, 10 s<br>10-100 Hz |
| *Sample rate [ms]* | 1 | 1 |
| *Taper [ms]* | 500 | 500 |
| *Record length [ms]* | 13.000 | 13.000 |
| *Geophones* | gimballed SM4,<br>14 Hz | gimballed SM4,<br>14 Hz |
| *Geophones per channel* | 8 | 8 |
| *Number of channels* | 60 | 60 |
| *Channel spacing [m]* | 25 | 25 |
| *Spread [m]* | 1500 | 1500 |
| *Distance from source to first geophone [m]* | 62.5 | 62.5 |
| *Fold coverage* | varying: 30, 15, 7.5 | 7.5 |
| *Shot spacing [m]* | varying: 25, 50, 100 | 100 |

## 4.2 Seismic data processing

This Chapter gives an introduction to the concept of seismic data processing in relation to this thesis. Many steps are necessary to produce a seismic profile out of a collection of shot gathers. In Fig. 27, the processing flow chart for this thesis is outlined. Such a flow chart is not definite, it can be changed in regard of special properties of the data, the survey area or the research objectives. All processing steps which were applied for this thesis shall be discussed here. The structure of this chapter is orientated on the main steps of the flow chart. The software that was used was Focus/Echos™ from Paradigm, Houston, Texas, USA. It is modular, like the flow chart in Fig. 27.

At the beginning it is necessary to define a geometric model for the record device delivery to assign the common reflection midpoints (CMP) to shoot locations. After the raw data was “Read in” from the record discs by the program, it has undergone first preparations. In “Edit”, bad shots and noisy traces were deleted; statically corrections were applied. Also mutes to exclude parts that only contain noise or more noise than signal will be applied here. In “Gain” is described how the signal was amplified by a spherical divergence correction. In the next module “Filter” unwanted frequencies were filtered out by several applications of filters. In “CMP sorting” the seismograms were assigned to their common mid points (Fig. 33). After the sorting it is possible to develop and establish a velocity model for the surveyed subsurface. This provides velocities of seismic waves for a certain depth and offset. This enables normal moveout correction (NMO correction) and thus multiple attenuation. The removal of multiples is an outstanding problem in seismic data processing. The theory of multiples and of their removing will be discussed here. Stacking is a compression of the data by summing them along the offset direction, here we got a good first seismic profile impression. After that we have a seismic profile which allows us geological interpretation and analysis of many parameters.

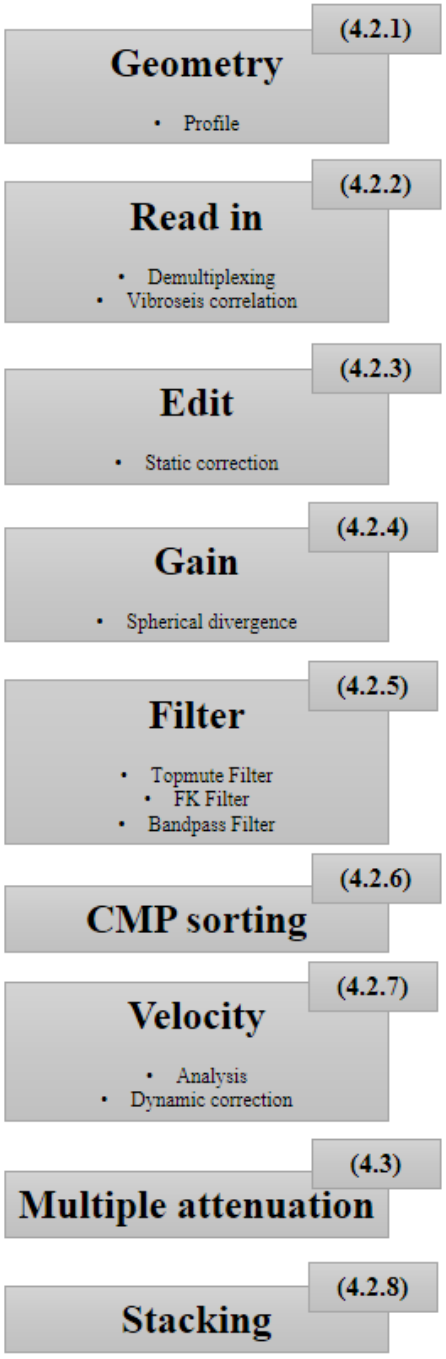


*Fig. 27; processing flow chart for seismic data processing.*

### 4.2.1 Acquisition geometry

In Chapter 4.1, Fig. 26 depicts a scheme about the shoot geometry. This information has to be stored in the processing software by defining a geometry model. The data will be linked to this model. It consists of three models:

- the station model: that describes a line along the whole profile, which contains the locations of the stations (shot and receiver positions)
- the CMP model: that contains the distance between CMP's and their number between the stations
- the shot model: it contains the record device delivery with the given parameters as first offset to geophone.

### 4.2.2 Read in

#### 4.2.2.1 Demultiplexing

Seismic data are recorded in sample order. That means the data is written on disc in the order they are sampled, this is called multiplexed. Consider a six-channel system that recorded six samples for each channel. Channels are named in capital letters from A to F, and samples are numbered from 1 to 6 (Fig. 28). "*Processing requires the application of mathematical operations to all samples of a channel*" (Gadallah & Fisher, 2009). The data has to be reorganized in a way that the samples for the same channel are stored together, separated by sample time. The Society of Exploration Geophysicists (SEG) adopted standard formats for digital recording. For this survey the SEG 2 file format was used. It gives automatically a demultiplexed output.

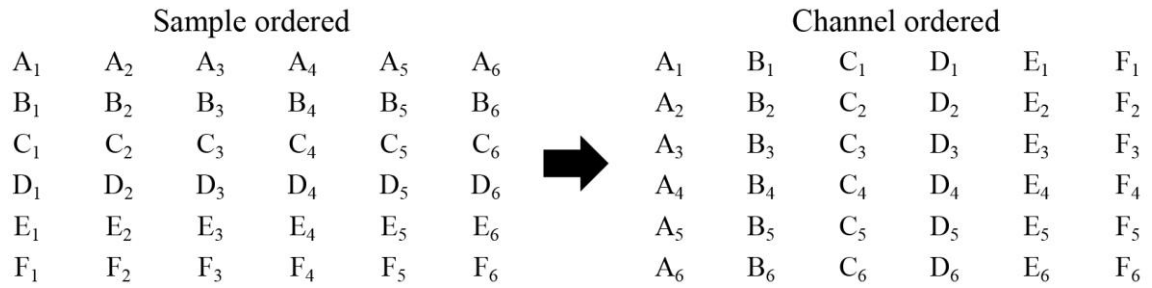


*Fig. 28; Demultiplexing of seismic data. Capital letters represent channels, numbers are samples. Modified after Gadallah & Fisher (2009)*

#### 4.2.2.2 Vibroseismic correlation

Let us assume the simple case of a horizontal layered Earth with three layers is given. The recorded trace of a Vibroseismic survey is a convolution between the Earth's vertical incidence reflectivity series (also called impulse response) and the sweep signal, or equivalently the summation of the three reflection series – responses to the downward traveling input sweep (Fig. 29). From the recorded trace we have to extract the reflection series via crosscorrelating the received signal with the sweep. For this purpose we need the input sweep, which is often recorded by a sensor mounted at the Vibrator-plate or as in this thesis, the raw data is cross-correlated with a synthetic sweep (Kristoffersen, et al., submitted). The recorded trace does not indicate arrival times of reflections ("events"), therefore it will be crosscorrelated with the sweep signal. If an event is detected, a zero-phase source signature is produced at the point that corresponds to the arrival time of that event, (Fig. 29, correlated trace).

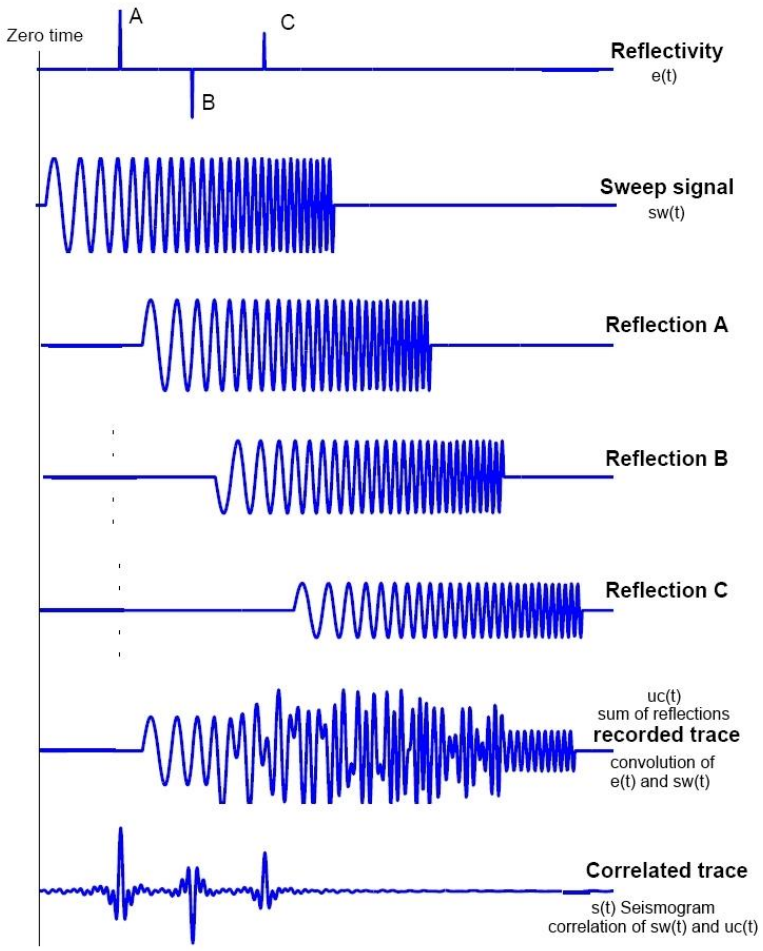


*Fig. 29; a Vibroseismic correlation outline. Signals from three geologic boundary layers are recorded (A,B,C), they contain the input sweep at a given time delay. Note the phase change of reflection B in both correlated trace and sweep. Courtesy of Petroleumgeophysics.com, modified.*

### 4.2.3 Edit

During recording some noise could occur, e. g. natural activities like strong wind and influence some traces or the whole seismogram. Traces could also be distorted by defect geophones. This should be noticed by the operator in the survey log or at least it is visible during the processing. It is recommended to take two records at one shotpoint for backup. Which is the way it was handled in this survey. Several distorted traces were selected and deleted by the processor, also whole seismograms. The best seismogram for a shotpoint was selected for further processing. A few shotpoints were bad and not used. But traces have not to be deleted if just a part of them is distorted. A mute can be applied to this part, so that the distorted part is excluded from further processing. In the following there are several muting applications.

#### 4.2.3.1 Static corrections

Elevations have to be considered for a common datum level of travel times. Differences in elevations of the source and the receivers or between the shotpoints have to be corrected with time shifts. This was not necessary in our data, but timing errors of a geophone occurred and had to be corrected with time shifts. This was also done manually. If reflections of a shot shift down or up in comparison to adjacent raw shots, a time delay was applied to the shot to correct the position of the reflection events in relation to the previous and the following raw shot. The ice-bottom and sea floor reflector was used to align the shots, because they were easy to identify.

### 4.2.4 Gain

Gain is a time-variant scaling of the traces. The aim is to improve weak signals for display like automatic gain control or to compensate amplitude attenuation for further processing. A loss of amplitude can be caused by spherical divergence spreading. An exponential gain correction for spherical divergence spreading was applied.

### 4.2.5 **Filter**

#### 4.2.5.1 Top mute

A top mute or front-end mute was applied to all raw shots to exclude the upper part of a raw shot that contains only noise, refractions and surface waves. Refractions can occur due to the far distance between the sweep and – especially rear – geophones. They can interfere with reflections of shallow reflectors. The mute zeros part of the traces, down to the time where first reflections of primaries appear. The position of the mute was set interactively and applied to all shots. It was set closely to the first primary reflection, but to prevent the mute from cutting off the primary reflection in other shots not too closely.

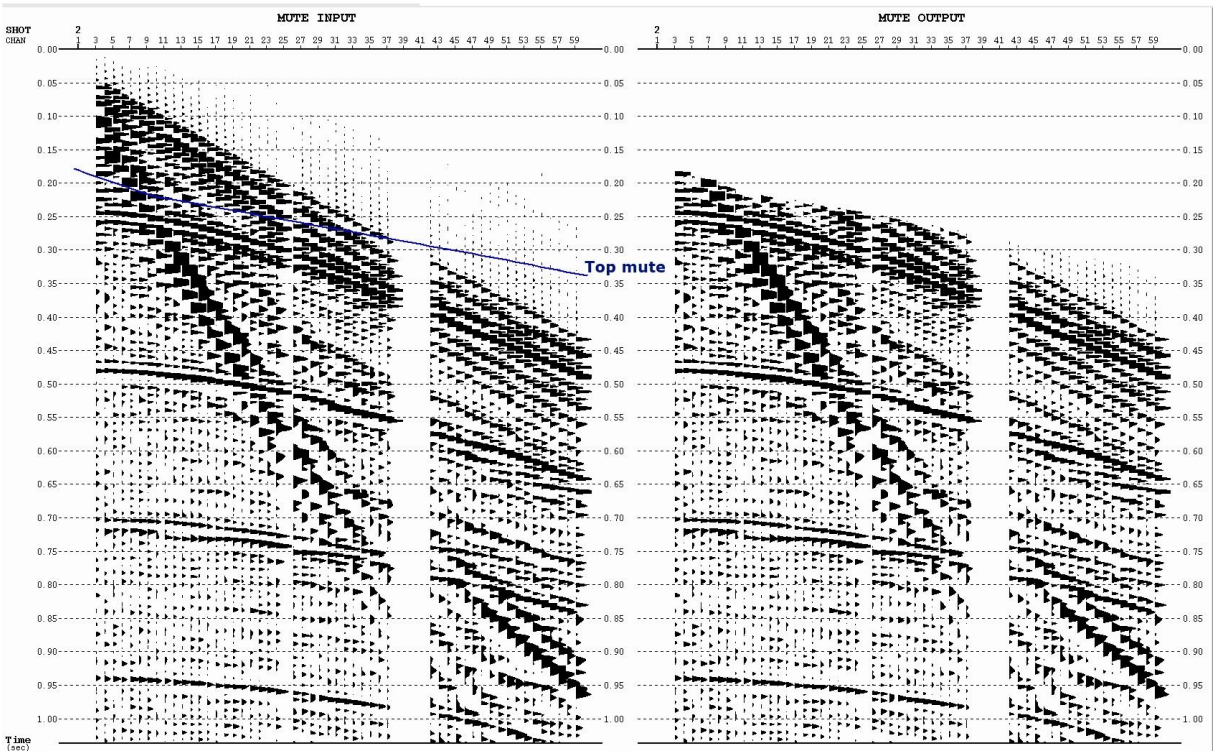


*Fig. 30; a raw shot of profile 1, a primary reflection is located at 0.25 s with following multiples between 0.45 s and 0.5 s and so on. The top mute (blue line) was set carefully in respect to the varying positions of the primary.*

#### 4.2.5.2 F – K filter

Via Fourier Transform the signals of the raw shots were transformed in the Frequency-Wavenumber (F – K) space (Fig. 31). The wavenumber (K) is the inverse of the wavelength (λ), $K = 2\pi/\lambda$ and measured in cycles per unit distance. An F – K filter is very common in seismic data processing and is used to eliminate certain types of unwanted energy like ground roll, diving and guided waves. These are coherent linear signals and can be distinguished by their phase velocity ($f\lambda$) which cause different dips in the F – K domain. Ground roll has a dispersive nature and appears in single events at the rim of the F – K domain. The signals of reflections are typically rather in the middle of this display with occurrence continuously, so the parts around then were cropped. Here we used a dip filter to exclude the unwanted ground roll and diving waves. With F – K filtering it was possible to filter out unwanted signals between reflections.

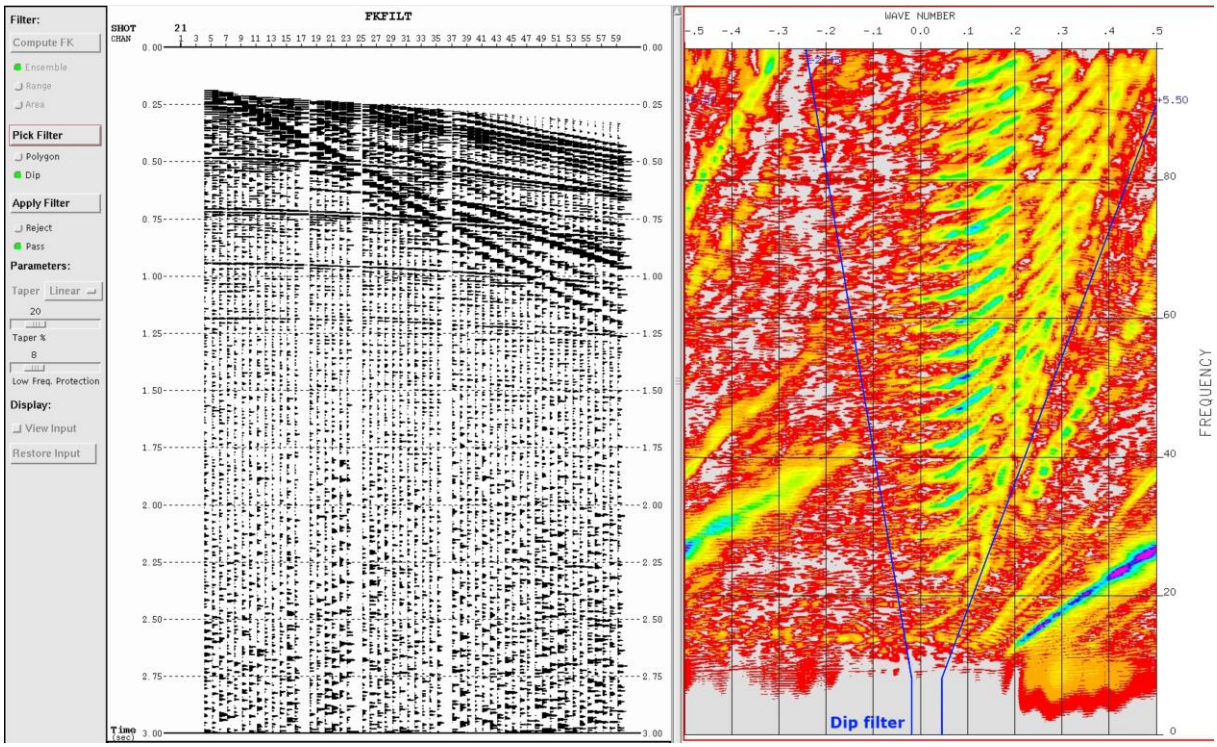


*Fig. 31; a raw shot of profile 1 (left) after transform into F – K space (right). Instead of a polygon a dip filter was established. Signals outside the dip filter-area were removed.*

The result is shown in Fig. 32, the signals of the raw shot were transformed back after applying a dip filter and only the energy of the reflection events was transformed back, too. As side effect some noise at the top was created, a top mute after F – K filtering was applied again.

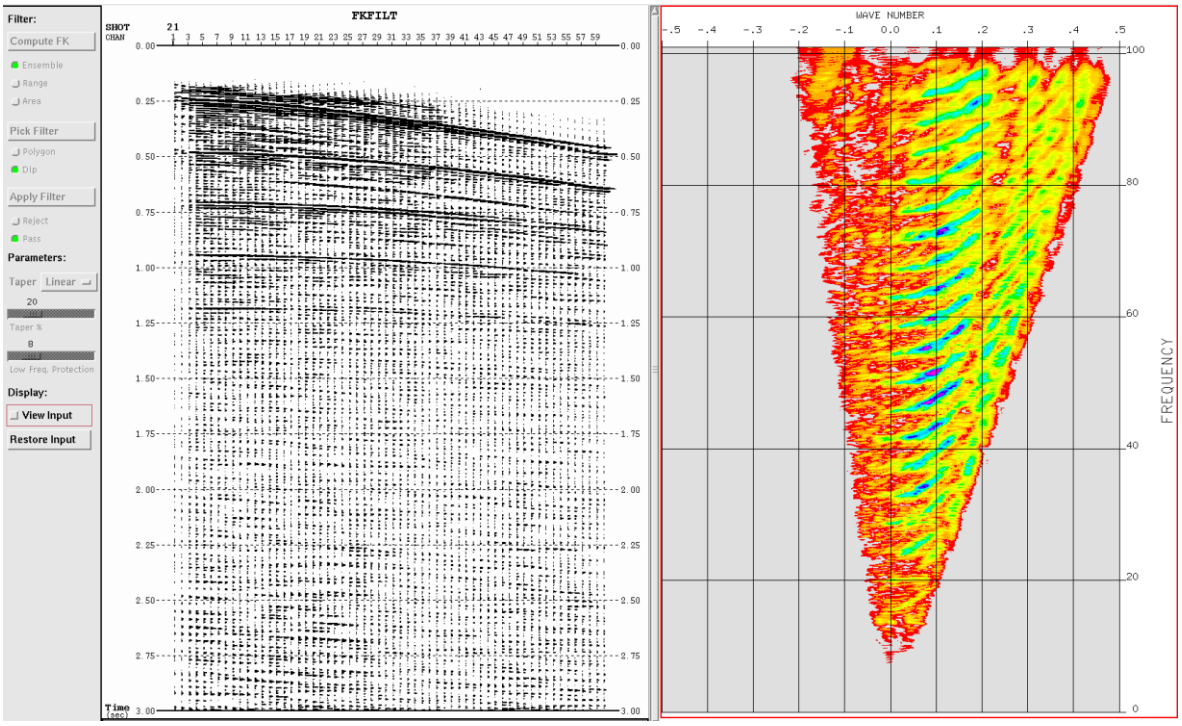


*Fig. 32; the raw shot from Fig. 31 after applying the dip filter. The diving wave and the ground roll are filtered out and the energy of reflections is left.*

#### 4.2.5.3 Bandpass filter

To eliminate frequencies outside the bandwidth of the input sweep (10 to 100 Hz) or artefacts that may have occurred after F – K filtering, a bandpass filter was applied (Butterworth, 10 to 100 Hz). Bandpass filters are the most used frequency filters in seismic data processing.

### 4.2.6 **CMP sorting**

After the record of a shot, the vibroseis source and the streamer were moved further down the profile line. The shot spacing is small enough that the reflection points are re-recorded with different offsets. That is called multifold coverage. Profile 2 has coverage of 7.5. Profile 1 was most time covered 7.5 times, near the grounding zone with 15 times and in the zone 30 times. A common midpoint (CMP) is a reflection point halfway between the source and receiver that is shared by numerous source – receiver pairs (Fig. 33).

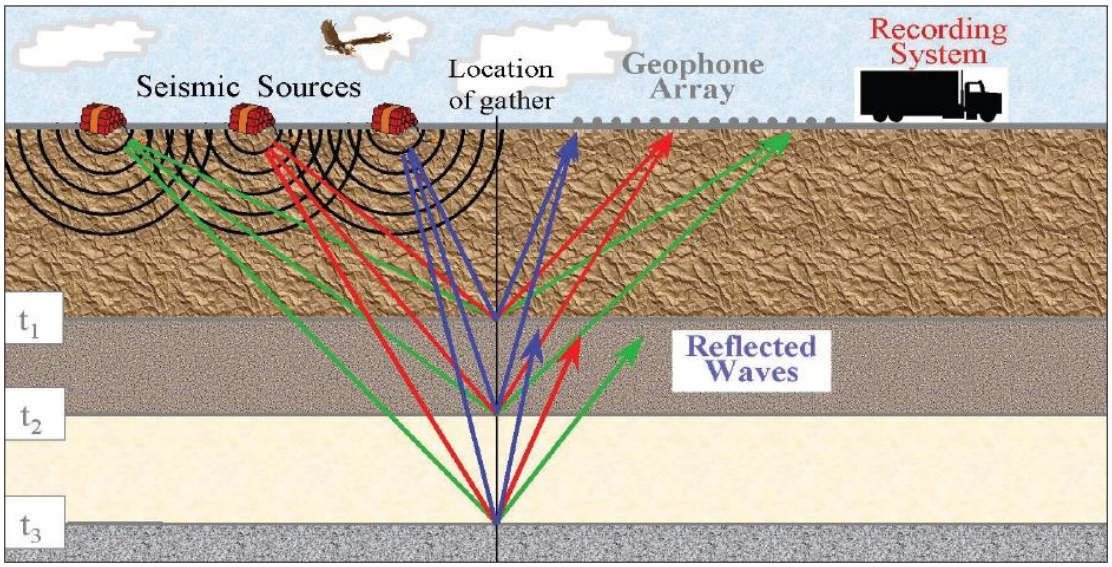


*Fig. 33; outline of a 2D-reflection seismic survey. The gather marks a reflection point for all ray paths, called common midpoint (CMP) and is here equal to the common depthpoint (CDP) due to the flat reflector. Courtesy of eSeis Inc.*

After CMP sorting these points are grouped together with respect to their midpoints. The geometry model enables this rearrangement of all traces, because a trace is associated to a certain midpoint. As a result the whole profile is subdivided in CMP gathers and a compression of the seismic dataset along the offset axis is achieved. Fig. 34(a) depicts the principle of CMP recording by means of stacking chart. The sweeps are displayed on the S-line and the receiver is displayed on the g-axis between FG. In case of a flat reflector with every shot the half length of the streamer registered the subsurface $(x/2)$ (Fig. 34(b,1)). Fig. 34(b) outlines different types of CMP acquisition and sorting.

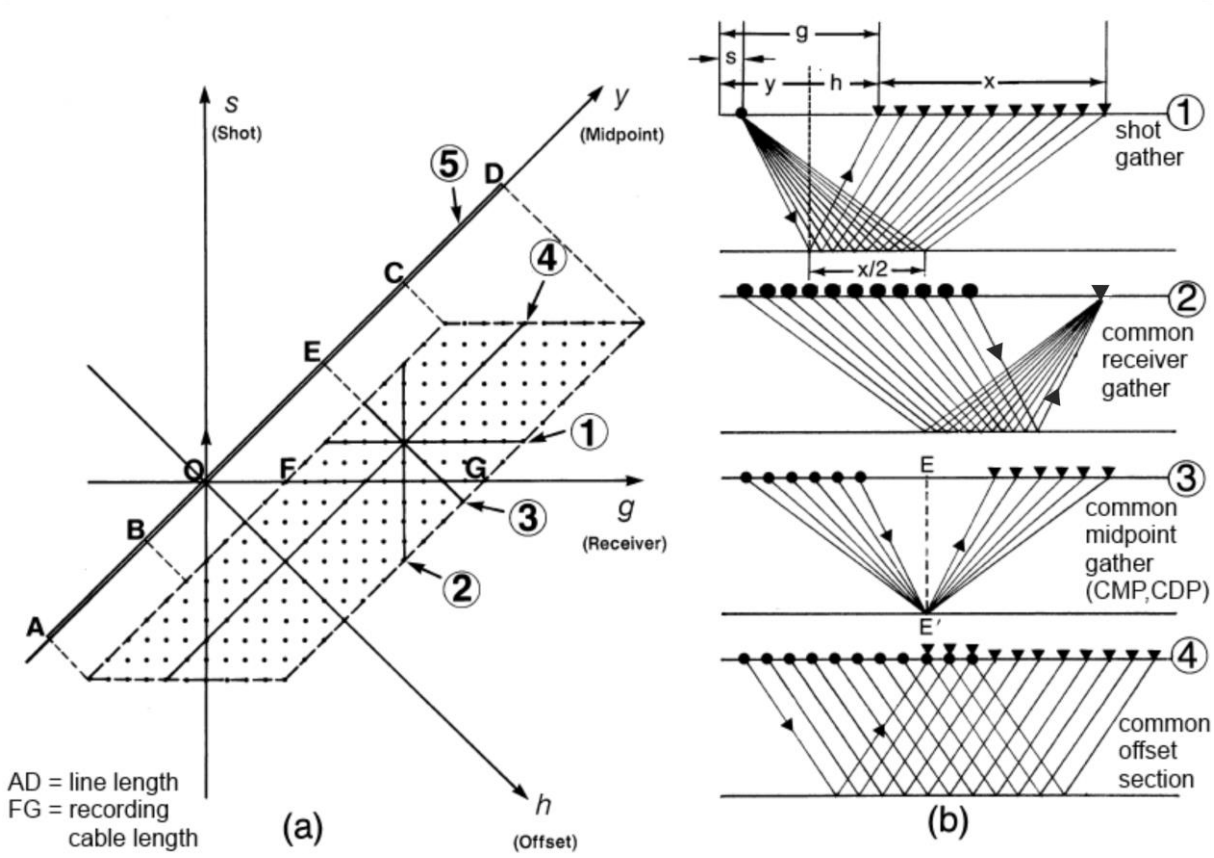


*Fig. 34(a); each dot represents a single trace with the time axis perpendicular to the plane of the page. Shot to geophone (s,g), and midpoint to offset (y,h) coordinates are superimposed with the (y,h) plane rotated 45 degrees with respect to the (s,g) plane. (b) solid triangles denote receiver locations and solid circles denote shot locations. x is the effective cable length, E denotes midpoint and E' denotes a depth point on a flat reflector. From Yilmaz (2001), modified.*

### 4.2.7 Seismic velocity

Seismic wave travels through the Earth and passes layers of different material. As outcome of this the wave travels with varying velocities. This fact enables seismic profiling. For a good interpretation it is necessary to know the velocities at each point on the path of the seismic wave. But for this purpose we have to know the exact lithology for the whole profile. Density data of firn and ice along the profile line will also be needed and the temperature and salinity of the sea water should be measured to calculate its density. Since collecting all this data would be too elaborate, we have to make good assumptions about the seismic velocity in a medium of a particular layer, which is named as interval velocity. Only then we are able to say if a layer lies in this depth and estimate its properties.

#### 4.2.7.1 Travel time and normal moveout correction (NMO)

Let us assume that we have only one flat reflector and a layer between it and the surface, with a thickness of $h_1$ and a velocity of $v_1$ (Fig. 35).

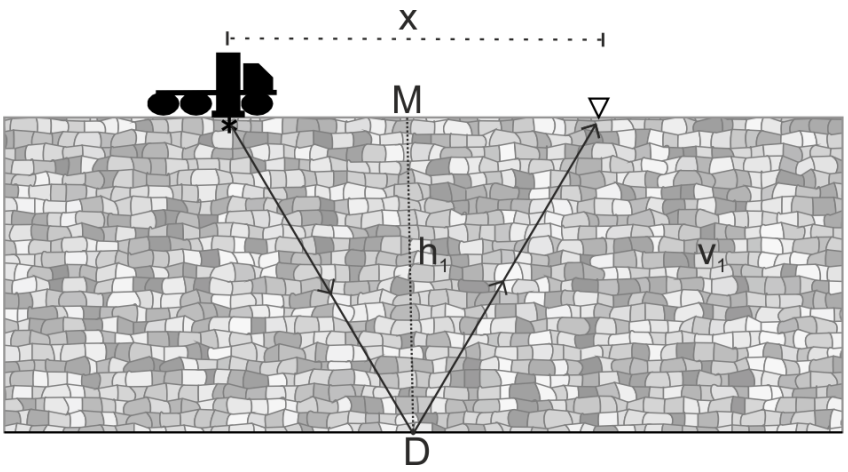


*Fig. 35; NMO geometry for a single, horizontal reflector. Star denotes source, triangle denotes receiver is midpoint, D is depthpoint. The travel time is described by a hyperbola in equation 32.*

The time that the seismic wave needs to travel from the source to the reflector (D) and upwards back to a receiver at the surface is called two-way travel time ($TWT$). Considering the Pythagorean Theorem the equation of $TWT$ as a function of offset ($x$) which is the distance from the source to the receiver, is (Yilmaz, 1987):

$$twt^2(x) = t^2(0) + \frac{x^2}{v_1^2} \quad (32)$$

The next geophone that records the same reflection has more offset. So the reflection pathway increases in length and thus the signal needs more time to arrive to the next geophone. That produces a hyperbolic shape in a CMP gather. The curvature depends on several factors:

- two-way travel time (TWT) with respect to offset,
- the two-way zero-offset time ($TWT_0$), which is the time required for a vertical signal from its source down to the reflector and back.
- dip of the reflector,
- the source-receiver azimuth with respect to the true-dip direction and
- the complexity of the near-surface.

The difference between the two-way zero-offset time and the two-way travel time at some offset ($TWT_x$) is called normal moveout (NMO, Fig. 36). To display a reflection event on its true position in the CMP gather, the reflection pathway has to be corrected for its normal moveout $\Delta t_{NMO}$ (Yilmaz, 2001)

$$\Delta t_{NMO} = (TWT_x - TWT_0) \quad (33)$$

Because of the reasons mentioned above, every offset needs its own velocity to correct for normal moveout. The velocity at which the reflections line becomes flat (Fig. 36) is the best correction and will be used ($v_{NMO}$). It will be determined through a velocity analysis. In conjunction with Equation (33) after Yilmaz, (2001),

$$\Delta t_{NMO} = TWT_0 \left[ \sqrt{1 + \left( \frac{x}{v_{NMO} TWT_0} \right)^2} - 1 \right] \quad (34)$$

If the normal moveout correction is applied correctly, the reflections become straight lines and only the multiples of them keep at least a roughly shape of a hyperbola. A too low velocity would result in overcorrecting, the event in Fig. 36b is then bending upwards and a

too high velocity would result in undercorrecting, the event would still be bending downwards.

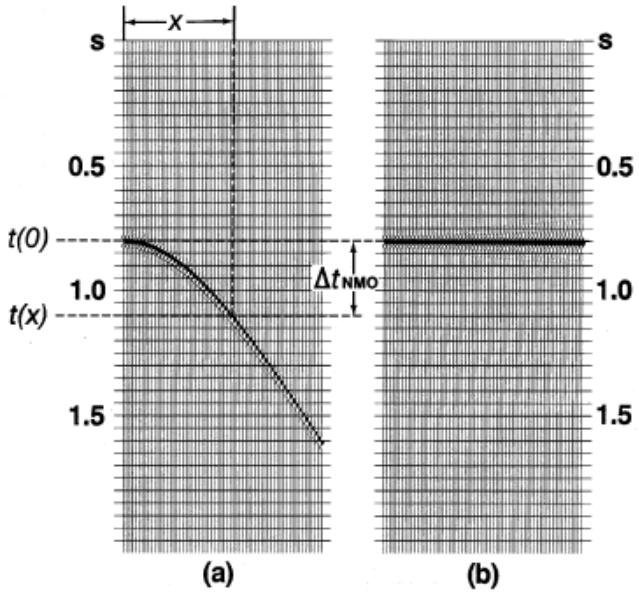


*Fig. 36; two CMP gathers, a without and b with NMO-Correction for offset x which involves mapping two-way travel time t(x) onto zero-offset two-way travel time t(o). From Yilmaz (2001).*

#### 4.2.7.2 Velocity analysis

Velocity analysis was done by visual inspection of adjacent CMP gathers, which was stacked over a range of test velocities for NMO corrections. First, several velocities were applied for NMO corrections and stacking of the whole profile. The aim was to make a first assumption in which velocity range the reflectors become flat and sharpened (Fig. 37). In Fig. 37, the upper part of profile 2 is shown under usage of different normal moveout corrections. Here are two strong events, the ice-water and the sea floor horizons. Fig. 37 suggests that an approximate velocity lies between $1450\ m/s$ and $1700\ m/s$. After that a small number of adjacent CMPs was selected and stacked again with several test velocities but with a smaller interval ($50\ m/s$) within the range ascertained above. This mini-stack panels were displayed next to each other, similar to Fig. 38, and velocities were picked where key events show the highest amplitude or greatest continuity.

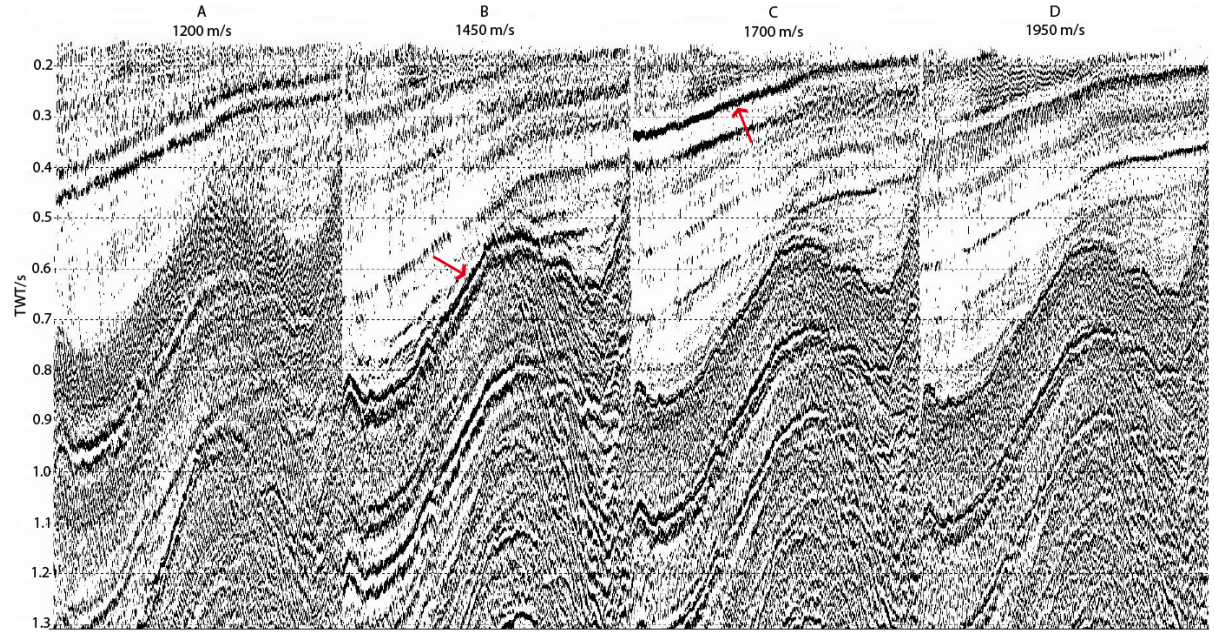


*Fig. 37; four different velocities were applied to profile 2, red arrows indicate important reflectors: A) the velocity is too low, the reflectors of the ice bed and sea bed are distorted because they are overcorrected. B) this velocity is better, because the sea floor is now sharpened, but for the ice horizon is even this velocity too low. C) here the velocity is adequate to both reflectors. D) through undercorrection, the lines bend downwards in each CDP gather, so in overall impression the events are dissolving.*

A whole series of time-velocities pairs were collected for every fiftieth CDP. The pairs were used to create a velocity model. In profile 1 (Fig. 39) the ice bed reflector has an average interval velocity about 3600 m/s and the sea floor was estimated with 1600 m/s, but with strong horizontal variations – up to 2000 m/s. In profile 2, the ice has an average interval velocity of 1775 $m/s$ and the sea bottom was estimated with 1450 $m/s$, this is nearly the same velocity for the water column, which was set here with 1500 m/s (Fig. 40).

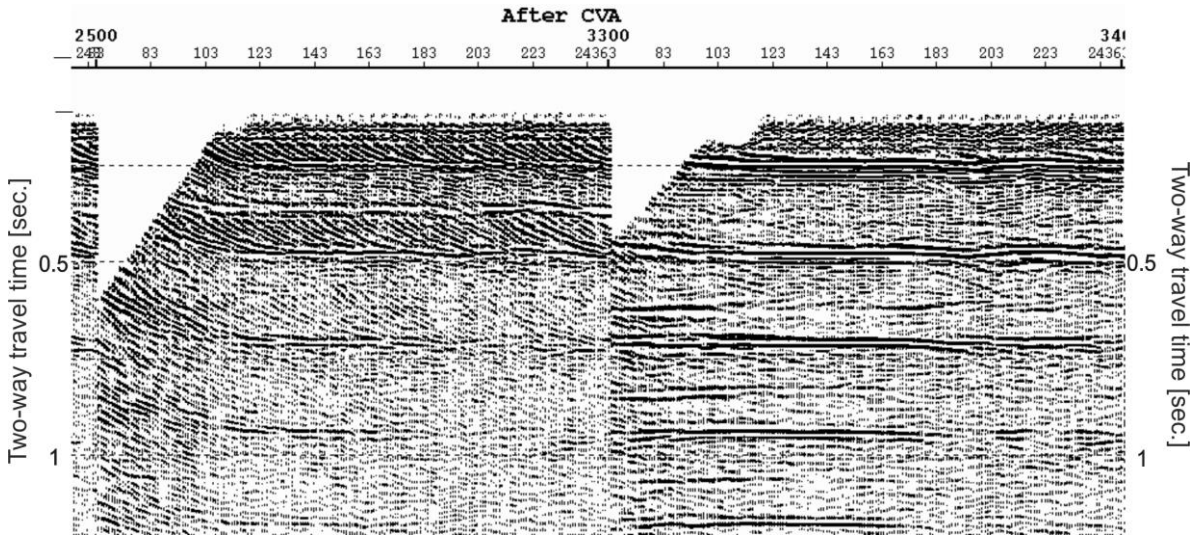


*Fig. 38; the first 250 CMP gathers of profile 1 with two different velocity functions. On the left side the velocity is too low, on the right side is proper velocity is applied.*

The resulting interval velocity models are shown in the next two figures.

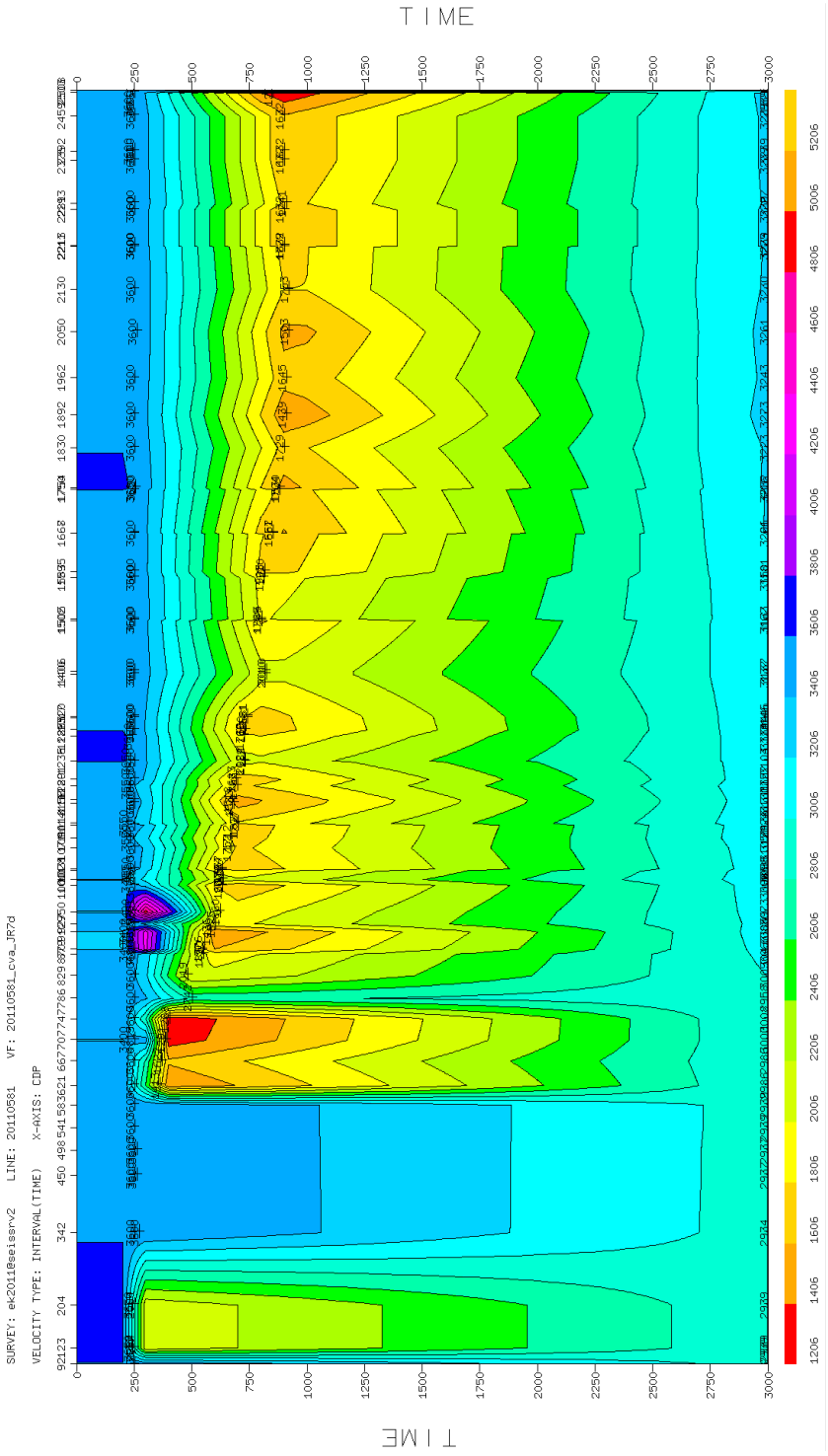


*Fig. 39; interval velocity model for profile 1, the two violet areas between CDP's 829 and 1000 are contributed from the shear zone, see section. 5.2.2*

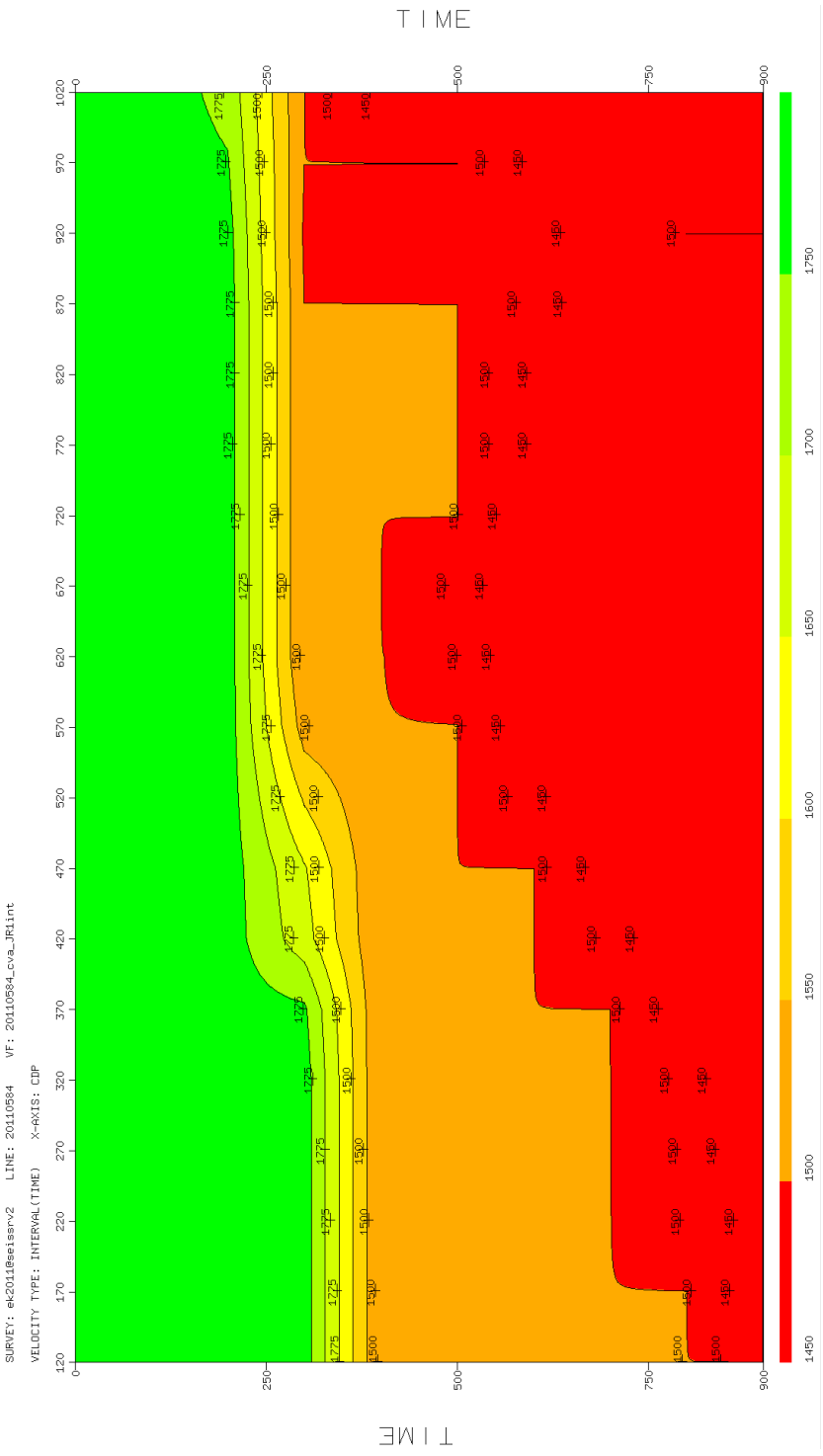


*Fig. 40; interval velocity model for profile 2, the ice reflector has a low velocity of 1775 m/s.*

### 4.2.8 **Stacking**

After applying NMO correction with velocity function for primary events, traces of the same CMP will be stacked together (Fig. 41). The primary associated signals are enhanced by summation over offsets while random noise is attenuated, since primaries are flat on NMO corrected gathers. If several random noises are stacked together, there will be some cancellation because they will be out of phase with each other. In best case, the sum of $n$ random signals will be proportional to $\sqrt{n}$. The sum of $n$ coherent in-phase signals will be proportional to $n$ so that the signal-to-noise ratio will be improved by the factor $\sqrt{n}$ (Sheriff & Geldart, 1982). A Median stacking was applied (Echos™-Module MEDSTK), it has advantages for records which contain multiple reflections with strong amplitudes.

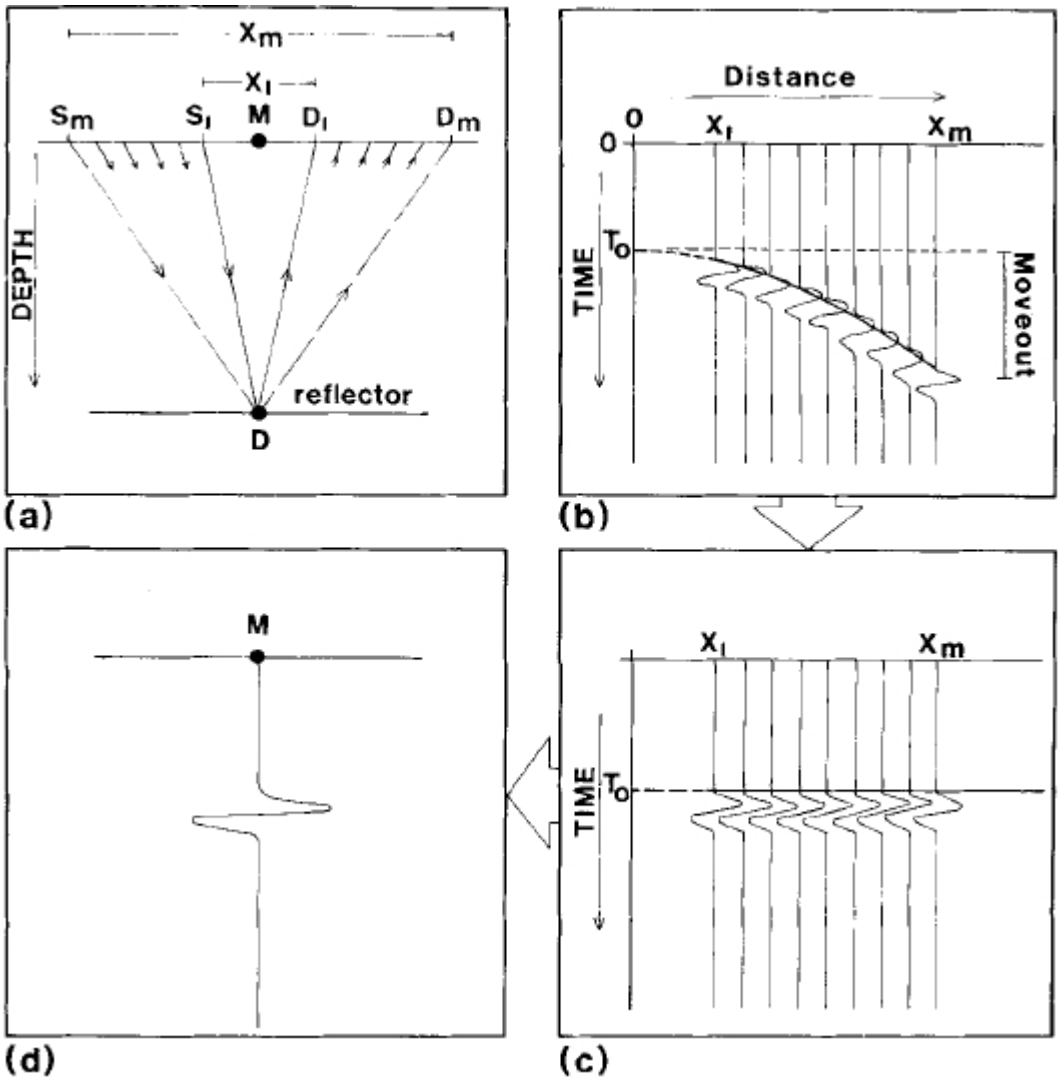


*Fig. 41; Common Depth-Point (CDP) stack. a) Ray diagram; S=Source, D=Detector, b) CDP record, note that each trace comes from a different field record, c) CDP record with NMO correction, d) Summation (stack) of all m traces. From O'Brien (1983).*

## 4.3 Application of multiple removal

In the following each profile shall be introduced with results of multiple suppression. NMO corrected seismic gathers was used to apply a multiple removal technique.

### 4.3.1 Multiple removal with Karhunen-Loeve

The best results for both profiles were reached using two eigenvalues and passing flat events. Multiple suppression with K – L transform did not work very well for profile 1 (Fig. 42), no multiple attenuation was achieved here, on the contrary the multiples in the water column were increased. Moreover, a notable attenuation was achieved for profile 2 (Fig. 43).

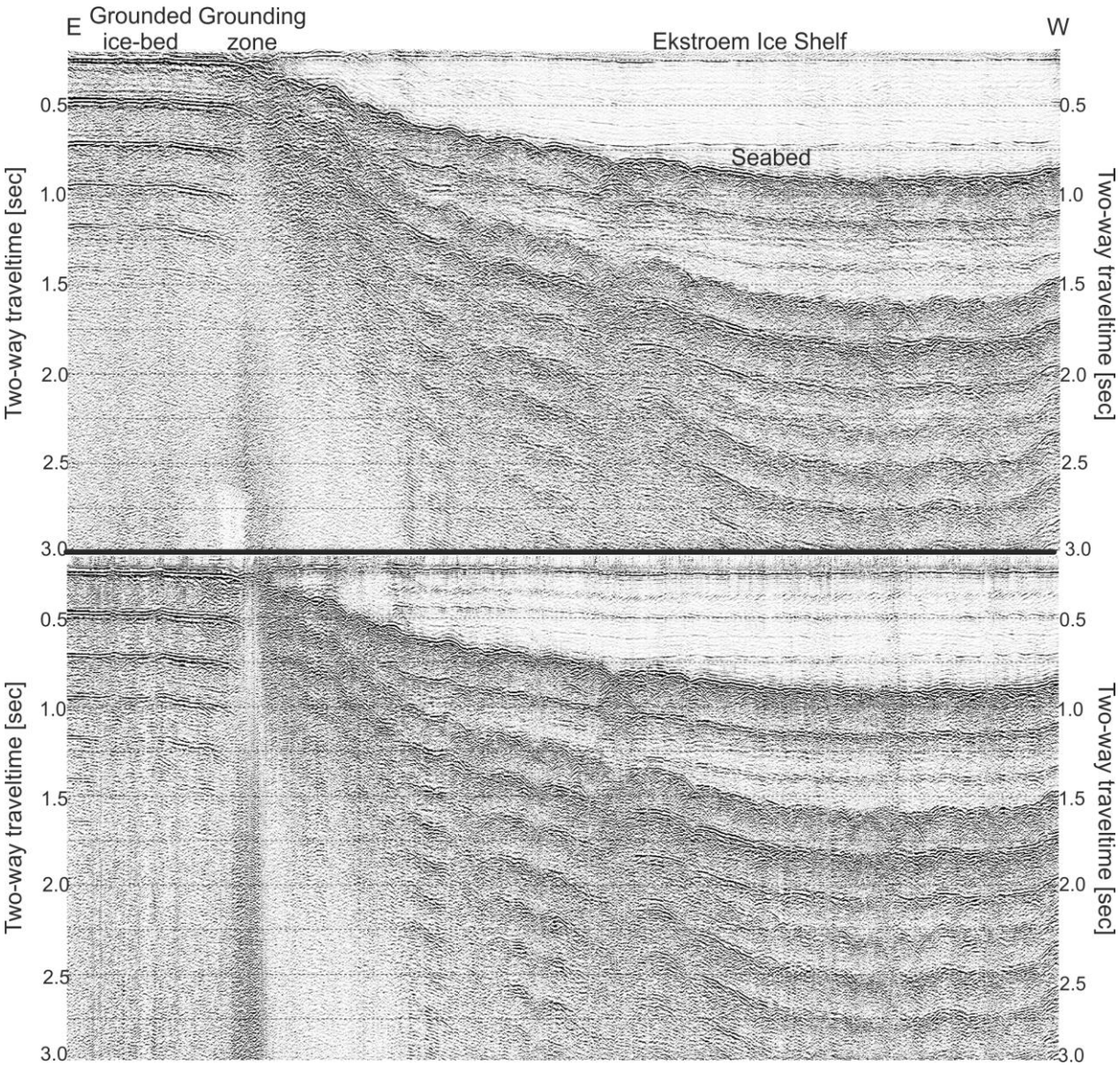


*Fig. 42; profile 1 stacked (top) and after K – L transform (bottom). The ice bed reflector has been improved after K – L transform and unfortunately its multiple at 0.5 s*

In profile 2 is multiple suppression for sea floor multiple achieved but the contour has suffered. The seaward dipping reflectors are now difficult to see.

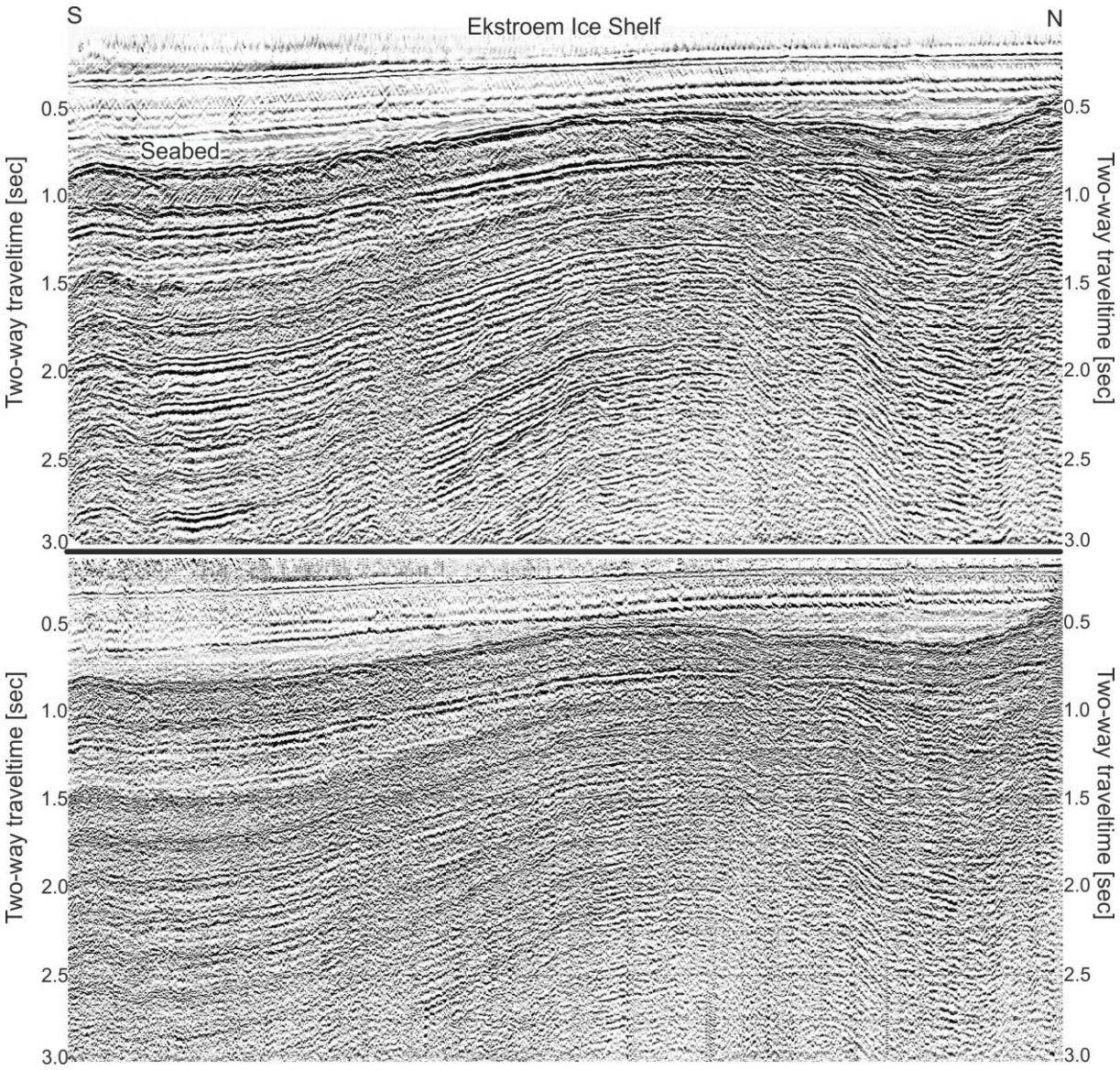


*Fig. 43; profile 2 stacked (top) and after K – L transform (bottom). The multiples in the sea water column were hardly suppressed but the deeper multiples of the sea floor boundary were attenuated. Both primary horizons experience a lag of contour.*

### 4.3.2 **Multiple removal with F – K Transform**

Undercorrected events were removed with F – K Transformation (ZMULT). For profile 1 was a stronger multiple attenuation achieved than with K – L Transformation. The sea water column is almost free of multiples (Fig. 44). The multiples of the ice-ground boundary are clearly reduced and the sea floor multiples are attenuated.

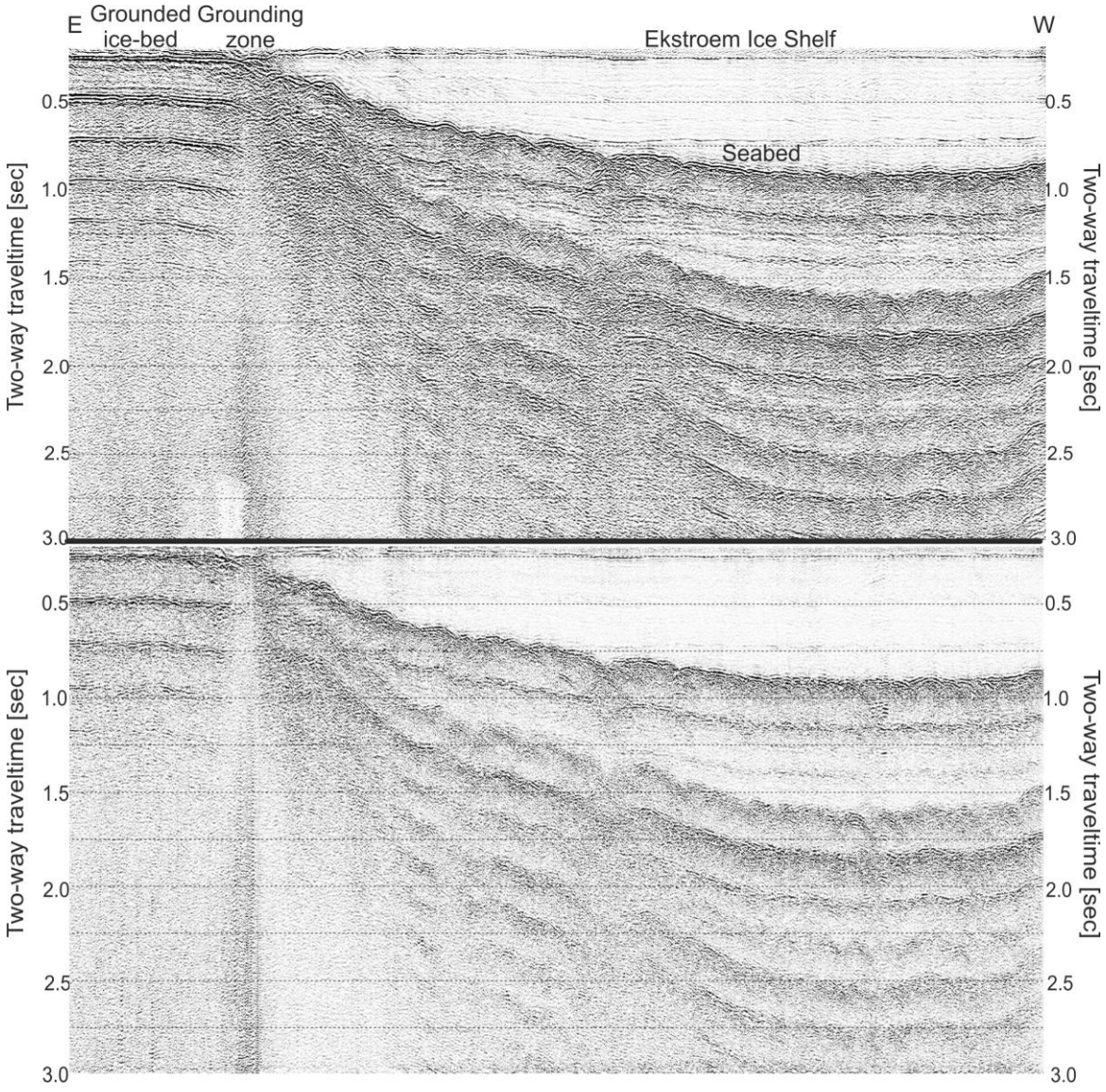


*Fig. 44; profile 1 stacked (top) and after multiple attenuation with F – K filtering (bottom).*

A frequency – wavenumber analysis of the Median stacked gather and after multiple removal with a F – K Transformation was applied to profile 1 (Fig. 45). After Median stack the energy of primary are close to each other between 40 Hz and 80 Hz and between wavenumber -0.1 and 0.1.

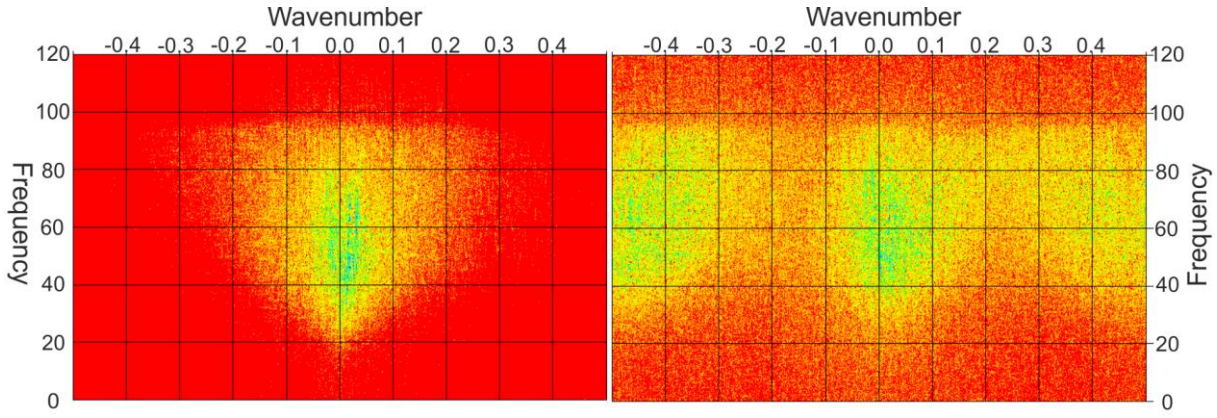


*Fig. 45; F – K spectrum of profile 1, the stacked gather (left) and after multiple suppression with ZMULT (right). The green and blue colors indicate strong amplitudes.*

For multiple removal the energy of multiple events should be clearly separated in groups of primary energy in different quadrants (positive or negative wavenumbers). Even with an overcorrection function it was not possible to obtain a better distinction. After filtering with ZMULT the spatial aliased energy has been distributed over a broader frequency and wavenumber range. As a result the section becomes more blurred. A similar situation for profile 2 is depicted in Fig. 46.

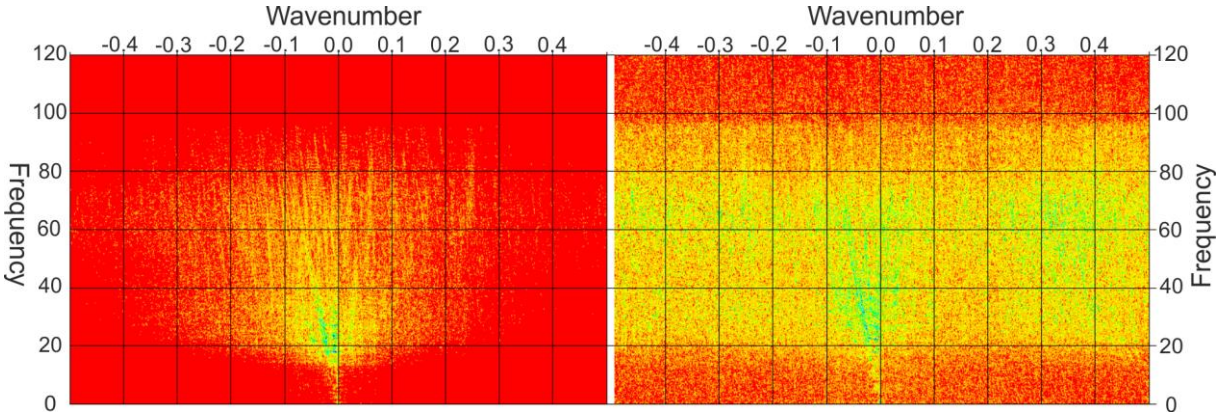


*Fig. 46; F – K spectrum of profile 2, the stacked gather (left) and after multiple suppression with ZMULT (right).*

In profile 2 after using ZMULT the southern part of the ice reflector was distraught, but multiples were attenuated.

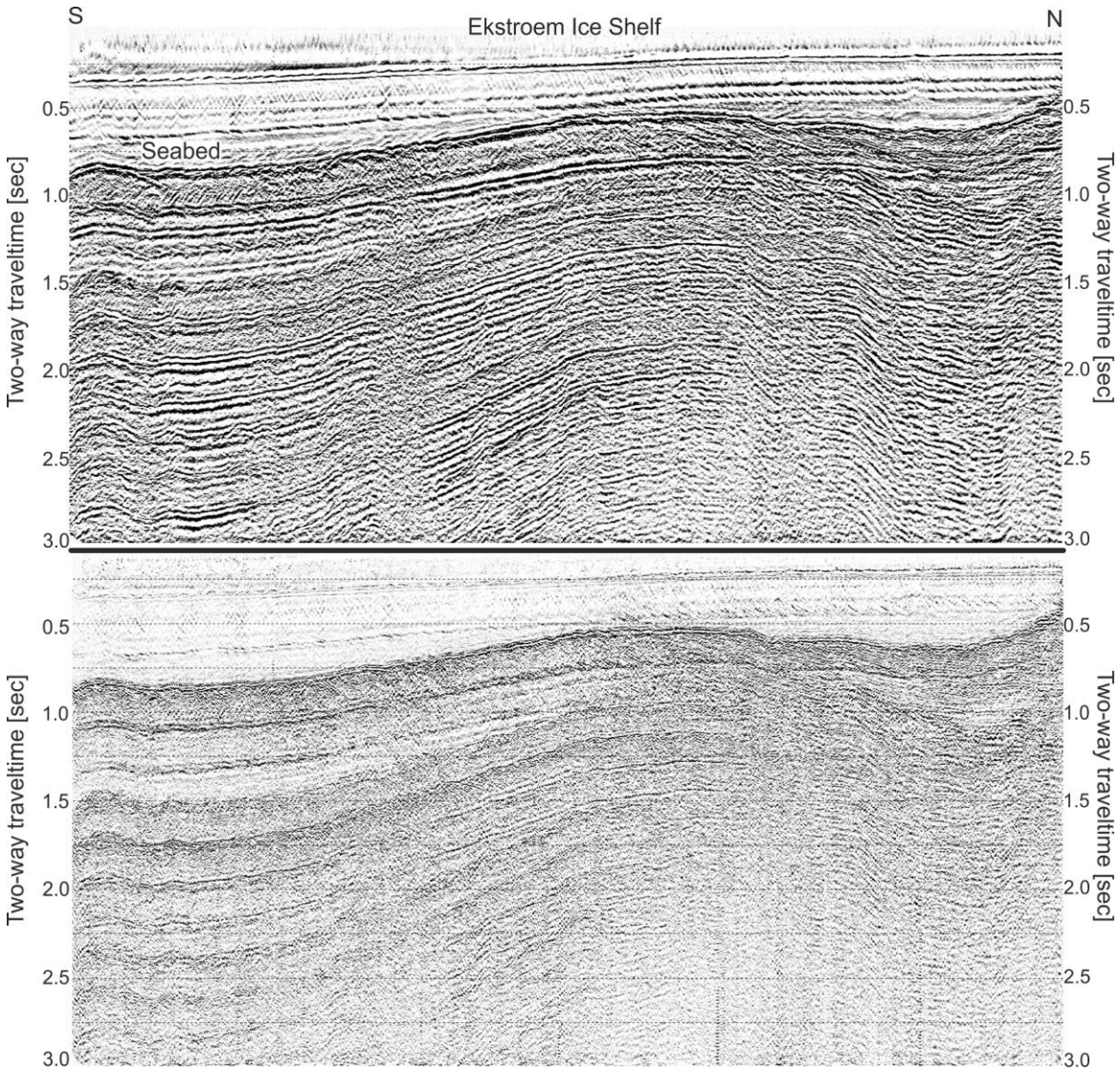


*Fig. 47; profile 2 stack (top) after multiple attenuation with ZMULT (bottom).*

### 4.3.3 **Multiple removal with parabolic Radon Transformation**

The result after filtering is that the shape of profile 1 is blurred and in profile 2 (Fig. 49) no effect was achieved.

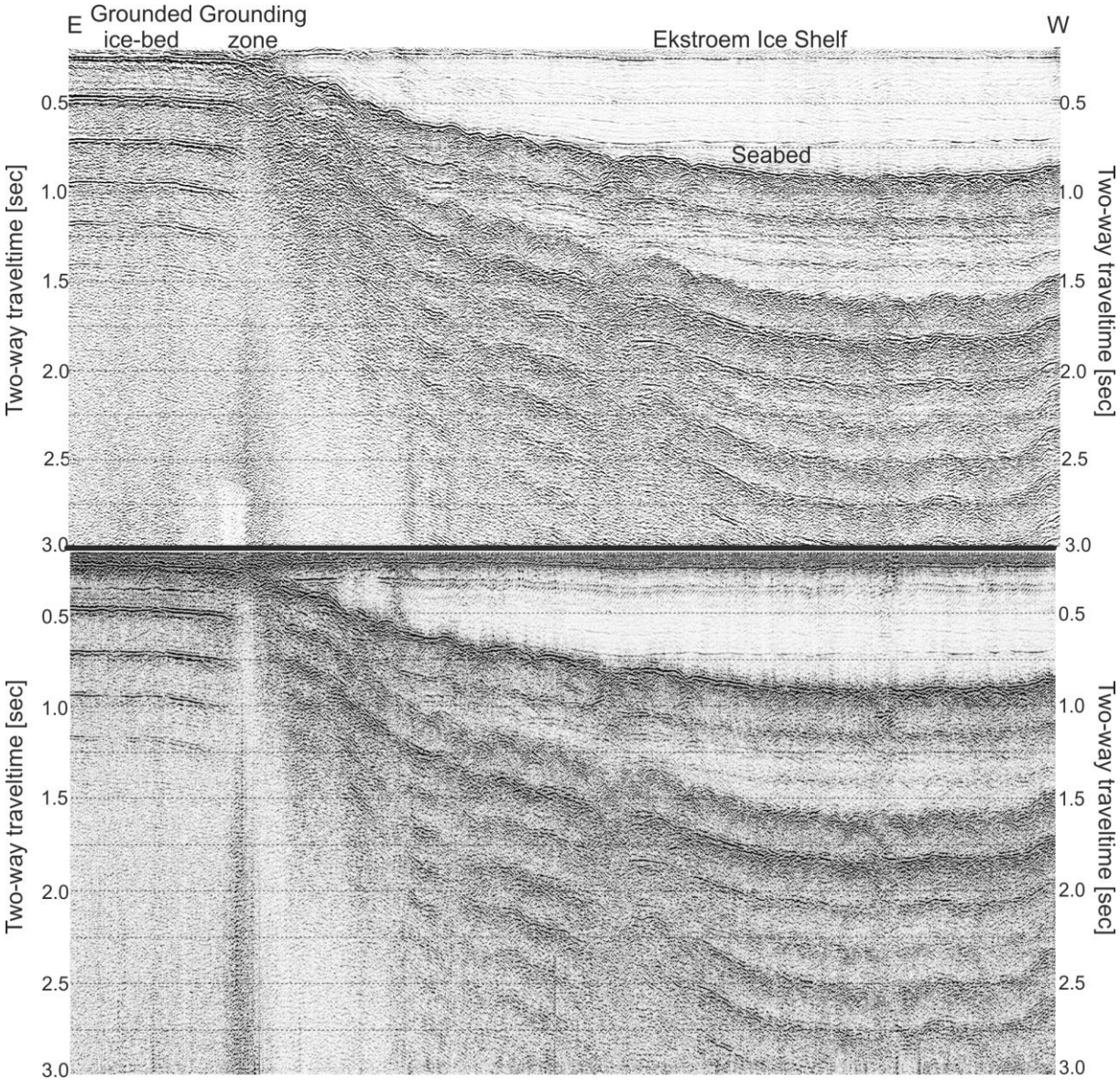


*Fig. 48; profile 1 stack (top) after multiple attenuation with parabolic Radon Transform (bottom).*

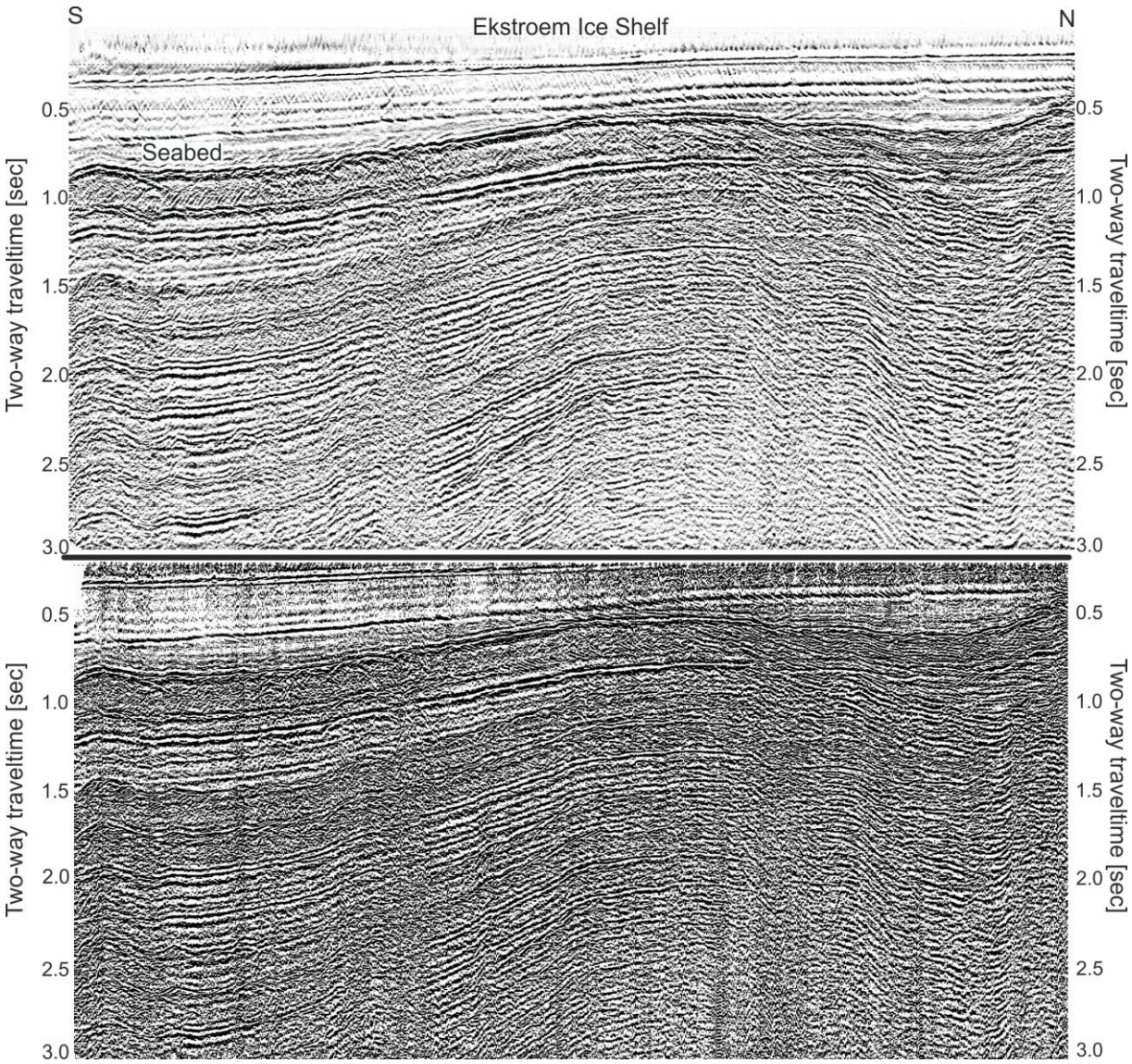


*Fig. 49; profile 2 stack (top) after multiple attenuation with parabolic Radon Transform (bottom). The lower picture has more contrast.*

# 5 Results

## 5.1 Stacked profiles

Fig. 50 shows the stacked seismic section of profile 1 without any multiple removal, also in large and without annotations in appendix A 1. A geologic interpretation is given in Ch. 5.2. The first important reflector, the ice bed boundary, is the thin line at 0.25 s TWT. At the east end, the ice rests on the ground. Here are five multiples visible. They are truncated by the grounding line. The second important reflector is the sea floor, dipping after the grounding line at 0.25 s down to 0.9 s TWT. The sea ground boundary generates more multiples than the ice-bed boundary. The ice-bed boundary produces two multiples, the first one is not visible at 0.35 s TWT, the second one visible at 0.75 s TWT. There are no further primary reflection events in the subsurface below the sea floor. The black, green and blue arrows indicate unconformities. The black arrows indicate a disturbance of the ice reflector. Green and blue arrows illustrate features at sea floor.

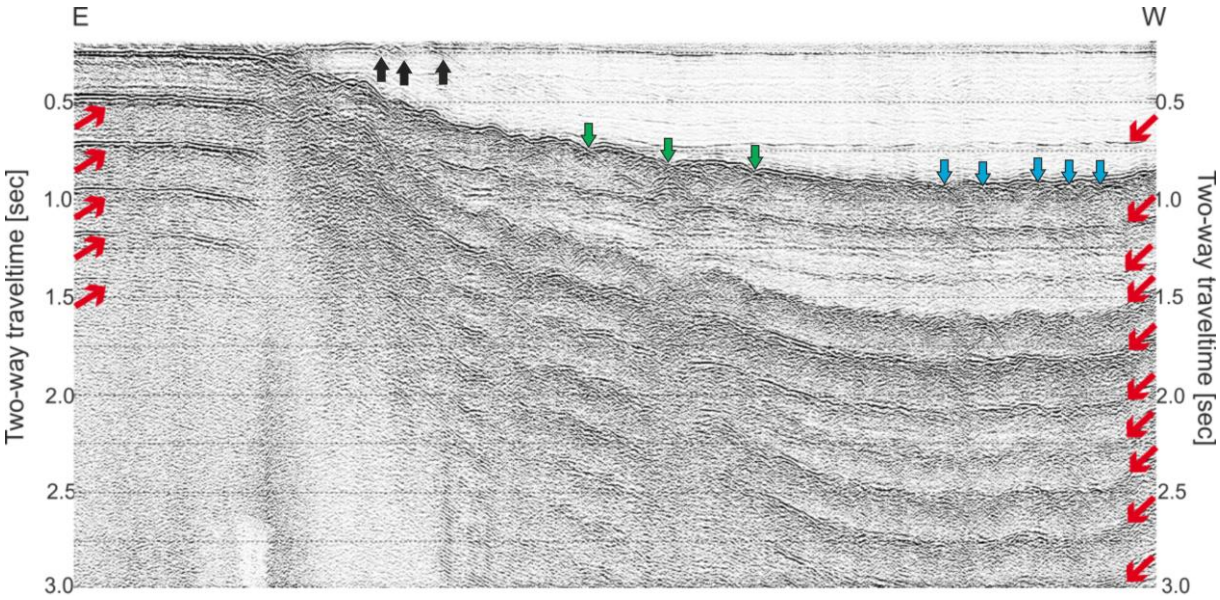


*Fig. 50; stacked profile 1 without any multiple suppression. Red arrows indicate multiples. Black arrows indicates a shear zone, greens are troughs and blues are unconformities of the sea floor.*

Fig. 51 shows the stacked profile 2 without any multiple attenuation, see also appendix A 2. Two important reflectors of layer boundaries are visible. The ice shelf/ocean reflector is at 0.3 s (south) and at 0.2 s (north). The multiples of this reflector are located below the ice shelf in the seawater column. The water bottom reaches from 0.9 s, (south) to 0.4 s, (north). There are dipping reflectors on the north side of the sea floor. A band of seaward (northward) dipping reflectors can be seen at the anticlinal reaching deep into the ground. The sea floor reflector generates multiples with strong amplitudes, they are visible in the entire seismic section below 0.9 s TWT.

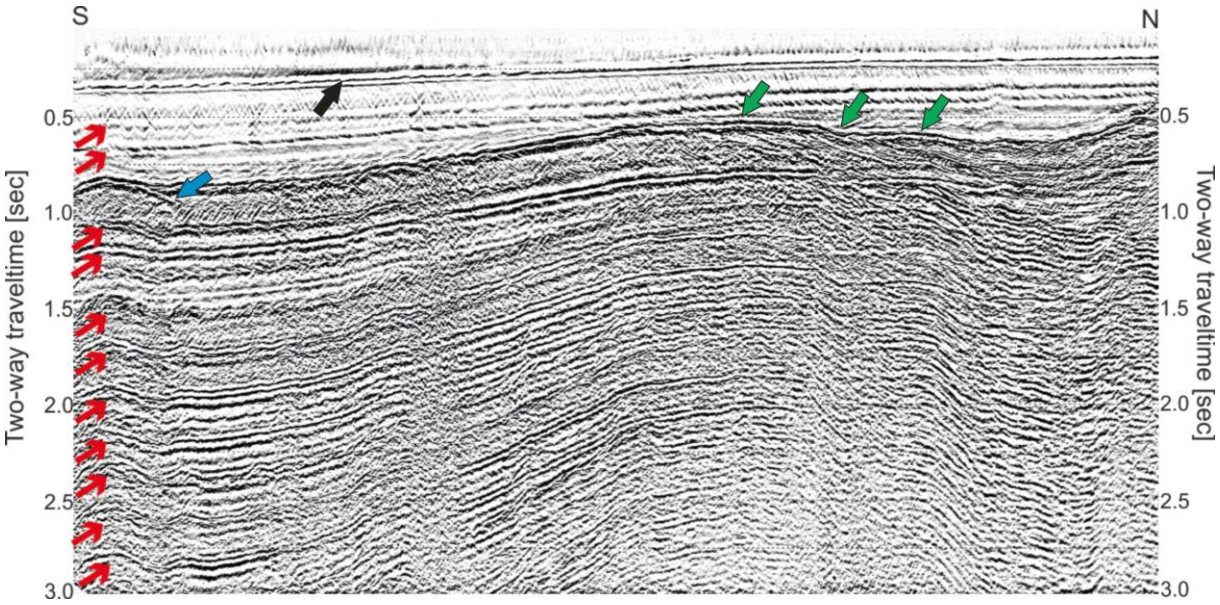


*Fig. 51; stacked profile 2 without any multiple suppression. Red arrows indicate multiples. The black arrow indicates the ice reflector, the blue one marks an unconformity of the sea floor and the green arrows indicates an outcrop.*

## 5.2 Interpretation of seismic sections

Based on the multiple attenuated seismic stacked gather and on the velocity models, an interpretation of the geologic and glaciological features is presented here.

### 5.2.1 Profile 1

Profile 1 has important features. Underneath the grounding zone the ice bed multiples are truncated before the grounding zone is reached. Below it in the continental basement is seismic noise, visible below 1.25 s TWT, embraced by the dotted lines in Fig. 52.

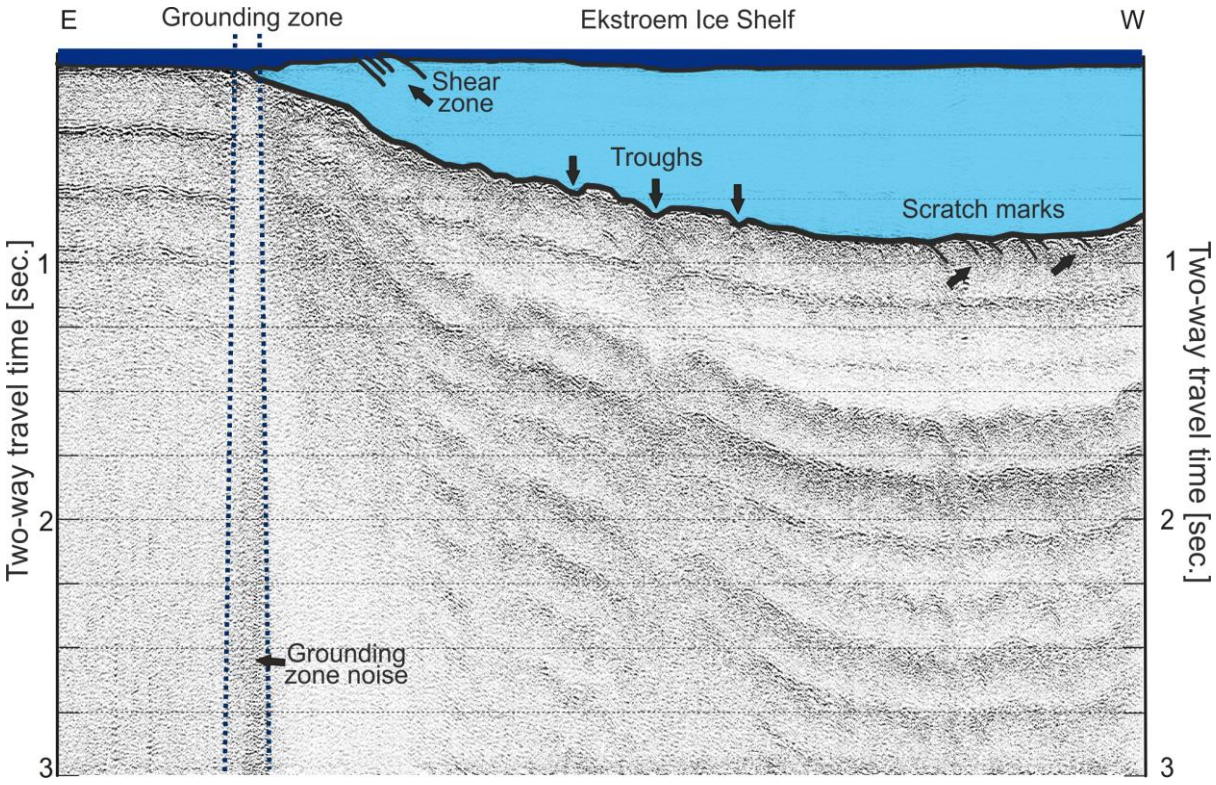


*Fig. 52; interpretation of seismic cross section of profile 1, based on multiple attenuation with F – K filtering, the ice flows into the direction of the reader, the resulting gather*

The multiples above 1 s TWT are interrupted here, thus this noise cannot be multiple reflections from the ice bed-ground boundary. In context to the missing multiples, this noise is only below the grounding zone, so the obviously explanation is that the noise rises from ice movement induced by ocean tidal motion. Robin (1958) had discovered that ocean tides influences ice shelves, he observed a vertical movement of the Quarisen Ice Shelf, during the Norwegian-British-Swedish Antarctic Expedition (NBSAE) from 1949 till 1952. The influence of ocean tides of do not end at the grounding zone, vertical movement of ice was

observed 2 km behind the grounding zone on grounded ice (Riedel, 2003). Bindschadler, et al. (2003) observed that west Antarctic ice streams can be discharged by sudden and brief periods of very rapid motion paced by oceanic tidal oscillations about 1 meter.

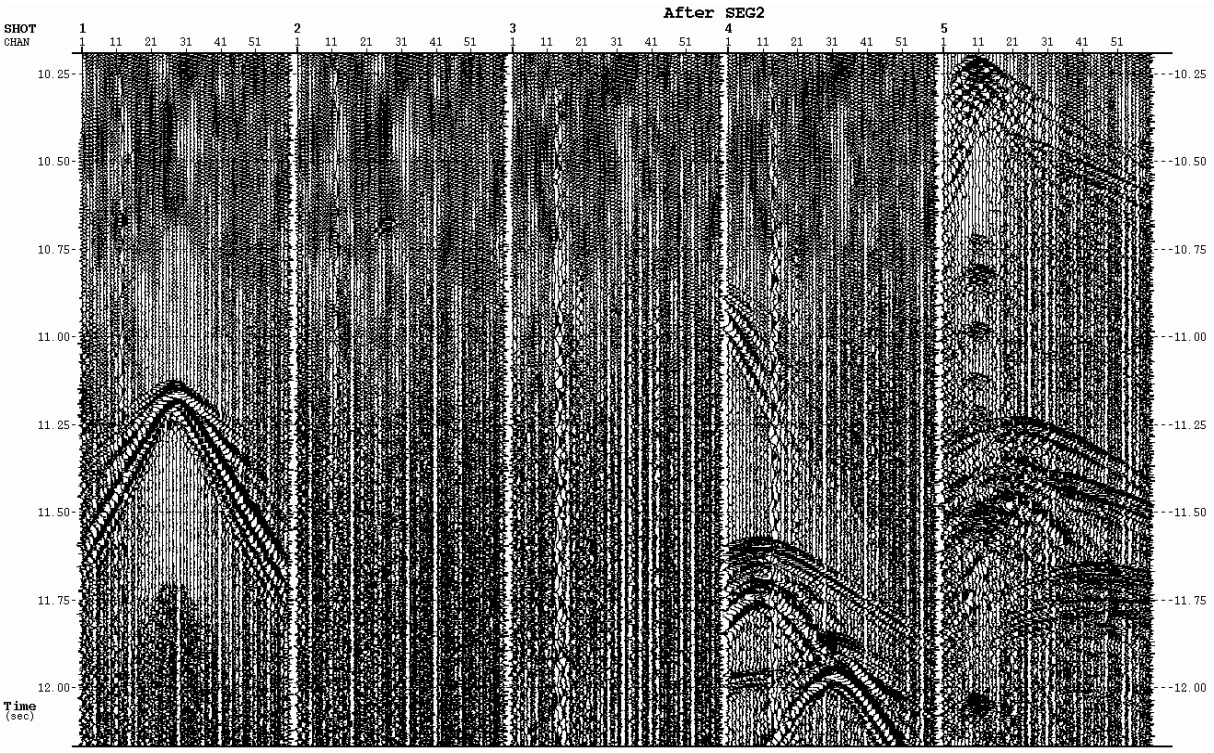


*Fig. 53; 5 shot gathers from the grounding zone showing much seismic noise in the uncorrelated data. The noise is properly generated by tidal motion of the ice.*

### 5.2.2 **Shear Zone**

Fig. 54 depicts an unconformity of the ice shelf, behind the grounding zone in western direction, it consists of dipping events. The sea bed is unaffected.

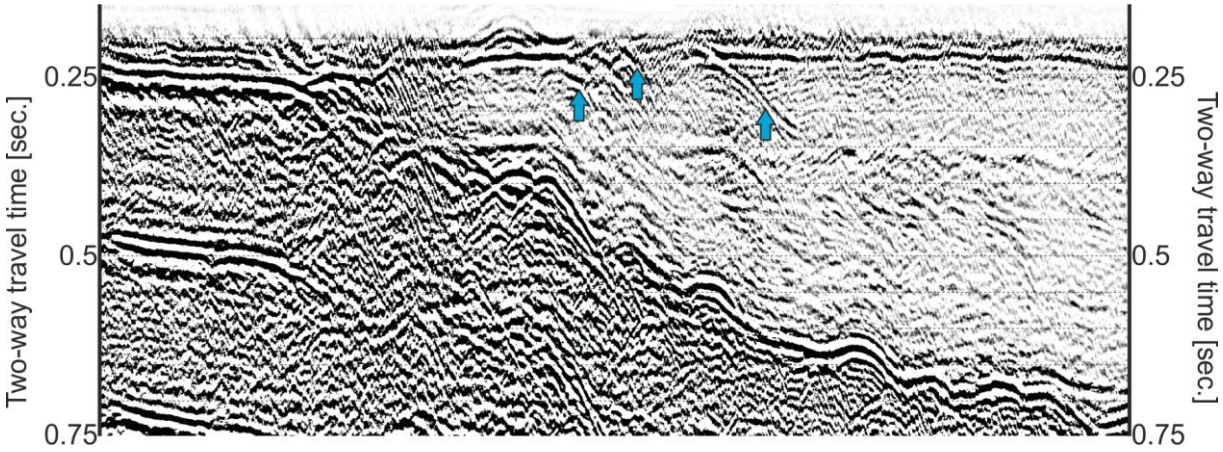


*Fig. 54; aperture of profile 1, Median stacked gather, blue arrows indicates the dipping events.*

Niklas Neckel (2010) has developed a surface velocity model for ice flows in the hinterland of Neumayer III station (Fig. 55). It outlines flow directions and velocities of ice flows and the black line marks profile 1. The profile line crosses two different ice flows. The sea bed is unaffected of the unconformity. This unconformity is caused by a shear zone. Here is the contact of two ice flows, which flow perpendicular with significant velocities differences to each other.

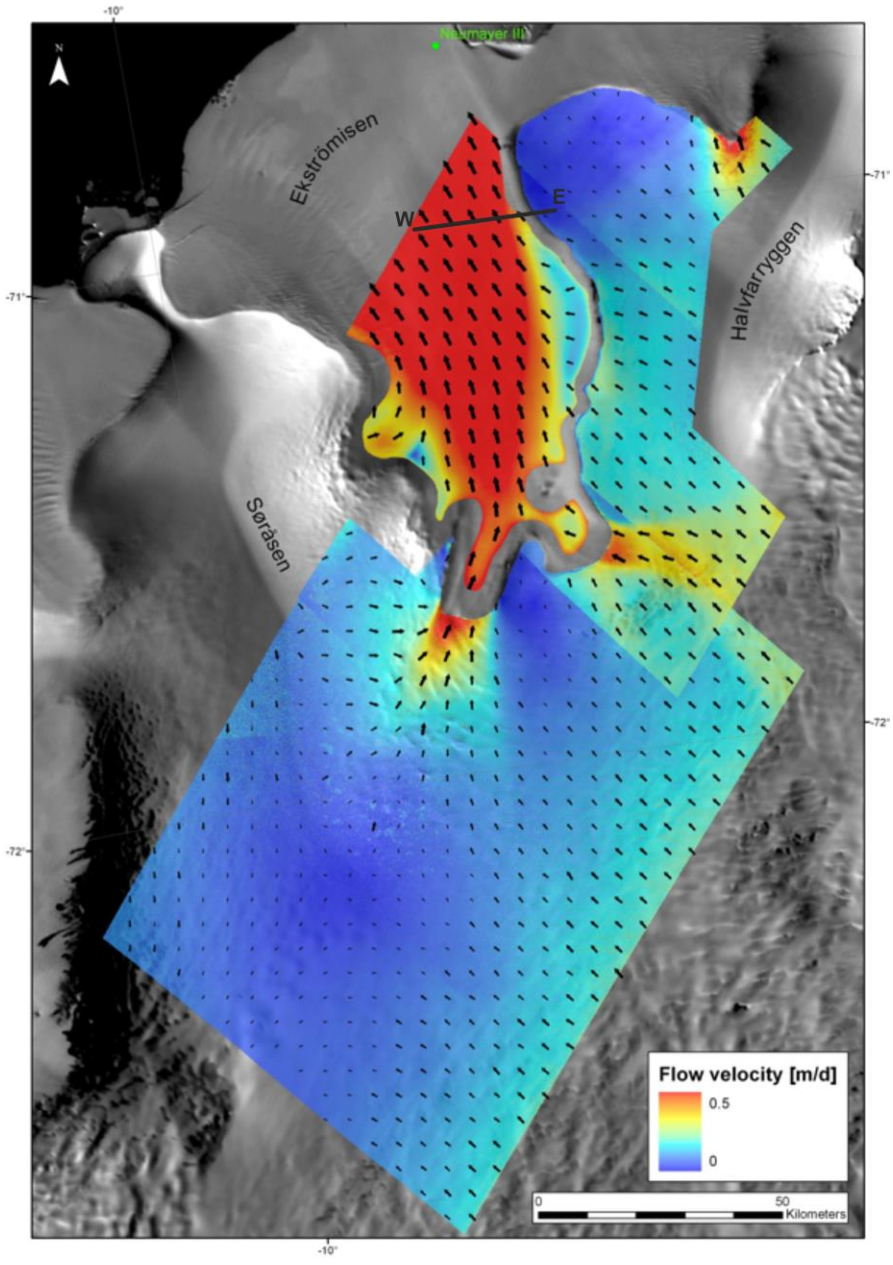


*Fig. 55; surface velocities in the hinterland of the German overwintering station Neumayer III in meter per day. The black arrows indicate the direction of the flow and their size is proportional to velocity. The NSDIC MODIS mosaic of Antarctica (MOA) is in the background. The black line marks the profile line of profile 1, from Niklas Neckel (2010).*

### 5.2.3 **Troughs and scratch marks**

Moving ice interacts with the ground and forms its surface in several ways. Glaciers transport debris, they push the bed load in their front and it will be deposited bit by bit. Also the soil gets solidified through the weight of ice masses.

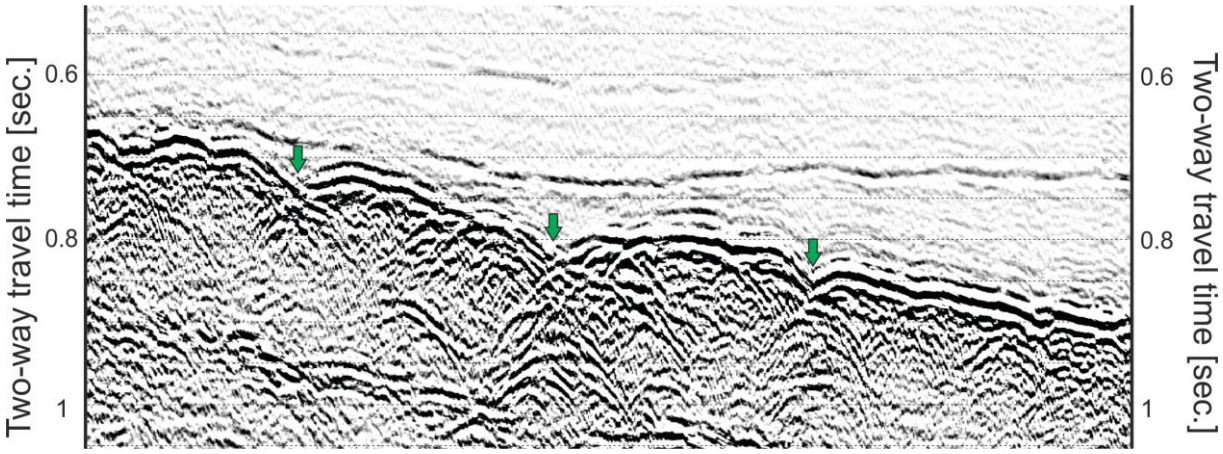


*Fig. 56; aperture of profile 1, Median stack gather, green arrows indicate bigger troughs at the sea floor.*

In Fig. 56 positions of troughs are indicated. The stacks are unmigrated, the typically structure of an unmigrated syncline is visible. These troughs can be created by former ice load. In Fig. 57 unconformities of the sea floor are outlined, these scratch marks could be created by the debris load of a glacier.

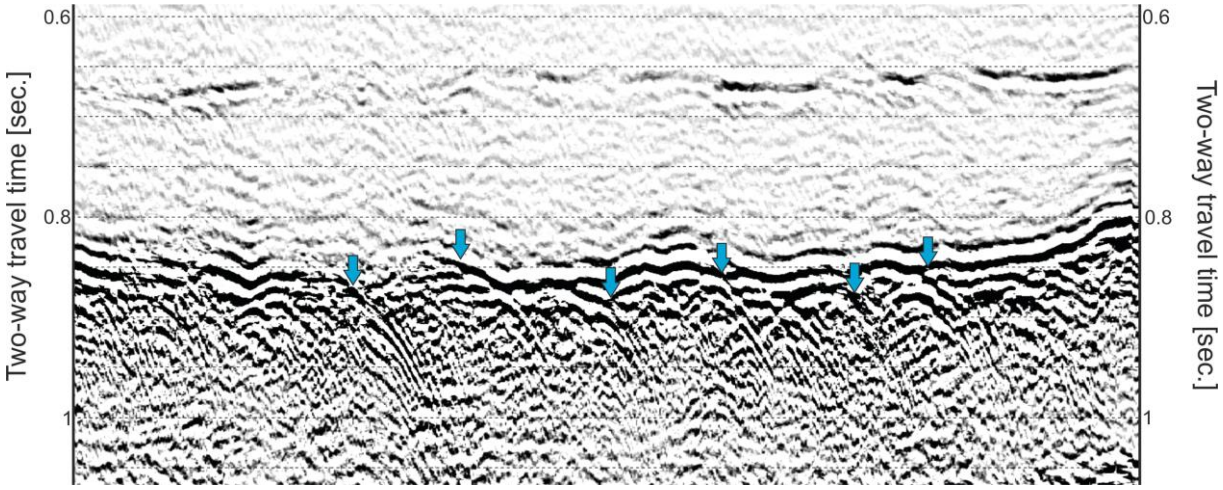


*Fig. 57; aperture of profile 1, Median stack gather, blue arrows indicate unconformities.*

### 5.2.4 **Profile 2**

A crustal section of the continental margin with position of the Ekstroem Ice Shelf is given in Fig. 58. Profile 2 extends to about -71°S till 70.53°S, so EWC3, the Explora Wedge (EW) is part of our data. Also the flat layer of sediments (maybe the Ritscherflya Supergroup) above the wedge with a seismic velocity about 2.1 km/s. For velocity modeling for our data, the velocities given in Fig. 58 were not important. The reason is that both profiles do not extend to such depth, so lower velocities were used.

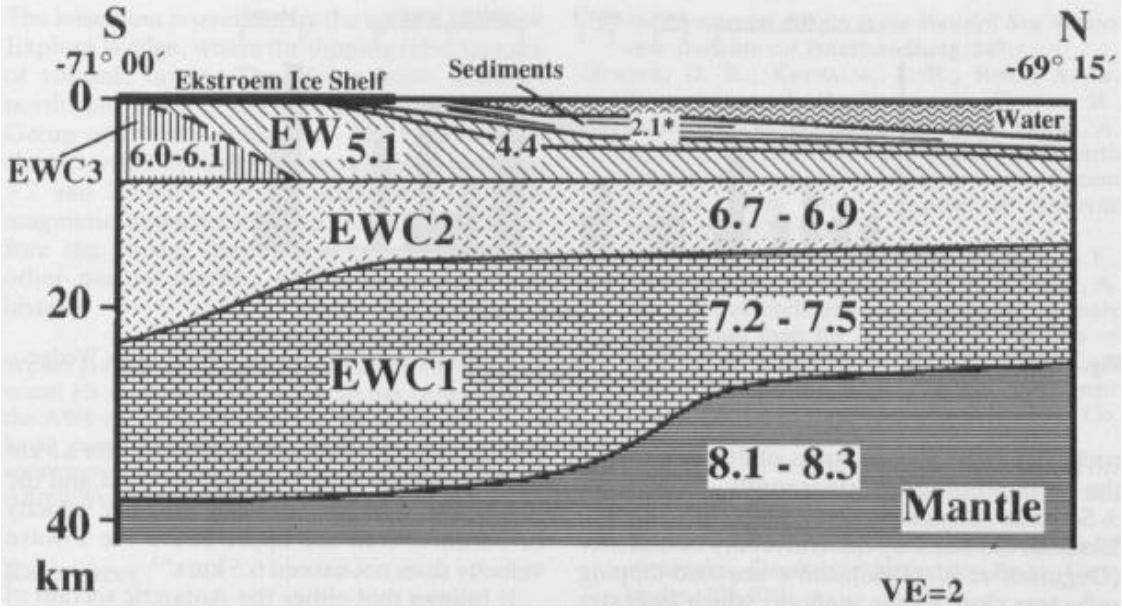


*Fig. 58; crustal section perpendicular to the continental margin in the Weddell Sea at 8°W. The interpreted layers are named as the East Weddell Sea Crust (EWC).The Explora Wedge is denoted with EW, numbers are seismic velocities in thousands of meters per second. From Hübscher et al. (1996). Please keep in mind there is also water under the ice shelf.*

The cross section along Ekstroem Ice Shelf provides three features (Fig. 59). The first one reaches from south to the middle of the profile. It is the continental basement, and consists of the granitic basement of the Archaean Grunehogna Craton, it is denoted as EWC 3 referring to Fig. 58. In this part are no primary reflectors. Within the second unit are divergent seaward dipping reflectors with a distinct unconformity at the upper boundary. The upper boundary is marked by a black line, which follows the uppermost reflector of this unit. These features had Hinz (1981) described as the volcanic Explora Wedge (EW). The dotted line outlines the estimated trend of the bottom of this unit. There is an outcrop at the sea floor (red circle) that disturbs the sea floor reflector. The Explora Wedge overlies the shelf edge (section. 2.1.2).

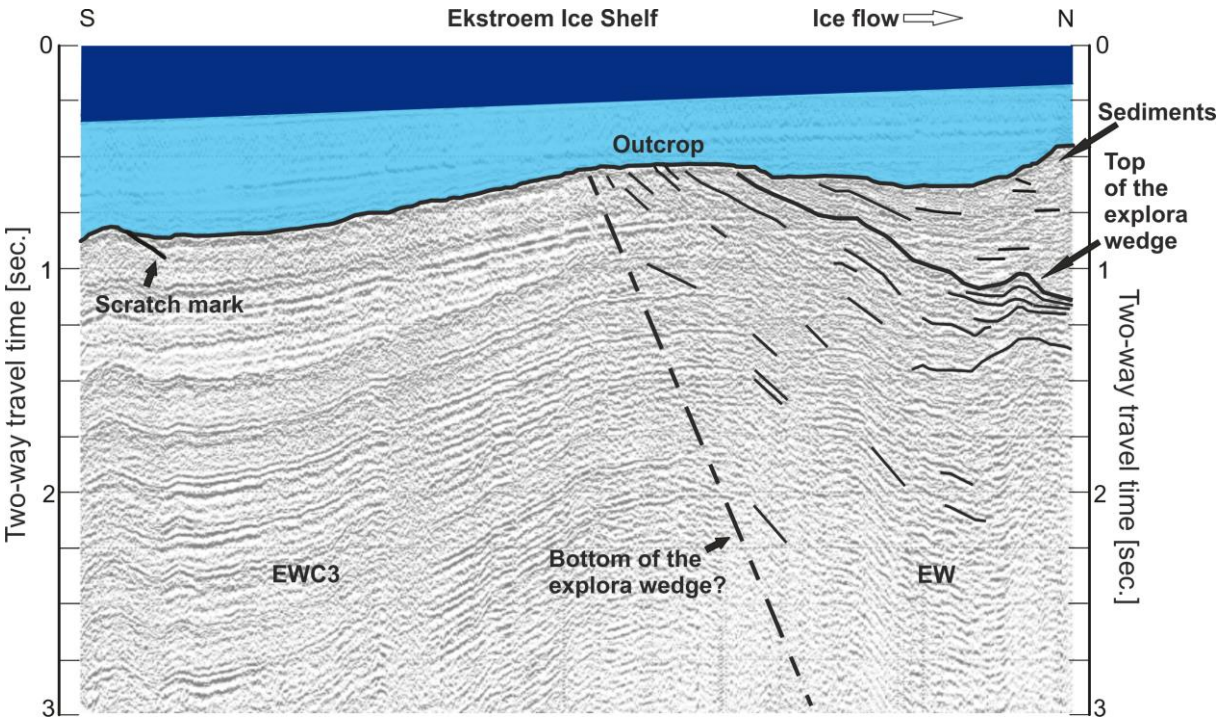


*Fig. 59; interpretation of seismic cross section of profile 2, based on Median stack gather. EW denotes Explora Wedge and EWC is East Weddell Sea Crust 3 in relation to Hübscher et al. (1996) Fig. 58.*

Above the top of the Explora Wedge is a layer with horizontal reflectors. After Hinz & Krause (1982) and Kristoffersen et al. (submitted) this is a layer of sediments. Till should be found here and as thin layer on the rest of the sea floor. Fig. 60 shows the sediment layer in relation to the Explora Wedge and the sea floor.

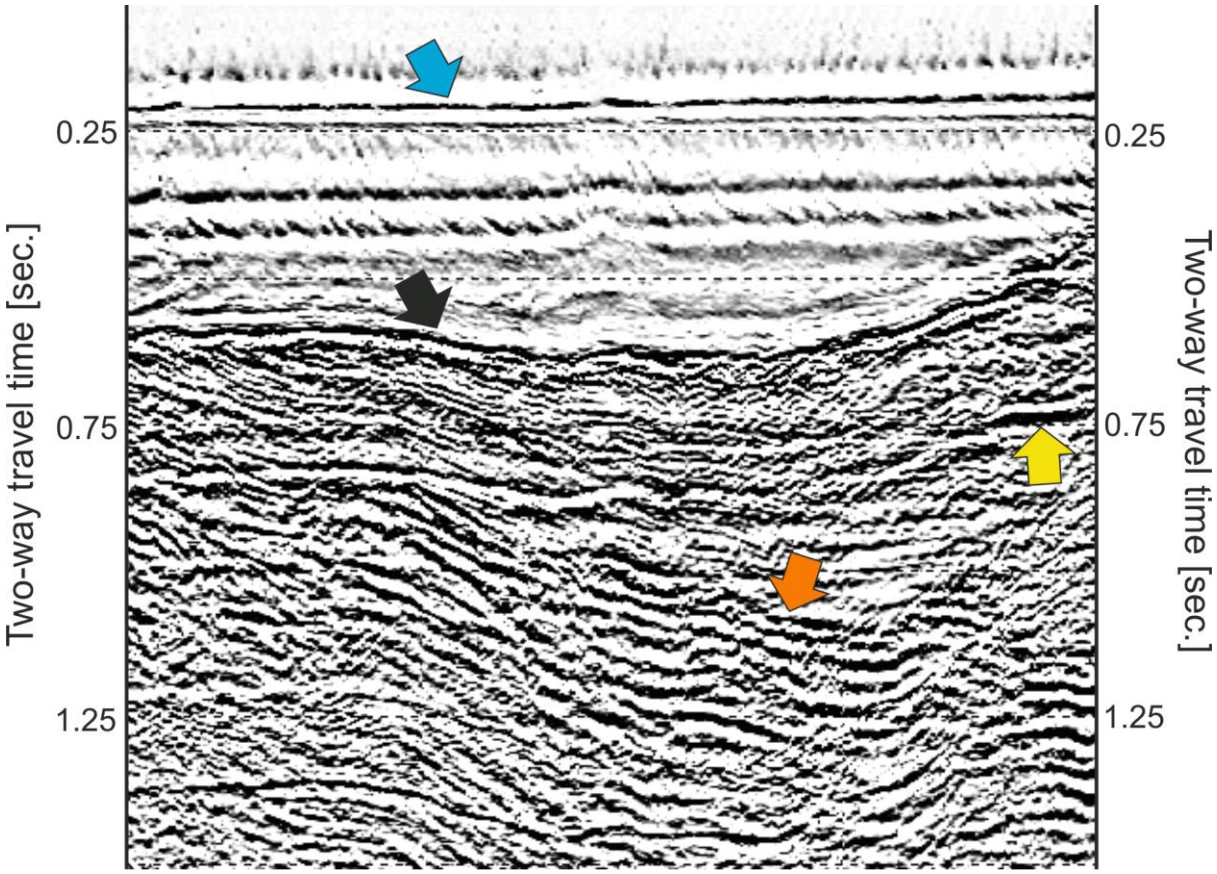


*Fig. 60; aperture of profile 2, Median stacked gather, the blue arrow indicates the ice reflector, the black one indicates the sea floor, the brown arrow marks the top of the Explora Wedge and the yellow one shows a horizontal reflector within the sediment layer.*

# 6 Discussion

The geological/glaciological setting of the survey area causes three crucial problems for seismic survey processing. The uppermost layer, the firn, determines on how much energy will be transferred into the ground, because the first few meters of this column works as energy trap due to its velocity gradient. Continuous densification over depth from about 350 kg/m³ to 915 kg/m³ causes an increase of speed of seismic waves from 970 m/s to 3255 m/s and a diving wave, too. The diving wave and ground roll were removed with F – K filtering before stacking. The second crucial part is the water column. A strong impedance contrast is given between ice and water that causes a strong multiple and appears in the seawater column. Thirdly, the sea bottom-multiple is responsible for the strongest and most reflected amplitudes. Its multiples interfere with the geological interpretation of the basement.

The NMO corrected CMP gathers were treated with several techniques for multiple removal. Periodicity-based methods like predictive deconvolution and slant stacking were not helpful. A predictive deconvolution can not effectively suppress multiple sea-floor reflections. "This method fails because the reflection coefficient varies markedly with angle of incidence and also because of the variation of arrival time with offset and because of dip" (Taner, 1980). Predictive deconvolution was not helpful in both profiles to attenuate multiples of the sea-floor horizon, no attenuation could be achieved. Gorbatschow (2011) who has worked on a part of profile 1 in his thesis, comes to the same result. But the length of the streamer should be long enough to cover a large range of reflection coefficients. In addition, if periodicity-based methods fail, it can be a hint of moveout in the CMP gathers. A problem is the bandlimited sweep (10 - 100 Hz). Resulting in a long time interval of the crosscorrelated source wavelet. As the range of high frequencies increase, the wavelet gets shorter and resolution improves (Fig. 61). The limitation of frequency bandwidth results in a relative small moveout in a CMP gather. The low fold coverage reinforces this problem, so that in our CMP gathers are insufficient traces (partially only 7 traces per CMP) to visualize the small moveout. Although an overcorrection could increase moveout differences, it could not help to improve the final results of the different multiple removal methods, because many elements of the multiples remained unchanged. This phenomenon was also observed for parabolic Radon Transform, elements that should be zeroed out in $\tau - p$ domain to restore them in x – t space (primaries) were not restored. The attempt to apply only an overcorrection to the primaries failed as well. Multiple attenuation was achieved with moveout-based methods. With F – K

filtering and K – L Transformation a good result was achieved in multiple removal. Multiple removal were accompained with a reduce of the contours of the reflectors. Thus for interpetation of profile 2 was the Median stack gather used.

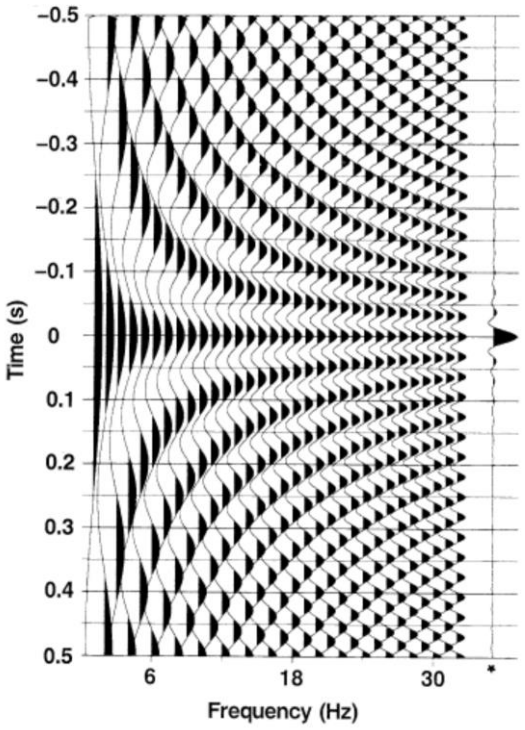


*Fig. 61; "Summation of a discrete number of sinusoids with no phase-lag, but with the same peak amplitude, yields a band-limited symmetric wavelet represented by the trace on the right (denoted by an asterisk). This is a zero-phase wavelet" (Yilmaz, 2001). This picture outlines the relation between seismic event resolution and frequency bandwidth.*

# 7 Conclusions

Two seismic datasets from the Ekstroem Ice Shelf, Antarctica were undergone a complete processing sequence in seismic data processing. Two images of the subsurface were created with a quite good quality. The buildup of the profiles down to a depth of around 5 km is visible now. It is possible to calculate the thickness of the ice (grounded and floating) and estimating the water depth. An impression of the topography of the ocean bottom is also given. The buildup of the continental basement, the crustal sections, is partially revealed. Structures within the sections are clearly indicated. That has enabled a visualization of sub-ice glaciological/geological features like the grounding zone, the shear zone, scratch marks, troughs, sediments and the Explora Wedge with a given interpretation. To achieve these outcomes in areas with tough climate conditions seismic surveys are the only way. In other regions autonomous underwater vehicles (AUV) are used to perform tasks like measuring the water depth and to explore the sea floor. But a commitment of AUV's under ice shelves in the Antarctic polar region is expected in only 10 till 15 years (Jenkins, 2013).

Once more, it has been shown that the removal of multiple reflections is an outstanding problem in seismic data processing. Many approaches were made in the last decades to solve this problem. Several techniques that have arisen were tested and used here. A really good multiple removal could not be applied due to the low fold coverage and the limitation of frequency of the input sweep. An attenuation of multiples could be attained with methods, which are exploiting time-based differences in the seismic signals. More fold coverage could improve the results. In addition, a Vibroseismic source that can produce a sweep with a frequency above 100 Hz will increase the resolution.

# 8 References


Albert, D. G., 1998. Theoretical modeling of seismic noise propagation in firn at the South Pole, Antarctica. *Geophysical Research Letters,* 25(23), pp. 4257-4260.

Baeten, G. & Ziolkowski, A., 1990. *The Vibroseis source.* Amsterdam; New York; New York, NY, U.S.A: Elsevier;Sole distributors for the U.S. and Canada Elsevier Science Pub. Co..

Bamber, J. L., 2000. Widespread Complex Flow in the Interior of the Antarctic Ice Sheet. *Science*, 287(5456), pp. 1248-1250.

Barton, J. J. et al., 1987. The geology and geochronology of the Annandagstoppane granite, Western Dronning Maud Land, Antarctica. *Contributions to Mineralogy and Petrology*, Issue 97, pp. 488-496.

Bell, R. E., 2008. Rutschgefährdete Eisschilde. *Spektrum der Wissenschaft*, Issue 5.

Bindschadler, R. A., 2003. Tidally Controlled Stick-Slip Discharge of a West Antarctic Ice. *Science*, 301(5636), pp. 1087-1089.

Boger, S. D., 2011. Antarctica — Before and after Gondwana. *Gondwana Research*, 19(2), pp. 335-371.

Claerbout, J. F., 1985. *Imaging the earth's interior.* Oxford [England]; Boston: Blackwell Scientific Publications.

Diez, A. et al., 2013. Joint interpretation of explosive and vibroseismic surveys on cold firn for the investigation of ice properties. *Annals of Glaciology,* 54(64), pp. 201-210.

Echos™ Manual 2011. Paradigm Ltd. Houston

Eisen, O. et al., 2010. A New Approach for Exploring Ice Sheets and Sub-Ice Geology. *Eos, Transactions American Geophysical Union,* 91(46), p. 429.

Fernandoy, F. et al., 2010. Temporal and spatial variation of stable-isotope ratios and accumulation rates in the hinterland of Neumayer station, East Antarctica. *Journal of Glaciology,* 56(198), pp. 673-687.

Foster, D. J. & Mosher, C. C., 1992. Suppression of multiple reflections using the Radon transform. *GEOPHYSICS*, 57(3), pp. 386-395.

Gadallah, M. R. & Fisher, R. L., 2009. *Exploration geophysics.* Berlin: Springer.

Gorbatschow, N., 2011. *Ekstroemisen 2011 - Groundingline Survey,* Berlin: Freie Universität Berlin.

Greve, R. & Blatter, H., 2009. *Dynamics of Ice Sheets and Glaciers.* s.l.:Springer.

Gu, Y. J. & Sacchi, M., 2009. Radon Transform Methods and Their Applications in Mapping Mantle Reflectivity Structure. *Surveys in Geophysics*, 30(4-5), pp. 327-354.

Halpern, M., 1970. Rubidium-Strontium Date of Possibly 3 Billion Years for a Granitic Rock from Antarctica. *Science*, 169(3949), pp. 977-978.

Helm, V., 2003. *Die Struktur des Kontinentalrandes im Gebiet des Larsenschelfes, Antarktische Halbinsel,* Freiberg: Institut für Geophysik Technische Universität Bergakademie Freiberg.

Hinz, K., 1981. *Wedges of very thick Oceanward Dipping Layers beneath Passive Continental Margins.* Hannover: s.n.

Hinz, K. & Krause, W., 1982. The Continental Margin of Queen Maud Land / Antartica: Seismic Sequences, Structural Elements and Geological Development. In: *Geologisches Jahrbuch.* s.l.:s.n., pp. 17-41.

Hofstede, C. et al., 2011. *Überblick der geophysikalischen Messungen am Colle Gnifetti.* s.l., s.n.

Hofstede, C. et al., 2013. Investigating englacial reflections with vibro- and explosive-seismic surveys at Halvfarryggen ice dome, Antarctica. *Annals of Glaciology,* 54(64), pp. 189-200.

Hübscher, C., Jokat, W. & Miller, H., 1996. Crustal structure of the Antartic continental margin in the eastern Weddell Sea. *Weddell Sea Tectonics and Gondwana Break-up,* Issue 108, pp. 166-174.

Hughes, T., 1977. West Antarctic ice streams. *Reviews of Geophysics,* 15(1), p. 1.

Jacobs, J., Pisarevsky, S., Thomas, R. & Becker, T., 2008. The Kalahari Craton during the assembly and dispersal of Rodinia. *Precambrian Research,* 160(1-2), pp. 142-158.

Jenkins, A., 2013. *Autonomous Underwater Vehicle* [Interview] (September 2013).

Jokat, W., 2003. Timing and geometry of early Gondwana breakup. *Journal of Geophysical Research,* 108(B9).

Kohnen, H., 1972. On the Relation between Seismic Velocities and Densities in Firn and Ice.. *Zeitschrift für Geophysik,* Issue 38.

Kristoffersen, Y. et al., 2010. Vibroseismic measurements on an ice shelf. *Geophysical Research Abstracts,* Band 12, EGU2010-1652.

Kristoffersen, Y. et al., kein Datum Exploring continental margin geology below a thick, floating ice shelf - a vibroseis survey of the Explora volcanic wedge, Dronning Maud Land, East Antarctica. *Tectonophysics*.

Lambrecht, A. et al., 2010. *Vibroseismics on ice: First results and implications from Antartic measurements.*. Milano, Italy: s.n.

Lawver, L. A. & Gahagan, L. M., 2003. Evolution of Cenozoic seaways in the circum-Antarctic region. *Palaeogeography, Palaeoclimatology, Palaeoecology*, 198(1-2), pp. 11-37.

Mari, J. L., Glangeaud, F. & Coppens, F., 1999. *Signal processing for geologists & geophysicists.* Paris: Editions Technip.

Müller, U., Sandhäger, H., Sievers, J. & Blindow, N., 2000. Glacio-kinematic analysis of ERS-1/2 SAR data of the Antarctic ice shelf Ekströmisen and the adjoining inland ice sheet. *Polarforschung*, pp. 15-26.

Niklas Neckel, 2010. *Surface velocities in the hinterland of the Neumayer III station (Antarctica) derived from SAR-Interferometry*, Heidelberg: Universität Heidelberg.

O'Brien, P. N. S., 1983. Aspects of seismic reflection prospecting for oil and gas. *Geophysical Journal International*, 74(1), pp. 97-127.

Riedel, B., 2003. *The elastic behaviour of Ekströmisen grounding zone.*. s.l.:s.n.

Riedel, S., Jacobs, J. & Jokat, W., 2013. Interpretation of new regional aeromagnetic data over Dronning Maud Land (East Antarctica). *Tectonophysics*, Band 585, pp. 161-171.

Riedel, S., Jokat, W. & Steinhage, D., 2012. Mapping tectonic provinces with airborne gravity and radar data in Dronning Maud Land, East Antarctica. *Geophysical Journal International*, 189(1), pp. 414-427.

Rignot, E., Mouginot, J. & Scheuchl, B., 2011. Antarctic grounding line mapping from differential satellite radar interferometry. *Geophysical Research Letters*, 38(10), p. n/a.

Robin, G. d. Q., 1958. Glaciology III. Seismic shooting and related investigations. In: *Norwegian-British-Swedish Antarctic Expedition, 1949-52 Scientific Results, Vol. V.* Oslo: Norsk Polarinstitutt.

Sheriff, R. E. & Geldart, L. P., 1982. *Exploration Seismology.* New York: s.n.

Stauffer, B., Schwander, J. & Oeschger, E., 1985. Enclosure of air during metamorphosis of dry firn to ice. *Annals of Glaciology*, Issue 6, pp. 108-112.

Stolldorf, T., Schenke, H.-W. & Anderson, J. B., 2012. LGM ice sheet extent in the Weddell Sea: evidence for diachronous behavior of Antarctic Ice Sheets. *Quaternary Science Reviews*, Band 48, pp. 20-31.

Studinger, M. & Miller, H., 1999. Crustal structure of the Filchner-Ronne Shelf and Coats Land, Antarctica, from gravity and magnetic data: Implications for the breakup of Gondwana. *Journal of Geophysical Research*, 104(B9), p. 20379.

Taner, M., 1980. Long Period Sea-Floor Multiples and their Suppression. *Geophysical Prospecting*, 28(1), pp. 30-48.

Telford, W. M., Geldart, L. P. & Sheriff, R. E., 1990. *Applied geophysics.* 2nd ed Hrsg. Cambridge [England]; New York: Cambridge University Press.

Thomas, R. H., 1979. The dynamics of marine ice sheets. *J. Glacio.*, 24(90), pp. 167-177.

Veevers, J., 2012. Reconstructions before rifting and drifting reveal the geological connections between Antarctica and its conjugates in Gondwanaland. *Earth-Science Reviews*, 111(3-4), pp. 249-318.

Yilmaz, Ö., 1987. *Seismic data processing.* Tulsa, OK: Society of Exploration Geophysicists.

Yilmaz, Ö., 2001. *Seismic data analysis.* 2nd ed Hrsg. Tulsa, OK: Society of Exploration Geophysicists.

# 9 Appendix – Processing results

## 9.1 Median stacks without multiple suppression

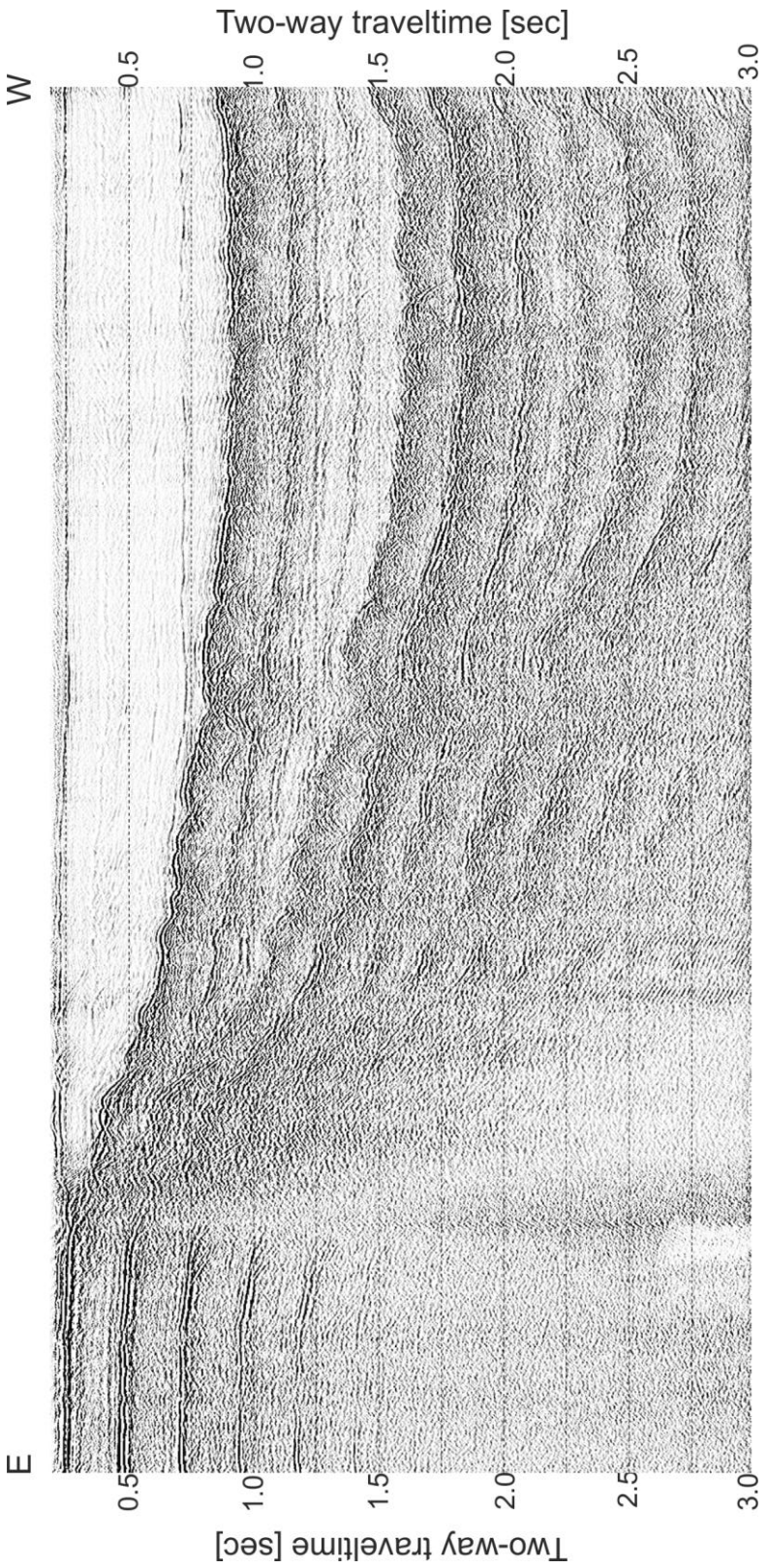


*A 1; Median stack of profile 1 (AWI 20110581) without multiple suppression.*

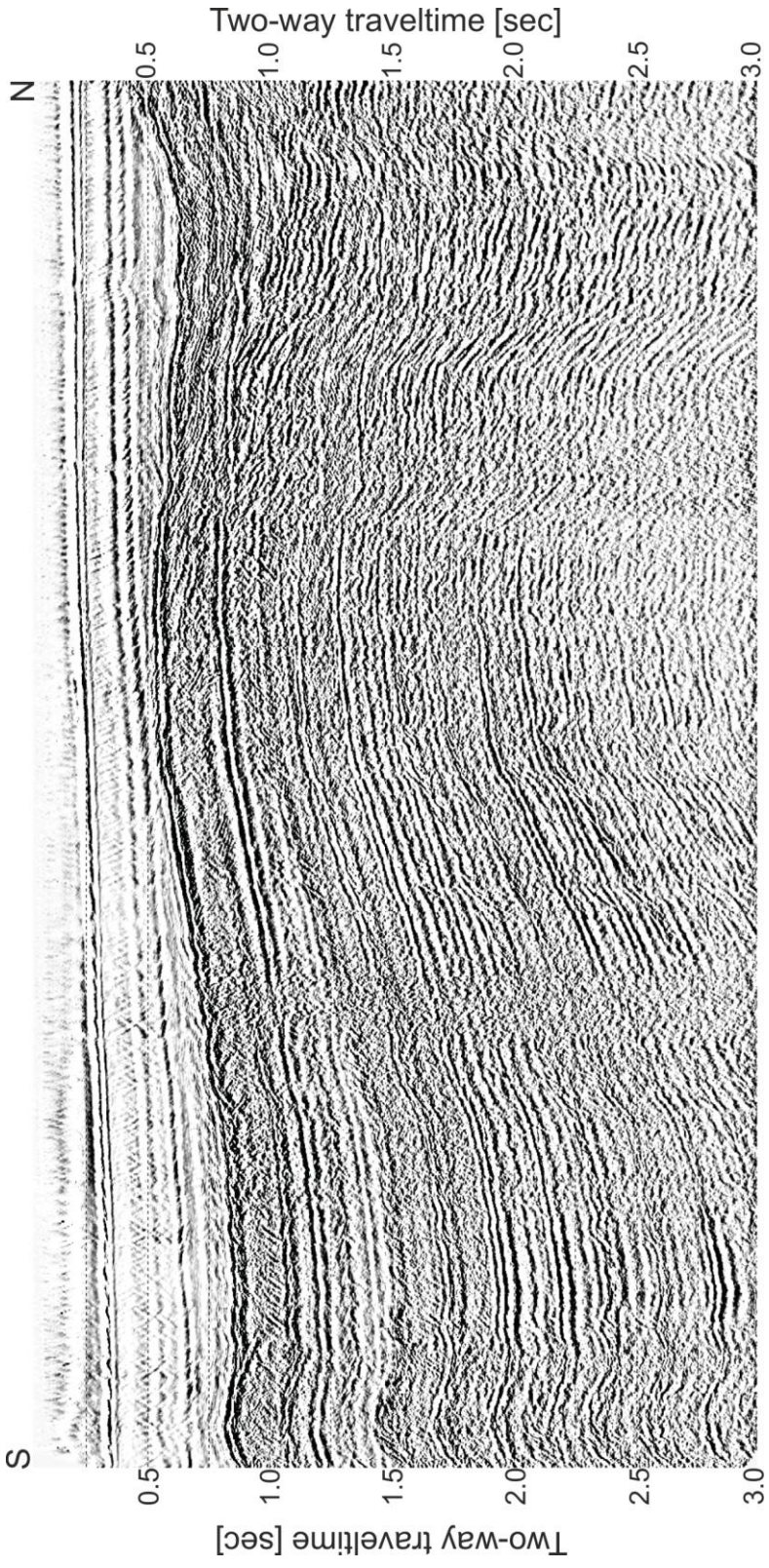


*A 2; Median stack of profile 2 (AWI 20110584) without multiple suppression.*